Total Word count without References ~12500

Age-associated failure of efficient cardiac proteostatic adaptations to chronic cAMP-stress is associated with accelerated heart aging

*Maria Grazia Perino[1], *Miguel Calvo-Rubio Barrera[2], Daniel R. Riordon[1], Giulio Agnetti[3,6], Admira Parveen[4], Christopher H. Morrell[1], Ismayil Ahmet[1], Khalid Chakir[1], Yelena S. Tarasova[1], Jia-Hua Qu[1,5], Kirill V Tarasov[1], Alexey E. Lyashkov[2], Yevgeniya O. Lukyanenko[2], Hikmet Kadioglu[3], Mark Ranek[3], Rafael deCabo[2], Edward G. Lakatta[1]

*Contributed equally

Correspondence to: Maria Grazia Perino, PhD, Laboratory of Cardiovascular Science, National Institute on Aging, National Institutes of Health, 251 Bayview Blvd, Baltimore (MD) 21224, United States, Email: mariagrazia.perino@nih.gov

Affiliations:

[1]Laboratory of Cardiovascular Science, National Institute on Aging, National Institutes of Health, Baltimore (MD), United States

[2]Translational Gerontology Branch, Intramural Research Program, National Institute on Aging, National Institutes of Health, Baltimore (MD), United States

[3]Division of Cardiology, Department of Medicine, Johns Hopkins University School of Medicine, Baltimore (MD), United States

[4]Department of Biochemistry and Molecular Biology, Johns Hopkins University School of Public Health, Baltimore (MD), United States

[5]St. Jude Children's Research Hospital, Memphis (TN), United States

[6]Dipartimento di Scienze Biomediche e Neuromotorie (DIBINEM), Università di Bologna, Bologna, Italy

ABSTRACT

Dysregulated proteostasis, leading to accumulation of misfolded proteins, electron-dense aggregates (lipofuscin, LF), preamyloid oligomers (PAOs), and proteotoxic stress is a hallmark of aging. We investigated how efficiently proteostatic adaptations to chronic cardiac cyclic adenosine monophosphate (cAMP)-dependent stress change with aging in mice harboring marked, cardiac-specific over-expression of adenylyl cyclase VIII (TG^{AC8}). We assessed protein quality control (PQC) mechanisms: ubiquitin proteasome system (UPS), autophagic flux via macroautophagy, and mitophagy in left ventricles (LVs) of TG^{AC8} and wild type littermates (WT) at 3-4 months and at 17-21 months of age. At 3-4 months of age TG^{AC8} mice exhibited markers of increased autophagic flux, measured by levels of microtubule-associated protein 1 light chain 3 (LC3), p62, and their phospho-forms in TG^{AC8} LV; cathepsin L1 activity was also significantly increased. In addition, canonical mitophagy signaling was enhanced, as receptors PARKIN, $p62^{S405}$ and $p62^{S351}$ were all upregulated, confirming a more efficient proteostasis in TG^{AC8} at 3-4 months vs WT. In advanced age, however, the PQC mechanisms were overwhelmed by proteotoxic stress, manifested in insufficient proteasome activity and an unbalanced autophagic flux (accelerated for markers such as LC3A in the context of a slower *overall* flux), leading to an increase in the accumulation of protein aggregates (increased ratio of insoluble/soluble protein fractions). Although both canonical (PARKIN, $p62^{S405}$ and $p62^{S351}$ receptors) and non-canonical (FKBP8 receptor) mitophagy signaling were upregulated in advanced age in TG^{AC8}, mitophagy was markedly impaired and mitochondrial dysfunction increased. Accumulation of LF bodies, of brownish-to-black pigments, and of $LC3^{+}$ and $p62^{+}$-inclusions of aberrant sizes, of desmin cardiac preamyloid oligomers (PAOs) and of

49 cleaved desmin, tagged for ubiquitination, were all increased in TG^{AC8} compared to young
50 TG^{AC8}. In contrast, the rate of protein synthesis and levels of soluble aggregates were
51 reduced in aged vs young TG^{AC8}, a sign of “normal” aging. Thus, increased proteostatic
52 mechanisms maintain cardiac health in TG^{AC8} in youth (3-4 months), but long-term
53 exposure to chronic cardiac stress, imposed by sustained activation of the
54 AC/cAMP/PKA/Ca^{2+} signaling axis, results in severely dysregulated proteostasis in TG^{AC8}
55 vs WT mice, associated with proteostatic insufficiency and increased cardiomyopathy that
56 leads to accelerated cardiac aging.
57

INTRODUCTION

Cardiac protein quality control (PQC) is required for the maintenance of cardiac health and function. Pathogenic aspects of protein misfolding and aggregation, collectively referred to *proteotoxicity*, accompany advancing age and can ultimately lead to heart dysfunction[1], and eventual cardiac failure[2]. Many protein aggregate–based diseases in the heart have been well characterized[3]. Plaque deposition (amyloidosis) or accumulation of soluble, oligomeric aggregates, and, more recently, desmin disorganization and the increase in cardiac desmin preamyloid oligomers (PAOs)[4] have also emerged as common hallmarks of aging, and acquired heart failure (HF)[5,6].

Many factors, including an imbalance of protein synthesis and degradation, exhaustion of proteostatic machinery, and downregulation of clearing mechanisms, e.g. the ubiquitin proteasome system (UPS)[7] and autophagy[8], can lead to collapse of proteostasis. Impaired autophagy and mitophagy that accompany advancing age due to reduced lysosomal[9] and mitochondrial fitness resulting from increased oxidative stress[10], have been linked to the accumulation of electron-dense aggregates, generally referred to lipofuscin (LF). As age advances, accumulation of LF occurs as PQC mechanisms become insufficient and begin to collapse[11]. The linear increase of LF as age advances is inversely correlated with longevity[12,13].

Our recent study demonstrated that chronic severe cardiac stress imposed by over-expression of adenylyl cyclase VIII (AC8) in mice (TG^{AC8}), induced concentric pattern of adaptations-signaling circuitry at a young age (3-4 months)[14]. This adaptive signaling circuitry included impressive upregulation of protein synthesis and degradation mechanisms (proteasome and autophagy) that protect against cardiac stress,

81 maintaining the remarkably high performance of the heart for up to about one year of
82 age[15,16]. However, signs of heart failure (HF) and cardiomyopathy begin to emerge in
83 TG^{AC8} as age advances[17,18]. Here we tested the hypothesis that the adaptive proteostatic
84 mechanisms in response to severe sustained cAMP-dependent chronic cardiac stress
85 become *more impaired* (overwhelmed) in TG^{AC8} than in WT in advanced age.

86 RESULTS

87 **Autophagy is <u>upregulated</u> in the TG^{AC8} heart at 3-4 months of age**

88 To assess basal autophagy in LVs in young TG^{AC8} and WT, we performed WB of the
89 established autophagy markers LC3 and p62/sequestosome-1, and assessed their
90 activity via measuring their phosphorylation states. Both LC3A and LC3B isoforms, which
91 localize on different autophagosomes[19] and exhibit distinct expression patterns and
92 functions[20], were assessed using isoform-specific antibodies.

93 Significant changes in cytosolic LC3I and its lipidated product, LC3II (LC3-PE),
94 recruited to the autophagosomal membrane during autophagy, were evident in TG^{AC8} vs
95 WT. Specifically at 3-4 months of age: LC3AI was significantly upregulated in TG^{AC8} vs
96 WT, whereas LC3AII was unchanged (**Figure 1Ai**); in contrast, cytosolic LC3BI did not
97 change in TG^{AC8}, whereas lipidated LC3BII was significantly downregulated (**Figure**
98 **1Aii**), compared to WT. Further, phosphorylation of LC3 at S12, which inhibits LC3
99 activity[21], was reduced by 50% (**Figure 1Bi**), and phosphorylation of LC3 at T50, which
100 increases LC3 activity[22], was increased by 30% (**Figure 1Bii**) in TG^{AC8} vs WT, suggesting
101 a <u>more efficient</u> autophagic context in TG^{AC8} vs WT.

102 Expression of total p62, an essential autophagy protein adaptor[23], was significantly
103 upregulated in TG^{AC8} vs WT (**Figure 1Ci**), and p62 was hyper-phosphorylated at S405

104 (p62^{S405}) (**Figure 1Cii**) and at S351 (p62^{S351}) (**Figure 1Ciii**), compared to WT; the ratios
105 of phospho-proteins at both sites to total p62 were also significantly elevated (**Figures**
106 **1Civ-v**), suggesting a higher detection of "aggregates"[24] (because phosphorylation at
107 S405 increases affinity to ubiquitinated cargo[25], including depolarized mitochondria[26]),
108 and more efficient oxidative stress management (phosphorylation at S351 activates
109 NRF2-pathway[27]) in the TG^{AC8} vs WT hearts, at 3-4 months of age.

110 Our previous work had shown that protein levels of lysosomal cathepsins are
111 upregulated in the TG^{AC8} at 3-4 months of age[14]. Here, we quantified relative changes in
112 different cathepsins in the TG^{AC8} LV, compared to WT. Cathepsins Z and S were *more*
113 *enriched* in TG^{AC8}, whereas cathepsin L1 showed the least significant change (**Figure**
114 **2A**, **Extended Data Table**). Because cathepsin L degrades not only lysosomal content
115 but also autophagosome membrane-components GABARAP-II and LC3-II[28], during the
116 autophagic proteolysis, we assessed its activity as a measure of lysosome function and
117 dispose of autophagy flux. A significantly higher cathepsin L1 activity was in TG^{AC8} vs WT
118 LV (**Figure 2B**) in the context of an increase in the lysosomal acid phosphatase ACP2
119 protein **(Figure 2C**), suggesting an <u>overall higher lysosomal fitness</u> (function) in TG^{AC8}
120 compared to WT.

121 **Autophagic flux is <u>optimized</u> to ensure efficient and effective clearance in the TG^{AC8}**
122 **heart at 3-4 months of age**

123 Because autophagy is a dynamic, multi-step process, we next evaluated stages of
124 autophagic flux by inhibiting lysosomal function with the lysosomotropic drug chloroquine
125 (CQ). Basal autophagy clearly differed in the young TG^{AC8} vs WT (**Figures 3Ai-iii,**
126 **Extended Data Figure S1**): autophagic "carrier flux" (flux of the "carrier" protein not the

127 actual cargo/substrate flux) of both LC3AI and LC3BI (**Figures 3Ai-ii**) became
128 significantly reduced following CQ treatment, compared to saline, whereas for LC3AII and
129 LC3BII remained unchanged; carrier-flux of the ubiquitin-binding protein[25] and NRF2-
130 signaling activator[29,30] p62 (**Figure 3Aiii**), was also downregulated (by 29%) in TG^{AC8} vs
131 WT, whereas the pattern of the carrier-flux of other important players involved in
132 autophagy following CQ was more variable. Specifically, the carrier-flux of the *autophagy*
133 *related 16 like 1* protein (ATG16L1), which participates in LC3 lipidation[31] and cell
134 homeostasis by regulating membrane cellular trafficking[32], was reduced (by 37%) (**Figure**
135 **3Bi**). In contrast, the carrier-flux of the *autophagy related 4B cysteine peptidase* (ATG4B)
136 (**Figure 3Bii**), which is involved in LC3 lifecycle[33] by processing pro-LC3 into LC3**I**[33], and
137 of the programmed cell death 6-interacting protein (PDCD6IP/ALIX), ancillary protein
138 contributing to the ESCRT signaling[34], were both increased (by 42% and 28%,
139 respectively) (**Figure 3Biii**). Finally, carrier-flux of the *peptidyl-prolyl cis-trans isomerase*
140 (FKBP8) (**Figure 3Biv**), non-canonical mitophagy receptor[35] that after recruitment on
141 mitochondria from LC3A translocates to the ER (avoiding to be degraded by
142 autophagosomes[36]), did not change between genotype.

143 Using transmission electron microscopy (TEM), we next assessed events-flux by
144 directly visualizing autophagic figures in saline vs CQ-treated TG^{AC8} and age-matched
145 WT controls. A significant increase in the numbers of autophagic events was detected in
146 TG^{AC8} vs WT (**Figures 3Ci-ii**), confirming the increase in autophagy/autophagic flux in
147 the TG^{AC8} LV at this age.

148 In summary, chronic cardiac-specific over-expression of AC8 in the young TG^{AC8}
149 heart[14] modulates protein levels of the autophagic machinery by fine-tuning key markers

150 of selective cargo recognition (LC3 isoforms), and of selective autophagy (LC3/p62
151 activation by phosphorylation), activates protection mechanisms against oxidative stress,
152 and enhances lysosomal degradation ensuring a more efficient and effective clearance
153 of misfolded proteins without accumulation of insoluble protein aggregates.

154 **Increased efficiency of autophagy/autophagic flux of the youthful TG^{AC8} heart**
155 **becomes insufficient in advanced age**

156 Because autophagy induction and clearance are known to decrease with aging[9], we
157 anticipated that expression of key autophagic proteins and dissipated autophagic flux
158 became reduced in LV of both aged TG^{AC8} and matched WT. Indeed, both LC3 isoforms
159 (**Figures 4Ai-ii**) and ATG4B (**Extended Data Figure S2**) were significantly
160 downregulated in both genotypes at 17-21 vs 3-4 months of age, with specific
161 accumulation of LC3II, an age-associated decrease in event number/volumetric density
162 at *early* stages (**Figures 4Bi-ii, 4Bv**), and an increase in event number/volumetric density
163 in *late* stages, measured by paired TEM micrograph analysis (planimetry and stereology)
164 (**Figures 4Biii-v**).

165 Assessment by fluorescence microscopy (IHC) of the number and size of endogenous
166 LC3^{+}-puncta (autophagosomes) and LAMP1^{+}-puncta (lysosomes/late endosomes),
167 (**Figure 4Ci**), in young and aged TG^{AC8} LVs and age-matched WT, revealed that puncta
168 count and size significantly increased in *aged* compared to *young* mice (**Figures 4Cii-vii**)
169 independently of genotype, suggesting downregulation of autophagy induction and
170 clearance, in aged mice.

171 TG^{AC8}, however, differed from WT in several aspects: both LAMP1^{+}-puncta and LC3^{+}-
172 puncta were *smaller* in TG^{AC8} vs matched WT, at *both* ages (**Figures 4Ciii, 4Cvi**); while

173 LC3^{+}-puncta counts were higher in numbers in *young* TG^{AC8} (**Figure 4Cv**), there was no
174 difference in the % of cell area covered by LC3^{+}-puncta in young TG^{AC8} vs WT (**Figure**
175 **4Cvii**), but as the TG^{AC8} *aged*, LC3^{+}-puncta count number decreased (**Figure 4Cv**),
176 whereas LAMP1^{+}-puncta counts significantly increased (**Figure 4Cii**), vs WT.
177 Additionally, independent of counts, both LAMP1^{+}-puncta and LC3^{+}-puncta covered a
178 smaller area of the cell in *aged* TG^{AC8} LV vs aged WT (**Figures 4Civ, 4Cvii**), but the latter
179 were much more heterogeneous in size (**Figures 4Di-ii**), and had a different frequency
180 distribution vs age-matched WT (**4Ei-ii**). A reduction in puncta size in TG^{AC8} vs WT at
181 both ages, indicates <u>differential modulation</u> of the autophagic process; relative changes
182 in LAMP1^{+}- vs LC3^{+}- puncta counts, in *aged* TG^{AC8}, suggest a <u>different</u> requirement in
183 <u>cargo detection</u> and transport (LAMP1 is also a marker of late endosomes) compared to
184 aging WT. Nonetheless, the greater accumulation and increased aggregation (increased
185 LC3^{+}-puncta size and smaller % of cell area covered by LC3^{+}-puncta) of insoluble
186 inclusions in the old TG^{AC8} heart compared to age-matched WT, suggests that effects of
187 aging are more severe in TG^{AC8} vs WT.

188 Measurement of specific LC3 isoforms, p62, and other proteins (ATG9A) involved in
189 the autophagic process (by WB), and assessment of autophagic flux (with CQ), showed
190 that LC3AI was significantly upregulated in old TG^{AC8}, compared to age-matched WT
191 (**Figure 5Ai**), similar to the genotypic difference at 3-4 months (**Figure 1Ai**), whereas
192 LC3AII protein levels did not significantly differ between genotypes at 17-21 months,
193 either in the soluble (**Figure 5Ai**) or insoluble (pellet) fraction (**Extended Data Figures**
194 **S3i, S3iii**). In contrast, LC3B forms did not differ in aged TG^{AC8} (**Figure 5Aii**),
195 demonstrating that LC3 isoform-specific modulation persists in old age, as we previously

196 observed in TG^{AC8} at younger age (**Figure 1Ai-ii**). p62 protein levels were also
197 significantly upregulated in old TG^{AC8} LVs, both in the soluble fraction (**Figure 5Aiii**),
198 similar to the younger age (**Figure 3Ci**), and in the insoluble fraction (**Extended Data**
199 **Figures S3ii-iii**), where *LC3AII-bound* p62 is present in LC3^{+}/p62^{+}
200 aggregates/inclusions[24], suggesting that unprocessed protein aggregates were increased
201 in the aged TG^{AC8}, vs WT. Protein levels of ATG9A were elevated at both ages in TG^{AC8}
202 vs age-matched WT (**Extended Data Figure S4**), but in *aged* TG^{AC8} was the highest
203 level, suggesting increased membrane delivery to the phagophore assembly site (PAS)[37],
204 a process that is essential for autophagosome formation[38], transport of lysosomal
205 hydrolases[39], and lipid mobilization to mitochondria[40].

206 Following CQ treatment, both LC3AI and LC3AII significantly *increased* in TG^{AC8} vs
207 WT-saline and WT-CQ (**Figure 5Ai**); LC3AII also increased vs TG^{AC8}-saline, an indication
208 of an *accelerated carrier-flux* for LC3A in old TG^{AC8} vs age-matched WT. LC3B forms
209 were not affected by CQ (**Figure 5Aii**), whereas CQ remarkably reduced p62 protein
210 levels (soluble fraction) in old TG^{AC8} (**Figure 5Aiii**), similar to younger age (**Figure 3Ci**).
211 Additionally, the carrier-flux of ATG16L1 (**Figure 5Bi**), of ALIX (**Figure 5Bii**) and of
212 FKPB8 (**Figure 5Biii**) were all significantly reduced in old TG^{AC8} LVs (by 68%, 20% and
213 49% respectively), an indication that *overall* autophagic flux in aged TG^{AC8} is significantly
214 reduced, compared to both younger TG^{AC8} and to aging WT. In contrast, the carrier-flux
215 of ATG4B (**Figure 5Biv**), LC3 phosphorylation (S12 and T50) and ACP2 protein levels
216 (**Extended Data Figures S5i-iii**) did not differ by genotype at 17-21 months of age.

217 Because the *Coordinated Lysosomal Expression and Regulation* (CLEAR) network[48]
218 orchestrates upstream signaling pathways of autophagy, lysosome biogenesis and

219 function[41], we assessed protein levels and activation of its master regulator, the
220 transcription factor TFEB, in young and old TG^{AC8} LVs and age-matched WT (**Extended**
221 **Data Figure S6i-iv**). We observed a significant increase in the phosphorylation at S210
222 ($TFEB^{S210}$), together with an increase in the ratio of $TFEB^{S210}$ to total TFEB (**Extended**
223 **Data Figure S6iii**), with aging in both genotypes (**Extended Data Figure S6i-iv**),
224 suggesting the lack of a genotype-effect on autophagy induction. However, and
225 remarkably, cytoplasmic and nuclear enrichment of LV tissue showed that the nuclear to
226 cytoplasmic ratio of total TFEB was significantly reduced in aged TG^{AC8} vs age-matched
227 WT (**Figures 5Ci-iv**). TFEB phosphorylation at S210 (by mTORC1[42]) increases its
228 interaction with 14-3-3 proteins in the cytoplasm, which prevents its translocation to the
229 nucleus[42] consequently turning off the activation of TFEB downstream pathways,
230 including autophagy (14-3-3:RAPTOR interaction), and mitophagy/ER-phagy (14-3-
231 3:BAD interaction, which shifts the balance towards survival, and BCL-2/BCL-XL binding
232 to BECLIN-1 (ATG6))[43]. 14-3-3 is a family of ubiquitously expressed adaptor proteins that
233 typically bind to “client proteins” at phosphorylated serine/threonine motifs, regulating
234 their stability, activity and/or localization[44]. We therefore assessed 14-3-3s’ transcriptional
235 expression (by qPCR) in TG^{AC8} vs WT with aging, and found that five (YWHAE, YWHAZ,
236 YWHAH, YWHAQ and Stratifin) of the 7 isoforms of 14-3-3s were significantly increased
237 in aged vs young TG^{AC8}, whereas 14-3-3’s transcripts did not change in WT with age
238 (**Figures 5Di-vii**). Additionally, mRNA of YWHAZ, YWHAH, YWHAQ and Stratifin were
239 also significantly increased in aged TG^{AC8} vs old WT (**Figures 5Div-vii**). Transcriptional
240 upregulation of 14-3-3s together with reduced levels of nuclear TFEB explain the greater
241 reduction in the activation of the CLEAR network in old TG^{AC8} vs WT hearts, strongly

242 suggesting that autophagic signaling becomes more severely downregulated in TG^{AC8}
243 with aging, compared to that in age-matched WT.

244 Taken together, data in figures suggest that autophagy declines with age in TG^{AC8} and
245 WT regardless of genotype, as shown by reduced protein levels of markers involved in
246 autophagy induction (LC3, ATG4B), accumulation of LC3II, increased puncta count and
247 size, and reduced numbers of *early* autophagic events in conjunction with higher
248 numbers/volumes of *late* figures.

249 However, further downregulation of the CLEAR network in old TG^{AC8} LVs compared
250 to age-matched WT, together with increased heterogeneity in $LC3^{+}$-puncta size, the
251 reduction in the cell area covered by $LC3^{+}$-puncta and the different modulation pattern of
252 $LAMP1^{+}$-puncta and $LC3^{+}$-puncta in old TG^{AC8}, all point to much more severe autophagy
253 downregulation in old TG^{AC8} vs age-matched WT, thus that the *optimized, highly efficient*
254 *autophagic flux* in young age that accommodated proper cargo clearance in TG^{AC8},
255 *manifests reduced kinetics and becomes dysfunctional* as TG^{AC8} ages, and would clearly
256 be insufficient for proper clearance of aggregates and inclusions of aberrant size, and
257 more prone to aggregation, compared to the young-TG^{AC8} and age-matched WT.

258 **Proteasome insufficiency and mitochondrial dysfunction lead to exaggerated age-**
259 **associated increase in aggregates accumulation in TG^{AC8}**

260 We next assessed PQC mechanisms (ubiquitin proteasome system (UPS) activity,
261 autophagy and mitophagy) and evaluated protein translation rates and aggregates
262 accumulation in young and aged TG^{AC8}, and age-matched WT. Our previous work in
263 young mice (3-4 months of age) demonstrated that: 1) UPS activity and autophagy,
264 including mitophagy, were all upregulated in TG^{AC8}, compared to WT, indicating

265 cooperation among PQC mechanisms[14]; 2) although the protein synthesis rate was 40%
266 higher in TG^{AC8} vs WT, UPS clearance of soluble aggregates was also upregulated, and
267 insoluble protein aggregates did not accumulate within cells[14]; 3) the numbers of healthy
268 mitochondria and the percent of cell volume these occupied, did not differ between TG^{AC8}
269 and WT[14]; and 4) although the canonical cargo receptors PARKIN was significantly
270 upregulated, mitochondrial fitness was comparable between genotypes[14].

271 Proteasome activity was not increased in old TG^{AC8}, compared to age-matched WT
272 and in contrast to younger age (**Figure 6A**). UPS function in TG^{AC8} declined with aging,
273 from 3 to 18 months, whereas it remained the same with aging in WT (**Figure 6A**). The
274 density of *soluble* aggregates also did not differ by genotype at both ages, but it
275 decreased with aging independent of genotype (**Figure 6Bi**). The ratio of insoluble to
276 soluble aggregates, however, significantly increased in TG^{AC8} between 3 and 18 months,
277 with no change in aging WT (**Figure 6Bii**), indicating the greater accumulation of *insoluble*
278 protein aggregates in the TG^{AC8} heart, during the aging process, compared to "normal"
279 aging WT.

280 Because accumulation of *insoluble* aggregates leads to proteotoxic stress[45], we
281 assessed, by WB, protein levels of heat shock protein 90 (HSP90), a stress-sensor that,
282 with its chaperon activity[46] activates protective mechanisms to reduce stress and maintain
283 cellular homeostasis and intracellular transport[47]. HSP90α, the HSP90 stress-inducible
284 form, significantly increased between 3 and 18 months in both genotypes (**Figure 6C**),
285 an indication that age, *per se*, increases cellular stress, as well as the need for increased
286 protein folding/refolding, maintenance and degradation. Additionally, HSP90α was
287 significantly upregulated in TG^{AC8} (**Figure 6C**) vs WT at both ages[14], but was increased

288 to a further extent in old TG^{AC8}, in parallel with the highest level of proteotoxic stress
289 (**Figure 6Bii**), and the persistent higher cAMP-derived chronic stress of the TG^{AC8} heart,
290 compared to "normal' aging WT.

291 Although protein synthesis did not differ by genotype in aged mice (**Figure 6D**), protein
292 translation rates, a hallmark of aging in health[48], significantly decreased in TG^{AC8}, from 3
293 to 18 months.

294 Mitochondrial failure, a hallmark of aging, occurs in diverse pathologic diseases
295 conditions, including heart failure[49], in response of a wide variety of stressors. We
296 evaluated protein levels (by WB) of key players of mitochondrial dynamics, including
297 fusion/fission[50], function[51], integrity[52] and clearance[53] in young and aged TG^{AC8} LVs, and
298 age-matched WT. *Mitofusin 1* (MFN1), located on the outer mitochondrial membrane
299 (OMM) and involved in the orchestration of OMM fusion, was significantly increased in
300 old TG^{AC8} (**Figure 7A**), suggesting that conditions for mitochondrial fusion and docking[54]
301 were more favorable, compared to old WT; however, levels of the mitochondrial GTPase
302 *dynamin-related protein 1* (DRP1), a cytosolic protein that controls late stages of the
303 mitofission process[55], and is recruited to the mitochondrial surface in response to various
304 physiological cues[56], did not differ between genotypes (**Figures 7B**). In contrast, levels
305 of the protein *dynamin-related GTPase optic atrophy type 1* (OPA1), which is localized in
306 the mitochondrial intermembrane space on the outer leaflet of the inner membrane
307 (IMM)[57] differed in TG^{AC8} vs WT. The expression of both the full length OPA1 (L-OPA1),
308 which has a role in IMM fusion and cristae remodeling[58], and of its cleaved form, S-OPA1,
309 which is associated with mitochondrial fission[59], and results from the proteolytic
310 processing of L-OPA1 constitutively (YME1L[60]), and upon stress-activation

311 (metalloprotease OMA1[61]), were significantly reduced in TG^{AC8} vs WT independent on
312 age (**Figure 7Ci-ii**). Remarkably, although TG^{AC8} expressed less S-OPA1 vs WT (**Figure**
313 **7Cii**), the ratio of S-OPA1 to L-OPA1 was significantly elevated in TG^{AC8} vs WT at both
314 ages (**Figure 7Ciii**), and was increased to a further extent in aged TG^{AC8} vs old WT,
315 suggesting that persistent chronic cardiac cAMP-derived stress in the TG^{AC8} heart
316 exacerbates the age-related increase in cellular stress[61] (**Figure 7Ciii**). Protein levels of
317 the mitochondrial heat-shock protein 60 (mtHSP60/HSPD1), an indispensable
318 chaperonin that regulates mitochondrial protein homeostasis and function by preventing
319 the aggregation of misfolded proteins[62], were also reduced in aged TG^{AC8} vs WT (**Figure**
320 **7D**), which in the context of imbalanced levels of OPA1 and the persistent chronic cAMP-
321 derived cardiac stress, show that decreased protection[52] of the mitochondrial matrix and
322 its associated functions[63] in the TG^{AC8} heart as age advances vs age-matched WT,
323 contribute to the greater mitochondrial dysfunction, eventually leading to heart failure[51].
324 Because the mitophagy process ensures disposal of malfunctional and/or
325 dysfunctional mitochondria, we next evaluated the expression of specific cargo receptors
326 involved in canonical and non-canonical mitophagy[64] in aged TG^{AC8} and age-matched
327 WT. Similar to young TG^{AC8}, the canonical cargo receptors PARKIN (**Figure 7Ei**), $p62^{S405}$
328 (**Figure 7Eii**), recruited to depolarized[65] and polyubitiquinated[26] mitochondria,
329 respectively, and $p62^{S351}$ (**Figure 7Eiii**), upregulated in conditions of oxidative stress[27],
330 were all significantly increased in aged TG^{AC8} vs WT, suggesting that canonical
331 mitophagy is incremented in TG^{AC8} vs WT. In contrast to young TG^{AC8} (**Figure 3Biv**), the
332 non-canonical cargo receptor FKBP8[66], which assists LC3A during mitophagy and in the
333 clearance of misfolded proteins, was also significantly upregulated (**Figure 7Eiv**) in the

old TG^{AC8} vs WT. In line with these results, TEM and light microscopic assessment of semi-thin sections of LV cardiomyocytes clearly demonstrated disruption of the mitochondrial network in old TG^{AC8} vs old WT (**Figures 7F-G**). Reduced signaling for disposal of oxidized lipoproteins, in old TG^{AC8}, together with disruption of the mitochondrial network, suggests that mitophagy failed in old TG^{AC8}, because the rate of damaged mitochondria accumulation *exceeded* the rate of aggregates clearance. In other terms, despite the concurrent activation of both canonical and non-canonical mitophagy in old TG^{AC8}, the system cannot cope with the increased mitochondrial dysfunction in old TG^{AC8}.

LF body quantification of the extent of accumulation of undigested material (in Palade's-stained semi-thin sections by light microscopy) (**Figure 8A**), showed that there was no difference in LF number (**Figure 8Bi**) or average body size (**Figure 8Bii**) in old TG^{AC8} vs WT. However, there was a marked heterogeneity within the LF population, and increased total volume of LF (**Figures 8Biii, 8Biv**), with LF covering a larger percentage of the cardiomyocyte area (**Figure 8Bv**), in TG^{AC8} vs WT. Interestingly, those vast insoluble aggregates reminded a myelin-like figure, with high electron-dense concentric lamellations, and displayed different pigmentation (brownish to blueish-black) (**Figure 8C**), and very heterogenous $LC3^{+}$-puncta/inclusions (**Figure 8D**) almost entirely covering the cardiac myocyte cell area ($LC3^{+}$-CMs) (**Figures 8Ei-iii**), and were only present in TG^{AC8} LVs, suggesting the presence of an "aged" (further oxidized) cargo accumulation of different lipoproteins and/or a denser composition.

Recent evidence has shown the involvement of desmin, whose filaments interlinks the contractile myofibrillar apparatus to mitochondria, nuclei and the sarcolemma, to impaired

357 mitochondrial fission[67] and proteostasis[67]. Furthermore, desmin disorganization has been
358 documented to be a component of the accumulation of preamyloid oligomer (PAO)
359 aggregates in the heart[68]. Desmin PAOs were increased with age in TG^{AC8} but not in WT,
360 and were higher in aged TG^{AC8} vs WT (**Figure 8F**). Further, a higher percentage of
361 desmin was tagged for ubiquitination (**Figure 8Gi**), and cleaved (**Figure 8Gii**), an
362 indication of severe alterations of the myofilament ultrastructure in the old TG^{AC8} heart vs
363 WT.

364 $HSP27^{S86}$ (S82 in human), the stress-induced phosphoform (by MAPK[69]) of the small
365 heat shock protein (sHSP) HSP27/HSPB1, which is a biomarker of cardiac damage[70] and
366 is upregulated during stress conditions to maintain myocardial function[71], was significantly
367 elevated in old TG^{AC8} vs WT LVs (**Figures 8Hi**), and specifically co-localized (via
368 fluorescence microscopy IHC) with $p62^{+}$-puncta/inclusions (**Figure 8Hii**), suggesting
369 higher stress and myofilament disruption, exactly at the site of electron-dense aggregates
370 accumulation, in aged TG^{AC8} cardiac myocytes vs old WT (**Figure 8Hii**). Thus, damaged
371 TG^{AC8}-cardiac myocytes ($HSP27^{S86+}$) present higher garbage accumulation ($p62^{+}$
372 aggregates), have a thinner wall and a sclerotic stroma, compared to old WT. Therefore,
373 failure of PQC mechanisms leads to poor cardiomyocyte "health", a phenotype
374 consistently associated with the context of cardiomyopathy.

375 **<u>Increased failure</u> of PQC mechanisms <u>exacerbates</u> cardiac aging in TG^{AC8}**

376 We next addressed what changes occurred in cardiac structure and function in the
377 context of dysregulated proteostasis. To this end, assessment of cardiac function and
378 structure by echocardiogram revealed that the small hyperdynamic heart at 3 months of
379 age in the AC8 group (significantly smaller LV chamber size and higher ejection fraction

380 (EF) and heart rate (HR), compared to young WT)[14], became a hypertrophic and dilated
381 heart at 19 months of age (**Figure 9Ai-iii**). Although the HR remained higher throughout
382 life in TG^{AC8} vs WT (**Figure 9Bi**), in aged TG^{AC8} the EF started to decline (**Figure 9Bii**)
383 between 14 and 19 months of age, whereas the left ventricular (LV) mass (**Figure 9Ci**),
384 the end diastolic volume (EDV) (**Figure 9Cii**) and the end systolic volume (ESV) (**Figure**
385 **9Ciii**) increased, demonstrating a reduced heart performance, vs old WT. Interestingly,
386 some hearts were more dilated and had a greater reduction in EF than others within the
387 aged TG^{AC8} group (**Figures 9Aii-iii, 9Bii**). This heterogeneity in LV reduced function
388 matches the increased heterogeneity present in aggregates (**Figures 4C-E, 6Bii**) and
389 oxidized lipoprotein accumulation in old TG^{AC8} (**Figures 8B, 8E**), compared to old WT
390 (**Figure 9Ai**).

391 In conclusion, increased proteasome insufficiency and greater proteotoxic stress, in
392 conjunction with a greater mitochondrial dysfunction and severe UPS and autophagy
393 dysregulation in aged TGAC8, lead to excessive accumulation of enlarged LF bodies,
394 brownish-to-black pigments and LC3+-/p62+-inclusions of heterogeneous size, and to the
395 disruption of the cardiac contractile machinery by desmin disorganization and increased
396 desmin PAOs. In addition, higher expression of HSP27S86 suggests increased cardiac
397 myocyte damage in the old TGAC8 heart vs WT, and its co-localization with p62+-
398 inclusions and LF aggregates points to these as mechanisms that underlie the
399 upregulation of stress responses to preserve cardiomyocyte structure and function. Thus,
400 increased failure of PQC mechanisms with aging leads to decreased heart function and
401 highly contributes to TGAC8 accelerated cardiac aging.

402 # DISCUSSION

403 It is widely recognized that marked chronic catecholamine-induced cardiac stress
404 leads to heart failure[72,73]. Our previous work in TG^{AC8} mice had shown that, up to 3-4
405 months of age, sustained upregulation of the AC/cAMP/PKA/Ca^{2+} axis[14] activates
406 numerous concentric adaptation mechanisms that protect heart health and function in
407 TG^{AC8} mice. Among other mechanisms, protein quality control (PQC), including the
408 ubiquitin proteasome system (UPS) and the autophagic machinery, became activated to
409 ensure more efficient proteostasis in the TG^{AC8} heart. The present study evaluated
410 proteostasis in the TG^{AC8} heart in more detail, focusing on key players involved in the
411 autophagic process at 3-4 months of age in TG^{AC8}, and probed whether PQC
412 mechanisms remained adequate in advanced age.

413 **Autophagy in the TG^{AC8} heart at 3-4 months of age**

414 Our results show that efficient modulation of LC3's isotype-specific functions[19] (by
415 interacting with specific adapters for cargo recruitment[20] and selection[74]) guarantees a
416 <u>more favorable</u> autophagic process and effective clearance of damaged proteins, that
417 essential PQC features in the context of a high cardiac workload and energy demands.
418 One manifestation of upregulated autophagy in TG^{AC8} vs WT is that LC3, and specifically
419 its isoforms LCA and LC3B, which localize to different phagophores/autophagosomes[19],
420 exhibit distinct expression patterns (**Figure 1A-B**). Specifically of the TG^{AC8} heart, at 3-4
421 months of age, LC3A orchestrates steady state autophagy, and *LC3A-mediated*
422 *autophagy* modulates the protein quality control network[75] to effectively resolve both
423 aggresome formation and disposal of failing mitochondria by mitophagy[35] (together with
424 FKBP8). We speculate that LC3A *upregulation* is important for efficient PQC in the

425 “stressed-out” TG^{AC8} heart, and that *downregulation* of LC3B is consistent with the idea
426 that LC3A and LC3B are involved in different signaling pathways (UPR-activated
427 response[75] vs mitophagy[35,54] vs apoptosis[76] vs endosome-mediated autophagy[77]). LC3
428 post-translational modifications (PTMs) by phosphorylation, that affect its activity[21,22],
429 were also differentially modulated in the young TG^{AC8} vs WT heart in a way that favored
430 both *early* and *late* stages of autophagy: specifically, phosphorylation of LC3 at S12 was
431 significantly reduced, whereas its phosphorylation at T50 was significantly increased.
432 Phosphorylation at S12 by PKA/PKC[78] inhibits autophagy by preventing autophagosome
433 wall elongation, whereas phosphorylation at T50 by STK3/4[22] stimulates the autophagic
434 process by promoting autophagolysosome fusion.

435 Another manifestation of fine-tuned, regulated efficient autophagy in TG^{AC8} vs WT was
436 that p62/sequestosome-1, an essential autophagy adaptor protein[79] that co-localizes with
437 ubiquitin and LC3, was upregulated in TG^{AC8} vs WT at 3-4 months (**Figure 1Ci**). p62 plays
438 a critical role in “aggresome” formation[80] and clearance[49] by activating autophagy while,
439 itself, becoming an autophagy substrate[81]. p62 phospho-forms p62^{S405} and p62^{S351} (and
440 their ratios to total p62) were also significantly upregulated in TG^{AC8} vs WT at 3-4 months
441 (**Figure 1Cii-v**). p62^{S405} correlates to ubiquitinated cargo[25] (including protein
442 aggregates[24]), cellular inclusion bodies (the aggregates of aggregates[45]), and
443 polyubitiquinated mitochondria[25], whereas p62^{S351} has a higher affinity for the ubiquitin
444 ligase adaptor Kelch-like ECH-associated protein 1 (KEAP1)[29], resulting in constitutive
445 activation of the transcription factor NF-E2-related factor 2 (NRF2) and regulation of its
446 downstream signaling pathways[30], with a positive feedback on p62 transcriptional
447 activation itself[27]. Transient accumulation of p62 bodies by upregulation of p62 and its

448 phospho-forms in the young TG^{AC8} heart, demonstrates its important role in the induction
449 of autophagy[82], and in both adaptation to the sequelae evoked by upregulation of
450 signaling for protein aggregate clearance, and increased ROS scavenging, a protection
451 mechanism from oxidative stress by sustained activation of the AC/cAMP/PKA/Ca^{2+} axis.
452 ATG9A, which is the only integral membrane ATG protein, and is essential for
453 autophagosome formation, was elevated in young TG^{AC8} LVs, vs WT (**Extended Data**
454 **Figure S3**). ATG9A partially co-localizes with LC3[38], and, as well as LC3, correlates with
455 the number of autophagic bodies and autophagosomes[37]. In addition, it also participates
456 in Parkin-mediated mitophagy via activation of the optineurin (OPTN)/ATG9A axis[83],
457 crucial for maintenance of healthy mitochondrial dynamics. $LC3^{+}$-puncta were more
458 numerous but smaller in TG^{AC8} at 3-4 months of age (**Figure 4Cv-vi**), and since cargo
459 detection is regulated by *flexibility in autophagosome size*[37], we interpret elevated levels
460 of ATG9A together with higher counts of smaller $LC3^{+}$-puncta, to indicate an increased
461 *frequency of autophagosome formation* and enhanced *"selective"* autophagy and
462 mitophagy in young TG^{AC8} vs WT.
463 Events-flux numbers were increased in $TG^{\mathbf{AC8}}$ vs WT at 3-4 months, following CQ
464 (**Figure 3C**), indicating accelerated flux. However, remarkably, LC3II did not accumulate,
465 following CQ (**Figure 3Ai-ii**). Interestingly, protein levels of LC3**I** (both LC3AI and LC3BI)
466 were *always decreased* in TG^{AC8}, following CQ (**Figure 3Ai-ii**), whether LC3 was
467 transcriptionally *upregulated* (LC3A) or *downregulated* (LC3B). We interpret this
468 reduction to be the result of an *accelerated LC3 turnover* that prevents accumulation of
469 LC3II at the lysosome. Specifically, increased protein levels of ATG4B (**Supplemental**
470 **Information Table 2**), ATG16L1 (**Figure 3Bi, Supplemental Information Table 2**), and

471 the trend towards accelerated flux of ATG4B in TG^{AC8} (**Figures 3Bii**), promote a *faster*
472 *LC3I to LC3II processing*; additionally, increased protein levels of ATG9A (**Extended**
473 **Data Figure S3**), of the lysosomal acid phosphatase ACP2 (**Figure 2C**), and of several
474 cathepsins (**Figure 2A**)[14], together with the upregulation of cathepsin L1 activity (**Figure**
475 **2B**), induce a *faster degradation of LC3II*. However, it might be argued that our conditions
476 to assess the autophagic flux were suboptimal for our transgenic mouse, since the
477 protocol was optimized to detect LC3II accumulation (following CQ) in WT controls. In
478 fact, saturating concentrations of lysosomal inhibitors are needed, considering the well-
479 known enhanced drug clearance of the heart compared to other organs[84], together with
480 the "high performance" of the TG^{AC8} heart[14] and the increase in lysosomal (cathepsin L1)
481 activity. Thus, we cannot exclude that the lack of accumulation of LC3II and p62 in TG^{AC8}
482 LVs, following CQ treatment, is due to a faster clearance of CQ from the TG^{AC8} heart
483 and/or because of the consequent reduced CQ concentration in TG^{AC8} LVs, the latter
484 been shown to further increase lysosomal activity[85], and autophagy flux in general. And
485 if that were to the case, lysosomal inhibition would be incomplete in young TG^{AC8} LVs,
486 leaving the existence of a remaining residual LC3-carrier flux in the TG^{AC8} heart, which
487 further accelerates endogenous LC3 turnover that deprives the cellular pool of LC3I
488 (lower levels of LC3AI and LC3BI) and prevents the accumulation of LC3II and p62 (no
489 changes in LC3II and lower levels of p62), following CQ.

490 Nonetheless, *in toto*, the present results, together with those of our previous study[14]
491 showing increased proteasome activity without accumulation of insoluble aggregates,
492 and increased levels of proteins involved in the autophagic machinery[14], strongly suggest
493 that UPS and autophagic pathways concurrently operate in a more efficient mode in the

494 young TG^{AC8} heart to manage its state of chronic, marked cardiac cAMP-derived
495 stress[49,86].

496 **PQC mechanisms in aged TG^{AC8} and WT**

497 **Autophagy**

498 Autophagy markers LC3 and ATG4B became significantly downregulated with age in
499 both TG^{AC8} and WT (**Figure 4A**, **Extended Data Figure S2**), and the number and the
500 size of autophagosomes ($LC3^{+}$-puncta) and lysosomes/late endosomes ($LAMP1^{+}$-
501 puncta), measured by fluorescence microscopy, dramatically increased (**Figure 4Cii-vi**).
502 Downregulation of proteins involved in induction of autophagy, in conjunction with
503 reduced numbers of *early* autophagy figures, and an increased number of *late* autophagic
504 events (by TEM quantification and fluorescence microscopy) (**Figure 4B**), an indication
505 of clearance impairment and of aggregates/inclusions accumulation, with age,
506 demonstrate that cardiac aging, *per se*, negatively impacts on PQC.

507 Although the present results clearly point to less efficient autophagy due to aging, *per*
508 *se*, several pieces of evidence suggest that some PQC mechanisms fail more severely
509 than others in a context of chronic exposure (up to 21 to months) to marked cardiac
510 cAMP-induced stress, and that autophagy is more severely compromised in TG^{AC8} than
511 in WT. Firstly, $LAMP1^{+}$-puncta *increased* in number whereas $LC3^{+}$-puncta *decreased*, in
512 old TG^{AC8}, vs old WT (**Figure 4Cii, 4Cv**); and, both $LAMP1^{+}$- and $LC3^{+}$-puncta covered a
513 smaller % of cell area in old TG^{AC8}, vs old WT (**Figure 4Civ, 4Cvii**). Secondly, a reduction
514 (by WB) of the nuclear to cytoplasm ratio of the master regulator protein of the CLEAR
515 network, TFEB, in old TG^{AC8} vs old WT (**Figure 5C**), together with the transcriptional
516 upregulation of several 14-3-3s isoforms in aged TG^{AC8} vs young TG^{AC8}, and vs old

517 WT(**Figure 5D**), demonstrate that the autophagic program is more severely suppressed
518 in the aged TG^{AC8} than that due to "normal" aging in WT, and that lysosomal clearance
519 more significantly impaired, manifested as the increased accumulation of insoluble $LC3^{+}$-
520 inclusions. Indeed, the fact that endogenous $LAMP1^{+}$- and $LC3^{+}$-puncta covered a
521 smaller % of cell area in TG^{AC8} vs WT of advanced age, and were highly heterogeneous
522 in size (**Figure 4D**), portrays a scenario compatible with the presence of increased
523 "aggresomes"[45,75] (the "aggregate of aggregates" encaged by intermediate filament
524 proteins[60]) resulting from a buildup of numerous small pre-aggresomal bodies which are,
525 at younger age, compartmentalized as a cytoprotective mechanism[87,88].

526 LC3A was transcriptionally *upregulated*[14] and its carrier-flux *accelerated* in old TG^{AC8},
527 vs WT (**Figure 5Ai**); however, *overall* autophagic flux was reduced more in TG^{AC8} than in
528 WT, as demonstrated by the reduced levels of p62 (**Figure 5Aiii**), ATG16L1, ATG4B and
529 ALIX (**Figure 5Bi-iii**), following CQ treatment. Inhibition of proteasome activity has been
530 linked to activation of LC3A specifically, as a general stress response[75], without
531 involvement of LC3B; additionally, LC3A silencing (by promoter methylation), primes cells
532 for aggresome formation to achieve cellular homeostasis, in conditions of altered
533 autophagy, such as in cancer cells[89]. Thus, we correlate *increased* LC3A levels and the
534 *accelerated LC3A-flux* to the presence of increased protein aggregates in aged TG^{AC8} vs
535 old WT. Indeed, accelerated flux has been shown to be a compensation mechanism that
536 can be maladaptive in disease conditions that contribute to the remodeling of the
537 myocardium under stress[90]. Thus, increased LC3A-flux in aged TG^{AC8} vs WT is another
538 index of an indication of initiated signaling of oxidized lipoprotein accumulation within the
539 context of chronic upregulation of the AC/cAMP/PKA/Ca^{2+} axis in old TG^{AC8}.

540 Damaged and/or dysfunctional mitochondria[8,49] are unable to support high energy
541 demands, and overall mitochondrial fitness declines, with deterioration of heart function
542 leading to disease conditions. Significant alterations in mitochondrial morphology,
543 reflected by mitochondrial dysfunction and increased ROS production, in response to
544 LC3A-induced autophagy, via the PERK-eIF2a-ATF4 axis of the UPR pathway, have
545 been shown to result in altered mitochondrial dynamics and stress induced senescence[75].
546 LC3A activation was greater, and its flux accelerated. In aged TG^{AC8}, it was accompanied
547 by mitochondrial dysfunction, also increased, vs WT, suggesting that greater
548 mitochondrial dysfunction may contribute to increased LC3A expression in old TG^{AC8} LVs.
549 The higher cellular stress-response and the need of a "*specialized autophagy*" to maintain
550 cellular/mitochondrial homeostasis, further emphasizes the intricate interplay between
551 autophagy and mitochondrial dynamics[75].

552 Although in aged TG^{AC8}, both L-OPA1 and S-OPA1 protein levels were significantly
553 decreased vs WT (by WB) (**Figure 7Ci-ii**), the ratio of S-OPA1 to L-OPA1 was
554 significantly increased (**Figure 7Ciii**). In contrast, protein levels of HSP60 (WB) were
555 reduced, in TG^{AC8} vs WT (**Figure 7D**). These results point to a reduction in mitochondrial
556 fusion in aged TG^{AC8} vs WT: excessive stress-induced processing of OPA1 by OMA1[60]
557 triggers mitochondrial fragmentation, accelerating mitochondrial fission[69]. Because
558 myocardial function depends on balanced mitochondrial fusion and fission[91], we conclude
559 that although mitophagy signaling was upregulated through a variety of pathways[53]
560 (**Figure 7E**), such altered mitochondrial dynamics and reduced protection by HSP60
561 contribute to mitochondrial dysfunction and failing of mitophagy to a greater extent, in

562 aged TG^{AC8} vs WT, resulting in poor mitochondrial fitness/function, and is further
563 aggravated by insufficient lysosomal activity.

564 Accumulation of $LC3^{+}$-bodies (**Figure 4C**) and $p62^{+}$-inclusions (**Figure 8H**), like LF
565 aggregates (**Figure 8A-B**) in late stages of autophagy that cannot be removed from the
566 cytosol by the UPS[92] because they are covalently cross-linked aggregates, is an
567 indication of a greater lysosomal impairment[93] in aged TG^{AC8} vs WT. In addition, the
568 black-to blueish pigment aggregates (**Figure 8C**), and $LC3^{+}$-cardiac cells (**Figure 8D-E**),
569 in older TG^{AC8}, but not in age-matched WT, suggests changes in cargo processing, and
570 accumulation of different material in TG^{AC8} LV vs WT. Because aggregates/inclusions are
571 a manifestation of "normal" aging, we interpret more marked changes in TG^{AC8} than in
572 WT to be an induction of accelerated aging in TG^{AC8}.

573 **Proteasome**

574 Although proteasome activity did not differ between genotypes at 18 months, between
575 3-4 months and 18 months, proteasome function progressively declined in TG^{AC8} but not
576 in WT (**Figure 6A**). In addition to failure at the lysosome, variations in UPS activity and
577 expression, reflecting age-associated metabolic, functional, or simply structural changes,
578 occur in response to the different demands for the turnover of signaling and structural
579 proteins. Specifically, cardiac proteasomal insufficiency has been linked to accumulation
580 of "aggresomes", leading to partial disorganization of protein filaments[60,61], that are
581 displaced from their normal cellular distribution[45]. In line with these results, accumulation
582 of insoluble misfolded proteins was increased in aged TG^{AC8} vs WT, whereas soluble
583 aggregates (soluble proteins undergoing normal turnover and misfolded proteins *en route*
584 to degradation by the UPS), became significantly reduced in *both* genotypes at 18 months

585 (**Figure 6B**). We interpret this result to indicate that protein insolubility increases with age,
586 *per se*, and that, with aging, misfolded proteins are more "aggregate-prone"[45]. Thus, the
587 presence of high molecular weight oligomers[45] in TG^{AC8}, more stable than the
588 intermediate conformers from which they are derived, clearly demonstrate that the
589 proteasome of the old TG^{AC8} heart is "out-won" in the competition for misfolded substrates
590 prior to their aggregation[94].

591 Although protein translation rates at older ages did not differ between genotypes,
592 protein synthesis decreased significantly more with aging in TG^{AC8} heart (**Figure 6D**) in
593 accordance with a "normal" aging process[48,95]. We interpret this reduction to indicate that,
594 exactly as in the age-matched WT, the old TG^{AC8} heart reduces energy use and load on
595 the protein quality control machinery, by directing proteases and chaperons activity
596 (**Figure 6C**) towards repair of existing proteins rather than the folding of new ones[48,95,96].
597 Thus, the old TG^{AC8} heart utilizes a mechanism that preserves and increases life span as
598 in healthy aging[96], to optimize energy use by reducing the formation of *de-novo* proteins,
599 in order to focus on repairing the existing proteome.

600 Disorganization of desmin filaments that interlink the contractile myofibrillar apparatus
601 with mitochondria, nuclei and the sarcolemma, has been shown to affect mitochondrial
602 positioning, therefore compromising mitochondrial function, and leading to cardiomyocyte
603 dysfunction[67,97]. Negative modulation of desmin's physical properties and assembly by its
604 PTMs leads to the build-up of cardiac preamyloid oligomers (PAOs) and has been
605 recently indicated to be an index of premature and acquired heart failure[4,6]. Desmin
606 tagging for ubiquitination and cleavage, and desmin PAOs accumulation (assessed by

607 protein fractionation and WB) was also highly increased in old vs WT TG^{AC8} hearts
608 (**Figures 8F-G**).

609 The number of cardiomyocytes expressing $HSP27^{S86}$ (assessed by fluorescence
610 microscopy) was also elevated in aged TG^{AC8} vs WT, and this increased expression was
611 co-localized with $p62^{+}$-inclusions (**Figures 8H**). $HSP27^{S86}$ co-localizes with contractile
612 proteins (cardiac troponin T) at sarcomeres[71,98] and it is upregulated in stress conditions
613 (including cardiac injury[99]) where it enhances heart tolerance to stress[100] while
614 maintaining myocardial function[71,98]. Co-localization of $HSP27^{S86}$ with $p62^{+}$-inclusions in
615 the aged TG^{AC8} suggests increased heart damage. Indeed, myocardial function and
616 cardiac structure progressively declined from 6 months to 21 months of age, leading to a
617 failing hypertrophic and dilated heart at 19 months of age (**Figures 9A-C**).

618 In conclusion, in response to chronic cardiac AC-dependent cAMP-stress that
619 activates protective concentric signaling circuitry, including autophagy/autophagic flux
620 and proteasome activity, and maintains PQC that preserve heart health early in life[14], with
621 age, <u>proteasomal insufficiency</u> and <u>compromised PQC</u>, in a context of a <u>dysregulated</u>
622 <u>autophagy flux</u> in the older TG^{AC8}, indicates the overall presence of maladaptive
623 responses with <u>ineffective cargo clearance</u> and <u>mitochondrial dysfunction</u>. This scenario
624 leads to severe loss of proteostasis in the old TG^{AC8} heart vs WT, contributing to increased
625 cardiac damage, accelerated cardiac aging (cardiomyopathy[15], desminopathy[90]) and
626 reduced cardiac health-span.

627 # METHODS

628 **Experimental animals**

629 All studies were performed in accordance with the Guide for the Care and Use of
630 Laboratory Animals published by the National Institutes of Health (NIH Publication no. 85-
631 23, revised 1996). All experimental protocols were approved by the Animal Care and Use
632 Committee of the National Institutes of Health (protocol #441-LCS-2025). Breeder pairs
633 of mice in which human TG^{AC8} was over-expressed under the murine α-myosin heavy
634 chain (α-MHC) promoter (TG^{AC8}), and wild-type littermates (WT) (background strain
635 C57BL/6 from Jackson Labs, Stock # 000664), were a gift from Nicole Defer/Jacques
636 Hanoune, Unite de Recherches, INSERM U- 99, Hôpital Henri Mondor, F-94010 Créteil,
637 France[15]. $HAC8^{+}$ mice were crossed with C57Bl6 mice, and housed in a climate-
638 controlled room with 12-hour light cycle and free access to food and water, as previously
639 described[72]. All assays were performed in 3-4-month-old (young) and 17-21-month-old
640 (old) males and compared to age-matched wild-type littermates (WT). Mice were
641 sacrificed using Ketamine/Xylazine mixture, by intraperitoneal (IP) administration, in
642 accordance with the approved protocol (#441-LCS-2025).

643 **Heart and cardiac tissue isolation**

644 The heart was quickly removed and placed into cold PBS solution. The left ventricle
645 (LV) free wall, without the septum, was identified anatomically under a dissecting
646 microscope, excised, snap-frozen in liquid nitrogen and stored at -80°C for further
647 analyses.

648 **Protein extraction and WB**

649 Flash frozen tissue was homogenized as previously described[14]. Briefly, snap-frozen
650 LVs were homogenized and lysed in ice cold RIPA buffer (Thermo Fisher Scientific: 25
651 mM Tris-HCl (pH 7.6), 150 mM NaCl, 1% NP-40, 1% sodium deoxycholate, 0.1% SDS)
652 supplemented with a Halt protease inhibitor cocktail (Thermo Fisher Scientific), Halt
653 phosphatase inhibitor cocktail (Thermo Fisher Scientific) and 1 mM phenylmethyl sulfonyl
654 fluoride, using a Precellys homogenizer (Bertin Instruments) with a tissue homogenization
655 kit CKMix (Bertin Instruments) at 4°C. Lysates were then centrifuged at 10,000g for 10
656 min at 4°C to separate insoluble material. Nuclear and cytosolic lysates were prepared
657 from snap-frozen LV using a subcellular protein fractionation kit for tissues (Thermo
658 Fisher Scientific) as per the manufacturer's instructions. The protein concentration of
659 samples was determined using the Bicinchoninic Acid (BCA) Assay (Thermo Fisher
660 Scientific). Samples were denatured in 4X Laemmli sample buffer (BioRad Laboratories)
661 containing 355 mM 2-mercaptoethanol at 95°C for 5 min, or DTT at 70°C for 10 min, and
662 proteins (25µg/lane) were resolved on 4-20% Criterion TGX Stain Free gels (Bio-Rad
663 Laboratories) by SDS/PAGE. For detection of HSP60, samples were denatured in XT
664 sample buffer containing 1X XT reducing reagent (BioRad Laboratories) at 95°C for 5
665 min, and 25µg protein resolved on a 12% Criterion™ XT Bis-Tris gel using XT MES
666 running buffer (BioRad Laboratories). For Stain-Free™ gels, to induce crosslinking of
667 trihalo compound with protein tryptophan residues, gels were exposed to UV
668 transillumination for 2-3 mins. Proteins were then transferred to low fluorescence
669 polyvinylidene difluoride (LF-PVDF) membranes (BioRad Laboratories), using an
670 electrophoretic transfer cell (Mini Trans-Blot, Bio-Rad). Membrane total protein was

671 visualized using an Amersham Imager 600 (AI600) (GE Healthcare Life Sciences) with
672 UV transillumination to induce and capture a fluorescence signal. Membranes were
673 blocked with either 5% milk/tris-buffered saline with Tween-20 (TBST) or EveryBlot
674 Blocking Buffer (BioRad Laboratories) as appropriate, and were then incubated with the
675 primary antibodies indicated in the **Supplemental Information Table 1** Primary
676 antibodies were then detected using horseradish peroxidase (HRP) conjugated antibody
677 (Invitrogen) at 1:10,000, and bands were visualized using Pierce SuperSignal West Pico
678 Plus ECL substrate kits (Thermo Scientific), the signal captured using an Amersham
679 Imager 600 (AI600) (GE Healthcare Life Sciences). Total protein for HSP60 blot was
680 visualized by staining membrane with 1X Amido Black solution (Millipore Sigma)
681 according to manufacturer's protocol. Band density was quantified using ImageQuant TL
682 software (GE Healthcare Life Sciences), normalized to total protein, and TG^{AC8} to average
683 of WT.

684 **Immunostaining (IHC)**

685 Endogenous macroautophagic puncta in young and aged TG^{AC8} and aged-matched
686 WT were determined in 5 μm thick paraffin sagittal sections of cardiac tissue. Following
687 standard procedures, deparaffinization and rehydration were followed by heat antigen
688 retrieval in a citric acid base solution (H-3300, VectorLabs). Autofluorescence was
689 quenched with a 10 min incubation with 1mg/ml Sodium Borohydride solution in PBS.
690 Cardiac sections were blocked in 10% goat serum for 30 min, and incubated at 4°C
691 overnight with the following primary antibodies: rabbit monoclonal LC3A/B (1:50,
692 cloneD3U4C, #12741 Cell Signaling), mouse monoclonal p62 (1:50, clone 2C11,
693 #ab56416; Abcam), rat monoclonal LAMP-1 (1:100, clone 1D4B, #1D4B; DSHB), rabbit

694 monoclonal p(S82)-HSP27 (1:100, clone D1H2F6, #9709; Cell Signaling), and Wheat
695 Germ Agglutinin (WGA) (1:100, #W21404; ThermoFisher Scientific). After incubation with
696 corresponding conjugated secondaries and counterstaining with 500 nM 4′,6-diamidino-
697 2-phenylindole (DAPI) for about 1 hr at RT, immunolabeled samples were mounted using
698 an antifade gel mounting medium (Vectashield Vibrance; Vectorlabs) and examined with
699 a Zeiss LSM 900 confocal microscope. At least 10 random fields of optical regions (100
700 μm2) of 5 μm thickness per cardiac section (n=3) were collected with a Plan-Apochromat
701 63x/1.40Oil DIC M27 objective and projected on a single extended projection image to
702 analyze. Puncta counting and areas of vesicles were measured using manual tracking
703 with ImageJ software by a blinded investigator.

704 **Transmission Electron Microscopy (TEM)**

705 Samples for transmission electron microscopy were fixed using 2.5% glutaraldehyde
706 in 0.1 M sodium cacodylate buffer, pH 7. Then, they were post-fixed in 1% osmium
707 tetroxide for 1 hr at 4°C in the same buffer, dehydrated, and then embedded in Embed
708 812 resin (Electron Microscopy Sciences, Hatfield, PA) through a series of resin resin-
709 propylene oxide gradients to pure resin. Blocks were formed in fresh resin contained in
710 silicon molds, and the resin was polymerized for 24-48 hrs at 65°C; blocks were then
711 trimmed and sectioned in an EM UC7 ultramicrotome (Leica Microsystems, Buffalo
712 Grove, IL) to obtain both semi-thick (0.5-1 μm width) and ultrathin (40-60 nm width)
713 sections. Semi-thick sections were mounted on glass slides and stained with 1% toluidine
714 blue in a 1% borax aqueous solution for 2 min. Palade-stained (OsO4) and Toluidine blue-
715 stained semi-thick sections were then imaged using a Leica AXIO Imager light
716 microscope with a 63x oil immersion objective, for quality control and Lipofuscin (LF)

717 quantification. Ultrathin sections were stained with uranyl acetate and lead citrate and
718 then imaged on a Talos L120C Transmission Electron Microscope (TEM) with a 4K Ceta
719 CMOS camera, for macroautophagic events quantification. Micrographs at ×2000 ×5000
720 and ×11000 magnification were obtained from randomly selected cytoplasmic areas of
721 cardiomyocytes, for illustration purposes and quantitative analysis of macroautophagic
722 events population. Two stereological parameters were determined: (a) the numerical
723 profile density Na (number of figures of interest / μm^2 of cell fraction), and (b) volume
724 density of figures of interest (Vv; i.e., the volume fraction of cardiomyocyte cytoplasm
725 occupied by figures of interest). Volume density was obtained following a point analysis
726 using a simple square lattice test system[101], with superposition of a virtual grid over the
727 micrographs where the user performs a point-counting method. Autophagosomes (also
728 referred in the text as early events) were identified as double-membrane vesicles with
729 identifiable cargo and comparable density to the surrounding cytosol. Autolysosomes
730 (late events) and residual bodies were denoted as single membrane vesicles containing
731 non-identifiable cargo of higher density than the surrounded cytosol and fragmented
732 organelles. Lipofuscin bodies were identified following Palade staining[102] by the presence
733 of densely packed lipids with a dark brown-black color against cardiomyocyte cytosol,
734 which allowed a straightforward segmentation of the image and posterior quantification
735 of the planimetric and stereological parameters. Point counting and areas of vesicles and
736 cytosol were measured using manual tracking with ImageJ software by a blinded
737 investigator.

738 **RT-qPCR**

739 RT-qPCR of LV tissue was performed to determine the transcript abundance of 14-3-
740 3 subunits. RNA was extracted from left ventricular myocytes (VM) with RNeasy Mini Kit
741 (Qiagen, Valencia, CA) and DNAse on column digestion. 1 µg of total RNA was used for
742 cDNA synthesis with MMLV reverse transcriptase (Promega). RT-qPCR was performed
743 using a QuantStudio 6 Flex Real-Time PCR System (Thermo Fisher Scientific) with a
744 384-well platform. The reaction was performed with a FastStart Universal SYBR Green
745 Master Kit with Rox (Roche) using the manufacturer's recommended conditions; the sizes
746 of amplicons were verified. Each well contained 0.5 µl of cDNA solution and 10 µl of
747 reaction mixture. Each sample was quadruplicated and repeated twice using de novo
748 synthesized cDNA sets. Preliminary reactions were performed to determine the efficiency
749 of amplification. RT-qPCR analysis was performed using the ddCt method. Primers were
750 selected with Primer Express 3.0 software (Applied Biosystems). The primers sequence
751 is indicated in the **Supplemental Information Table 2**.

752 **Cathepsin L1 activity assay**

753 Cathepsin L1 activity was measured using the fluorimetric kit (Abcam, ab65306)
754 according to the manufacturer's instructions. Briefly, snap-frozen LVs stored at -80°C
755 were thawed on ice, and 10 mg of tissue was resuspended in 50 µl of CL Buffer, then
756 homogenized with a Dounce homogenizer sitting on ice, with 10–15 passes. Samples
757 were centrifuged for 2–5 mins at 4°C at top speed using a cold microcentrifuge to remove
758 any insoluble material, then supernatants were collected and transferred to a clean tube,
759 on ice. Activity was performed at different dilutions to reach Vmax, in the presence of Ac-
760 FR-AFC fluorogenic substrate (200 µM final concentration), at 37°C for 1–2 hours, at an

761 excitation wavelength of 400 nm and an emission wavelength of 505 nm using the
762 Cytation 5 microplate reader (Biotek). Fold-increase in Cathepsin L activity was
763 determined by comparing the relative fluorescence units (RFU) with the level of the
764 uninduced control, after subtraction of the negative control sample. TG^{AC8} values were
765 normalized to average of WT.

766 **Proteasome activity assay**

767 Proteasome activity was measured with Proteasome-Glo™ Chymotrypsin-Like
768 Assay G8621, accordingly to the manufacturer's instructions. Briefly, lysed tissue was
769 diluted with the provided buffer and 50 µg of the sample was loaded on a 96 well
770 microplate. The resulting "glow-type" luminescent signal was then quantified utilizing the
771 Spectramax microplate reader (San Jose), with luminescence recorded at 500. Human
772 20S Proteosome was used as a positive control.

773 **Protein aggregation assay**

774 The isolation of protein aggregates and the assessment of protein aggregation was
775 conducted using the Proteostat kit (Enzo Life Science, ENZ-51023), as previously
776 published[14]. Specifically, 50 µg of proteins were loaded into a 96-well plate for analysis.
777 Fluorescence measurements were obtained with an excitation wavelength of 550 nm and
778 emission wavelength of 600 nm, employing a time interval of 15 minutes between
779 readings, and background readings were subtracted from sample recordings.

780 **Protein synthesis assessment**

781 Protein synthesis was assessed by SUnSET-Western Blot as previously
782 described[14,103]. Briefly, the puromycin solution was prepared in PBS, sterilized by
783 filtration, and a volume of 200 µl was injected in TG^{AC8} mice and age-matched WT

784 controls intraperitoneally, to achieve a final concentration of 0.04 μmol/g of body mass.
785 After 30 min, mice were sacrificed, the LV was harvested and snap frozen in liquid
786 nitrogen. Protein extraction was performed using Precellys, quantified with BCA assay 25
787 μg of total protein were separated by SDS-PAGE; proteins were then transferred onto
788 PVDF membrane and incubated overnight in the anti-puromycin primary antibody
789 (MABE343, Sigma-Aldrich, St. Louis, MO). Visualization of puromycin-labeled bands was
790 obtained using horseradish peroxidase conjugated anti-mouse IgG Fc 2 a secondary
791 antibody (Jackson ImmunoResearch Laboratories Inc, West Grove, PA, USA), using
792 Pierce Super Signal ECL substrate kit (Pierce/ Thermo Scientific Rockford, IL).
793 Chemiluminescence was captured with the Imager AI600 and densitometry analysis was
794 performed using ImageQuantTL software (both by GE, Boston, MA). Total protein was
795 used as control for protein loading. Genotypic differences of protein synthesis were tested
796 via an as unpaired t-test.

797 **Quantification of desmin preamyloid oligomers (PAOs)**

798 Proteins were extracted according to the method described in *Li Z et al*
799 (https://doi.org/10.1101/2023.05.09.540017). Myofilament-enriched, insoluble fractions
800 were prepared as described previously[6]. Fractions were separated using precast
801 NuPAGE gels (Thermo Fisher Scientific) with MES buffer, and probed with the desmin
802 antibody (DE-U-10, Sigma, 1:10,000) or the A11 antibody (kindly provided by Dr. Charles
803 Glabe at UC Irvine[104], 1:1,500). TG^{AC8} values were normalized to WT.

804 **Echocardiography**

805 Mice underwent echocardiographic (Echo) examination (40- MHz transducer; Visual
806 Sonics 3100; Fuji Film Inc, Seattle, WA) under light anesthesia with isoflurane (2% in

807 oxygen) via nose cone; temperature was maintained at 37°C using a heating pad. Mice
808 were placed in the supine position; skin hair in the chest area was shaved. Standard
809 electrocardiogram (ECG) electrodes were placed on the limbs and ECG Lead II was
810 recorded simultaneously with acquisition of echo images. Each Echo examination was
811 completed within 10 min. Parasternal long-axis views of the LV were obtained and
812 recorded to ensure that mitral and aortic valves and the LV apex were visualized. From
813 the parasternal long-axis view of the LV, M-mode tracings of LV were obtained at mid-
814 papillary muscle level. Parasternal short-axis views of the LV were recorded at the mid-
815 papillary muscle level. Endocardial area tracings, using the leading-edge method, were
816 performed in the 2D mode (short-axis and long-axis views) from digital images captured
817 on a cine loop to calculate the end-diastolic and end-systolic LV areas. LV End-Diastolic
818 Volume (EDV) and End-Systolic Volume (ESV) were calculated by a Hemisphere
819 Cylinder Model method. Ejection Fraction (EF) was derived as EF = 100*(EDV -
820 ESV)/EDV. LV mass (LVM) was calculated from EDV, septal thickness (IVS) and LV
821 Posterior Wall (PW). All measurements were made by a single observer who was blinded
822 to the identity of the tracings. All measurements were reported an average of five
823 consecutive cardiac cycles covering at least one respiration cycle (100 times/min in
824 average). The reproducibility of measurements was assessed by repeated measurement
825 a week apart in randomly selected images; the repeated measure variability was less
826 than 5%.

827 **Sample extraction and proteoOMICs analysis**

828 LV proteome analysis was done accordingly to our previous work[14]. Briefly, four LV
829 samples from WT and TG^{AC8} mouse hearts were snap frozen in liquid nitrogen and stored

830 at -80°C. On average, 2 mg of muscle tissue from each sample was pulverized in liquid
831 nitrogen and mixed with a lysis buffer containing (4% SDS, 1% Triton X-114, 50 mM Tris,
832 150 mM NaCl, protease inhibitor cocktail (Sigma)), pH 7.6. Samples were sonicated on
833 ice using a tip sonicator for 1 min with 3s pulses and 15s rest periods at 40% power.
834 Lysates were centrifuged at +4°C for 15 min at 14,000 rpm, aliquoted and stored at -80°C
835 until further processing. Protein concentration was determined using the commercially
836 available 2-D quant kit (GE Healthcare Life Sciences). Sample quality was confirmed
837 using NuPAGE protein gels stained with fluorescent SyproRuby protein stain
838 (ThermoFisher). In order to remove detergents and lipids, 500 µg of muscle tissue lysate
839 was precipitated using a methanol/chloroform extraction protocol
840 (sample:methanol:chloroform:water 1:4:1:3) (Wessel and Flugge[105]). Proteins were
841 resuspended in 50 µl of concentrated urea buffer (8 M Urea, 150 mM NaCl [Sigma]),
842 reduced with 50 mM DTT for 1 hour at 36°C and alkylated with 100 mM iodoacetamide
843 for 1 hr at 36°C in the dark. The concentrated urea/protein mixture was diluted 12 times
844 with 50 mM ammonium bicarbonate buffer, and proteins were digested for 18 hr at 36°C,
845 using trypsin/LysC mixture (Promega) in 1:50 (w/w) enzyme to protein ratio. Protein
846 digests were desalted on 10x4.0 mm C18 cartridge (Restek, cat# 917450210) using
847 Agilent 1260 Bio-inert HPLC system with a fraction collector. Purified peptides were
848 speed vacuum dried and stored at -80°C until further processing. A subset of 8 muscle
849 samples (100 µg) each corresponding to 4 controls and 4 TG^{AC8} LVs and one averaged
850 reference sample were labeled with 10-plex tandem mass spectrometry tags (TMT) using
851 standard TMT labeling protocol (Thermo Fisher). 200 femtomole (fM) of bacterial beta-
852 galactosidase digest (SCIEX) was spiked into each sample prior to TMT labeling to

853 control for labeling efficiency and overall instrument performance. Labeled peptides from
854 10 different TMT channels were combined into one experiment and fractionated.

855 **Statistics**

856 Data are presented as median ±range or median ±interquartile range, except for the
857 echocardiography, expressed as mean along with all the data points. Representative
858 TEM and IHC images, and western blots were chosen based on the resemblance to the
859 average values. The number of samples per group are indicated in each legend.
860 Statistical analyses were performed in GraphPad Prism 10 and with R. ROUT analyses
861 were applied to identify outliers, which were excluded from group comparison analyses.
862 Student *t* test with Welch's correction was used to compare data between 2 groups. Two-
863 way ANOVA followed by Original FDR method of Benjamini and Hochberg was used for
864 multiple comparisons[106]. For datasets with matching LC3I and LC3II from the same
865 animal, a repeated-measures approach with three-way mixed ANOVA or mixed-effect
866 analysis for repeated-measures was taken, followed by Original FDR method of
867 Benjamini and Hochberg. Statistical significance was assumed at $p<0.05$.

868 # ACKNOWLEDGMENTS

869 The study was designed by M.G.P. and E.G.L. The experiments were conducted by
870 M.G.P., M.C.B., D.R.R., G.A., A.P., I.A., K.C., Y.S.T, and H.K.. The data were analyzed
871 by M.G.P., M.C.B., D.R.R, G.A., C.H.M., I.A., K.V.T, and J.Q. The article was written by
872 M.G.P., M.C.B. and E.G.L., and approved by all authors.

Total Word count without References ~12500

SOURCES OF FUNDING

This research was supported in part by the Intramural Research Program of the NIH, National Institute on Aging (USA), and in part by the Leducq Foundation (TNE ID#673168 to GA).

DISCLOSURES

None.

REFERENCES

1 Taylor, R. C. & Dillin, A. Aging as an event of proteostasis collapse. *Cold Spring Harb Perspect Biol* **3** (2011). https://doi.org:10.1101/cshperspect.a004440

2 Willis, M. S. & Patterson, C. Proteotoxicity and cardiac dysfunction--Alzheimer's disease of the heart? *N Engl J Med* **368**, 455-464 (2013). https://doi.org:10.1056/NEJMra1106180

3 Kholova, I. & Niessen, H. W. Amyloid in the cardiovascular system: a review. *J Clin Pathol* **58**, 125-133 (2005). https://doi.org:10.1136/jcp.2004.017293

4 Agnetti, G. *et al.* Desmin modifications associate with amyloid-like oligomers deposition in heart failure. *Cardiovasc Res* **102**, 24-34 (2014). https://doi.org:10.1093/cvr/cvu003

5 Sanbe, A. *et al.* Desmin-related cardiomyopathy in transgenic mice: a cardiac amyloidosis. *Proc Natl Acad Sci U S A* **101**, 10132-10136 (2004). https://doi.org:10.1073/pnas.0401900101

6 Rainer, P. P. *et al.* Desmin Phosphorylation Triggers Preamyloid Oligomers Formation and Myocyte Dysfunction in Acquired Heart Failure. *Circ Res* **122**, e75-e83 (2018). https://doi.org:10.1161/CIRCRESAHA.117.312082

7 Day, S. M. The ubiquitin proteasome system in human cardiomyopathies and heart failure. *Am J Physiol Heart Circ Physiol* **304**, H1283-1293 (2013). https://doi.org:10.1152/ajpheart.00249.2012

8 Linton, P. J., Gurney, M., Sengstock, D., Mentzer, R. M., Jr. & Gottlieb, R. A. This old heart: Cardiac aging and autophagy. *J Mol Cell Cardiol* **83**, 44-54 (2015). https://doi.org:10.1016/j.yjmcc.2014.12.017

9 Wilhelm, T. & Richly, H. Autophagy during ageing - from Dr Jekyll to Mr Hyde. *FEBS J* **285**, 2367-2376 (2018). https://doi.org:10.1111/febs.14453

10 Marzabadi, M. R., Sohal, R. S. & Brunk, U. T. Mechanisms of lipofuscinogenesis: effect of the inhibition of lysosomal proteinases and lipases under varying concentrations of ambient oxygen in cultured rat neonatal myocardial cells. *APMIS* **99**, 416-426 (1991). https://doi.org:10.1111/j.1699-0463.1991.tb05170.x

11 Lopez-Otin, C., Blasco, M. A., Partridge, L., Serrano, M. & Kroemer, G. Hallmarks of aging: An expanding universe. *Cell* **186**, 243-278 (2023). https://doi.org:10.1016/j.cell.2022.11.001

12 Munnell, J. F. & Getty, R. Rate of accumulation of cardiac lipofuscin in the aging canine. *J Gerontol* **23**, 154-158 (1968). https://doi.org:10.1093/geronj/23.2.154

13 Nakano, M., Oenzil, F., Mizuno, T. & Gotoh, S. Age-related changes in the lipofuscin accumulation of brain and heart. *Gerontology* **41 Suppl 2**, 69-79 (1995). https://doi.org:10.1159/000213726

910 14 Tarasov, K. V. *et al.* A remarkable adaptive paradigm of heart performance and protection
911 emerges in response to marked cardiac-specific overexpression of ADCY8. *Elife* **11** (2022).
912 https://doi.org:10.7554/eLife.80949
913 15 Lipskaia, L. *et al.* Enhanced cardiac function in transgenic mice expressing a Ca(2+)-stimulated
914 adenylyl cyclase. *Circ Res* **86**, 795-801 (2000). https://doi.org:10.1161/01.res.86.7.795
915 16 Georget, M. *et al.* Augmentation of cardiac contractility with no change in L-type Ca2+ current in
916 transgenic mice with a cardiac-directed expression of the human adenylyl cyclase type 8 (AC8).
917 *FASEB J* **16**, 1636-1638 (2002). https://doi.org:10.1096/fj.02-0292fje
918 17 Mougenot, N. *et al.* Cardiac adenylyl cyclase overexpression precipitates and aggravates age-
919 related myocardial dysfunction. *Cardiovasc Res* **115**, 1778-1790 (2019).
920 https://doi.org:10.1093/cvr/cvy306
921 18 Liu, Y. *et al.* In Mice Subjected to Chronic Stress, Exogenous cBIN1 Preserves Calcium-Handling
922 Machinery and Cardiac Function. *JACC Basic Transl Sci* **5**, 561-578 (2020).
923 https://doi.org:10.1016/j.jacbts.2020.03.006
924 19 Koukourakis, M. I. *et al.* Autophagosome Proteins LC3A, LC3B and LC3C Have Distinct Subcellular
925 Distribution Kinetics and Expression in Cancer Cell Lines. *PLoS One* **10**, e0137675 (2015).
926 https://doi.org:10.1371/journal.pone.0137675
927 20 Baeken, M. W. *et al.* Novel Insights into the Cellular Localization and Regulation of the
928 Autophagosomal Proteins LC3A, LC3B and LC3C. *Cells* **9** (2020).
929 https://doi.org:10.3390/cells9102315
930 21 Cherra, S. J., 3rd *et al.* Regulation of the autophagy protein LC3 by phosphorylation. *J Cell Biol* **190**,
931 533-539 (2010). https://doi.org:10.1083/jcb.201002108
932 22 Wilkinson, D. S. *et al.* Phosphorylation of LC3 by the Hippo kinases STK3/STK4 is essential for
933 autophagy. *Mol Cell* **57**, 55-68 (2015). https://doi.org:10.1016/j.molcel.2014.11.019
934 23 Katsuragi, Y., Ichimura, Y. & Komatsu, M. p62/SQSTM1 functions as a signaling hub and an
935 autophagy adaptor. *FEBS J* **282**, 4672-4678 (2015). https://doi.org:10.1111/febs.13540
936 24 Lim, J. *et al.* Proteotoxic stress induces phosphorylation of p62/SQSTM1 by ULK1 to regulate
937 selective autophagic clearance of protein aggregates. *PLoS Genet* **11**, e1004987 (2015).
938 https://doi.org:10.1371/journal.pgen.1004987
939 25 Matsumoto, G., Wada, K., Okuno, M., Kurosawa, M. & Nukina, N. Serine 403 phosphorylation of
940 p62/SQSTM1 regulates selective autophagic clearance of ubiquitinated proteins. *Mol Cell* **44**, 279-
941 289 (2011). https://doi.org:10.1016/j.molcel.2011.07.039
942 26 Matsumoto, G., Shimogori, T., Hattori, N. & Nukina, N. TBK1 controls autophagosomal engulfment
943 of polyubiquitinated mitochondria through p62/SQSTM1 phosphorylation. *Hum Mol Genet* **24**,
944 4429-4442 (2015). https://doi.org:10.1093/hmg/ddv179
945 27 Jain, A. *et al.* p62/SQSTM1 is a target gene for transcription factor NRF2 and creates a positive
946 feedback loop by inducing antioxidant response element-driven gene transcription. *J Biol Chem*
947 **285**, 22576-22591 (2010). https://doi.org:10.1074/jbc.M110.118976
948 28 Ueno, T. & Takahashi, K. A cathepsin L-specific inhibitor preferentially inhibits degradation of
949 autophagosomal LC3 and GABARAP in HeLa and Huh-7 cells. *Autophagy* **5**, 878-879 (2009).
950 https://doi.org:10.4161/auto.9097
951 29 Ichimura, Y. *et al.* Phosphorylation of p62 activates the Keap1-Nrf2 pathway during selective
952 autophagy. *Mol Cell* **51**, 618-631 (2013). https://doi.org:10.1016/j.molcel.2013.08.003
953 30 Jiang, T. *et al.* p62 links autophagy and Nrf2 signaling. *Free Radic Biol Med* **88**, 199-204 (2015).
954 https://doi.org:10.1016/j.freeradbiomed.2015.06.014
955 31 Gammoh, N. The multifaceted functions of ATG16L1 in autophagy and related processes. *J Cell Sci*
956 **133** (2020). https://doi.org:10.1242/jcs.249227

32 Hamaoui, D. & Subtil, A. ATG16L1 functions in cell homeostasis beyond autophagy. *FEBS J* **289**, 1779-1800 (2022). https://doi.org:10.1111/febs.15833

33 Scherz-Shouval, R. *et al.* Reactive oxygen species are essential for autophagy and specifically regulate the activity of Atg4. *EMBO J* **26**, 1749-1760 (2007). https://doi.org:10.1038/sj.emboj.7601623

34 Petiot, A. *et al.* Alix differs from ESCRT proteins in the control of autophagy. *Biochem Biophys Res Commun* **375**, 63-68 (2008). https://doi.org:10.1016/j.bbrc.2008.07.136

35 Bhujabal, Z. *et al.* FKBP8 recruits LC3A to mediate Parkin-independent mitophagy. *EMBO Rep* **18**, 947-961 (2017). https://doi.org:10.15252/embr.201643147

36 Wang, S. *et al.* The mitophagy pathway and its implications in human diseases. *Signal Transduct Target Ther* **8**, 304 (2023). https://doi.org:10.1038/s41392-023-01503-7

37 Jin, M. & Klionsky, D. J. Regulation of autophagy: modulation of the size and number of autophagosomes. *FEBS Lett* **588**, 2457-2463 (2014). https://doi.org:10.1016/j.febslet.2014.06.015

38 Young, A. R. *et al.* Starvation and ULK1-dependent cycling of mammalian Atg9 between the TGN and endosomes. *J Cell Sci* **119**, 3888-3900 (2006). https://doi.org:10.1242/jcs.03172

39 Jia, S. *et al.* Mammalian Atg9 contributes to the post-Golgi transport of lysosomal hydrolases by interacting with adaptor protein-1. *FEBS Lett* **591**, 4027-4038 (2017). https://doi.org:10.1002/1873-3468.12916

40 Tatsuta, T., Scharwey, M. & Langer, T. Mitochondrial lipid trafficking. *Trends Cell Biol* **24**, 44-52 (2014). https://doi.org:10.1016/j.tcb.2013.07.011

41 Palmieri, M. *et al.* Characterization of the CLEAR network reveals an integrated control of cellular clearance pathways. *Hum Mol Genet* **20**, 3852-3866 (2011). https://doi.org:10.1093/hmg/ddr306

42 Martina, J. A., Chen, Y., Gucek, M. & Puertollano, R. MTORC1 functions as a transcriptional regulator of autophagy by preventing nuclear transport of TFEB. *Autophagy* **8**, 903-914 (2012). https://doi.org:10.4161/auto.19653

43 Kleppe, R., Martinez, A., Doskeland, S. O. & Haavik, J. The 14-3-3 proteins in regulation of cellular metabolism. *Semin Cell Dev Biol* **22**, 713-719 (2011). https://doi.org:10.1016/j.semcdb.2011.08.008

44 Kaplan, A., Ottmann, C. & Fournier, A. E. 14-3-3 adaptor protein-protein interactions as therapeutic targets for CNS diseases. *Pharmacol Res* **125**, 114-121 (2017). https://doi.org:10.1016/j.phrs.2017.09.007

45 Kopito, R. R. Aggresomes, inclusion bodies and protein aggregation. *Trends Cell Biol* **10**, 524-530 (2000). https://doi.org:10.1016/s0962-8924(00)01852-3

46 Backe, S. J., Heritz, J. A. & Mollapour, M. The HSP90 chaperone code regulates the crosstalk between proteostasis and autophagy. *Autophagy* **20**, 1689-1691 (2024). https://doi.org:10.1080/15548627.2024.2323259

47 Chiosis, G., Digwal, C. S., Trepel, J. B. & Neckers, L. Structural and functional complexity of HSP90 in cellular homeostasis and disease. *Nat Rev Mol Cell Biol* **24**, 797-815 (2023). https://doi.org:10.1038/s41580-023-00640-9

48 Anisimova, A. S. *et al.* Multifaceted deregulation of gene expression and protein synthesis with age. *Proc Natl Acad Sci U S A* **117**, 15581-15590 (2020). https://doi.org:10.1073/pnas.2001788117

49 Gottlieb, R. A. & Carreira, R. S. Autophagy in health and disease. 5. Mitophagy as a way of life. *Am J Physiol Cell Physiol* **299**, C203-210 (2010). https://doi.org:10.1152/ajpcell.00097.2010

50 Westermann, B. Molecular machinery of mitochondrial fusion and fission. *J Biol Chem* **283**, 13501-13505 (2008). https://doi.org:10.1074/jbc.R800011200

1003 51 Krishnan-Sivadoss, I. *et al.* Heat shock protein 60 and cardiovascular diseases: An intricate love-
1004 hate story. *Med Res Rev* **41**, 29-71 (2021). https://doi.org:10.1002/med.21723
1005 52 Lin, K. M. *et al.* Combined and individual mitochondrial HSP60 and HSP10 expression in cardiac
1006 myocytes protects mitochondrial function and prevents apoptotic cell deaths induced by
1007 simulated ischemia-reoxygenation. *Circulation* **103**, 1787-1792 (2001).
1008 https://doi.org:10.1161/01.cir.103.13.1787
1009 53 Moyzis, A. G., Sadoshima, J. & Gustafsson, A. B. Mending a broken heart: the role of mitophagy in
1010 cardioprotection. *Am J Physiol Heart Circ Physiol* **308**, H183-192 (2015).
1011 https://doi.org:10.1152/ajpheart.00708.2014
1012 54 Chu, C. T., Bayir, H. & Kagan, V. E. LC3 binds externalized cardiolipin on injured mitochondria to
1013 signal mitophagy in neurons: implications for Parkinson disease. *Autophagy* **10**, 376-378 (2014).
1014 https://doi.org:10.4161/auto.27191
1015 55 Hoppins, S., Lackner, L. & Nunnari, J. The machines that divide and fuse mitochondria. *Annu Rev*
1016 *Biochem* **76**, 751-780 (2007). https://doi.org:10.1146/annurev.biochem.76.071905.090048
1017 56 Smirnova, E., Griparic, L., Shurland, D. L. & van der Bliek, A. M. Dynamin-related protein Drp1 is
1018 required for mitochondrial division in mammalian cells. *Mol Biol Cell* **12**, 2245-2256 (2001).
1019 https://doi.org:10.1091/mbc.12.8.2245
1020 57 Griparic, L., van der Wel, N. N., Orozco, I. J., Peters, P. J. & van der Bliek, A. M. Loss of the
1021 intermembrane space protein Mgm1/OPA1 induces swelling and localized constrictions along the
1022 lengths of mitochondria. *J Biol Chem* **279**, 18792-18798 (2004).
1023 https://doi.org:10.1074/jbc.M400920200
1024 58 Frezza, C. *et al.* OPA1 controls apoptotic cristae remodeling independently from mitochondrial
1025 fusion. *Cell* **126**, 177-189 (2006). https://doi.org:10.1016/j.cell.2006.06.025
1026 59 Anand, R. *et al.* The i-AAA protease YME1L and OMA1 cleave OPA1 to balance mitochondrial
1027 fusion and fission. *J Cell Biol* **204**, 919-929 (2014). https://doi.org:10.1083/jcb.201308006
1028 60 Head, B., Griparic, L., Amiri, M., Gandre-Babbe, S. & van der Bliek, A. M. Inducible proteolytic
1029 inactivation of OPA1 mediated by the OMA1 protease in mammalian cells. *J Cell Biol* **187**, 959-966
1030 (2009). https://doi.org:10.1083/jcb.200906083
1031 61 Lee, H., Smith, S. B., Sheu, S. S. & Yoon, Y. The short variant of optic atrophy 1 (OPA1) improves
1032 cell survival under oxidative stress. *J Biol Chem* **295**, 6543-6560 (2020).
1033 https://doi.org:10.1074/jbc.RA119.010983
1034 62 Rodriguez, A., Von Salzen, D., Holguin, B. A. & Bernal, R. A. Complex Destabilization in the
1035 Mitochondrial Chaperonin Hsp60 Leads to Disease. *Front Mol Biosci* **7**, 159 (2020).
1036 https://doi.org:10.3389/fmolb.2020.00159
1037 63 Comert, C. *et al.* HSP60 chaperone deficiency disrupts the mitochondrial matrix proteome and
1038 dysregulates cholesterol synthesis. *Mol Metab* **88**, 102009 (2024).
1039 https://doi.org:10.1016/j.molmet.2024.102009
1040 64 Moyzis, A. & Gustafsson, A. B. Multiple recycling routes: Canonical vs. non-canonical mitophagy
1041 in the heart. *Biochim Biophys Acta Mol Basis Dis* **1865**, 797-809 (2019).
1042 https://doi.org:10.1016/j.bbadis.2018.09.034
1043 65 Narendra, D., Tanaka, A., Suen, D. F. & Youle, R. J. Parkin is recruited selectively to impaired
1044 mitochondria and promotes their autophagy. *J Cell Biol* **183**, 795-803 (2008).
1045 https://doi.org:10.1083/jcb.200809125
1046 66 Misaka, T. *et al.* FKBP8 protects the heart from hemodynamic stress by preventing the
1047 accumulation of misfolded proteins and endoplasmic reticulum-associated apoptosis in mice. *J*
1048 *Mol Cell Cardiol* **114**, 93-104 (2018). https://doi.org:10.1016/j.yjmcc.2017.11.004

1049 67 Alam, S. *et al.* Aberrant Mitochondrial Fission Is Maladaptive in Desmin Mutation-Induced Cardiac
1050 Proteotoxicity. *J Am Heart Assoc* **7** (2018). https://doi.org:10.1161/JAHA.118.009289
1051 68 Agnetti, G., Herrmann, H. & Cohen, S. New roles for desmin in the maintenance of muscle
1052 homeostasis. *FEBS J* **289**, 2755-2770 (2022). https://doi.org:10.1111/febs.15864
1053 69 Guay, J. *et al.* Regulation of actin filament dynamics by p38 map kinase-mediated phosphorylation
1054 of heat shock protein 27. *J Cell Sci* **110 (Pt 3)**, 357-368 (1997).
1055 https://doi.org:10.1242/jcs.110.3.357
1056 70 Dohke, T. *et al.* Proteomic analysis reveals significant alternations of cardiac small heat shock
1057 protein expression in congestive heart failure. *J Card Fail* **12**, 77-84 (2006).
1058 https://doi.org:10.1016/j.cardfail.2005.07.006
1059 71 Brundel, B. J. *et al.* Heat shock protein upregulation protects against pacing-induced myolysis in
1060 HL-1 atrial myocytes and in human atrial fibrillation. *J Mol Cell Cardiol* **41**, 555-562 (2006).
1061 https://doi.org:10.1016/j.yjmcc.2006.06.068
1062 72 Moen, J. M. *et al.* Overexpression of a Neuronal Type Adenylyl Cyclase (Type 8) in Sinoatrial Node
1063 Markedly Impacts Heart Rate and Rhythm. *Front Neurosci* **13**, 615 (2019).
1064 https://doi.org:10.3389/fnins.2019.00615
1065 73 Zhang, X. *et al.* Cardiotoxic and cardioprotective features of chronic beta-adrenergic signaling. *Circ*
1066 *Res* **112**, 498-509 (2013). https://doi.org:10.1161/CIRCRESAHA.112.273896
1067 74 Kwon, D. H. *et al.* A novel conformation of the LC3-interacting region motif revealed by the
1068 structure of a complex between LC3B and RavZ. *Biochem Biophys Res Commun* **490**, 1093-1099
1069 (2017). https://doi.org:10.1016/j.bbrc.2017.06.173
1070 75 Amer, N. *et al.* LC3A-mediated autophagy elicits PERK-eIF2alpha-ATF4 axis activation and
1071 mitochondrial dysfunction: Exposing vulnerability in aggresome-positive cancer cells. *J Biol Chem*
1072 **300**, 107398 (2024). https://doi.org:10.1016/j.jbc.2024.107398
1073 76 Satyavarapu, E. M., Das, R., Mandal, C., Mukhopadhyay, A. & Mandal, C. Autophagy-independent
1074 induction of LC3B through oxidative stress reveals its non-canonical role in anoikis of ovarian
1075 cancer cells. *Cell Death Dis* **9**, 934 (2018). https://doi.org:10.1038/s41419-018-0989-8
1076 77 Kondylis, V. *et al.* Endosome-mediated autophagy: an unconventional MIIC-driven autophagic
1077 pathway operational in dendritic cells. *Autophagy* **9**, 861-880 (2013).
1078 https://doi.org:10.4161/auto.24111
1079 78 Jiang, H., Cheng, D., Liu, W., Peng, J. & Feng, J. Protein kinase C inhibits autophagy and
1080 phosphorylates LC3. *Biochem Biophys Res Commun* **395**, 471-476 (2010).
1081 https://doi.org:10.1016/j.bbrc.2010.04.030
1082 79 Rusten, T. E. & Stenmark, H. p62, an autophagy hero or culprit? *Nat Cell Biol* **12**, 207-209 (2010).
1083 https://doi.org:10.1038/ncb0310-207
1084 80 Pankiv, S. *et al.* p62/SQSTM1 binds directly to Atg8/LC3 to facilitate degradation of ubiquitinated
1085 protein aggregates by autophagy. *J Biol Chem* **282**, 24131-24145 (2007).
1086 https://doi.org:10.1074/jbc.M702824200
1087 81 Bjorkoy, G. *et al.* p62/SQSTM1 forms protein aggregates degraded by autophagy and has a
1088 protective effect on huntingtin-induced cell death. *J Cell Biol* **171**, 603-614 (2005).
1089 https://doi.org:10.1083/jcb.200507002
1090 82 Szeto, J. *et al.* ALIS are stress-induced protein storage compartments for substrates of the
1091 proteasome and autophagy. *Autophagy* **2**, 189-199 (2006). https://doi.org:10.4161/auto.2731
1092 83 Yamano, K. *et al.* Critical role of mitochondrial ubiquitination and the OPTN-ATG9A axis in
1093 mitophagy. *J Cell Biol* **219** (2020). https://doi.org:10.1083/jcb.201912144
1094 84 Haspel, J. *et al.* Characterization of macroautophagic flux in vivo using a leupeptin-based assay.
1095 *Autophagy* **7**, 629-642 (2011). https://doi.org:10.4161/auto.7.6.15100

85 Bahr, B. A., Wisniewski, M. L. & Butler, D. Positive lysosomal modulation as a unique strategy to treat age-related protein accumulation diseases. *Rejuvenation Res* **15**, 189-197 (2012). https://doi.org:10.1089/rej.2011.1282

86 McBride, H. M., Neuspiel, M. & Wasiak, S. Mitochondria: more than just a powerhouse. *Curr Biol* **16**, R551-560 (2006). https://doi.org:10.1016/j.cub.2006.06.054

87 Garcia-Mata, R., Gao, Y. S. & Sztul, E. Hassles with taking out the garbage: aggravating aggresomes. *Traffic* **3**, 388-396 (2002). https://doi.org:10.1034/j.1600-0854.2002.30602.x

88 Johnston, J. A., Ward, C. L. & Kopito, R. R. Aggresomes: a cellular response to misfolded proteins. *J Cell Biol* **143**, 1883-1898 (1998). https://doi.org:10.1083/jcb.143.7.1883

89 Nassar, M. *et al.* LC3A Silencing Hinders Aggresome Vimentin Cage Clearance in Primary Choroid Plexus Carcinoma. *Sci Rep* **7**, 8022 (2017). https://doi.org:10.1038/s41598-017-07403-5

90 Zheng, Q., Su, H., Ranek, M. J. & Wang, X. Autophagy and p62 in cardiac proteinopathy. *Circ Res* **109**, 296-308 (2011). https://doi.org:10.1161/CIRCRESAHA.111.244707

91 Wai, T. *et al.* Imbalanced OPA1 processing and mitochondrial fragmentation cause heart failure in mice. *Science* **350**, aad0116 (2015). https://doi.org:10.1126/science.aad0116

92 Hohn, A. *et al.* Lipofuscin inhibits the proteasome by binding to surface motifs. *Free Radic Biol Med* **50**, 585-591 (2011). https://doi.org:10.1016/j.freeradbiomed.2010.12.011

93 Hohn, A., Sittig, A., Jung, T., Grimm, S. & Grune, T. Lipofuscin is formed independently of macroautophagy and lysosomal activity in stress-induced prematurely senescent human fibroblasts. *Free Radic Biol Med* **53**, 1760-1769 (2012). https://doi.org:10.1016/j.freeradbiomed.2012.08.591

94 DiLoreto, R. & Murphy, C. T. The cell biology of aging. *Mol Biol Cell* **26**, 4524-4531 (2015). https://doi.org:10.1091/mbc.E14-06-1084

95 Anisimova, A. S., Alexandrov, A. I., Makarova, N. E., Gladyshev, V. N. & Dmitriev, S. E. Protein synthesis and quality control in aging. *Aging (Albany NY)* **10**, 4269-4288 (2018). https://doi.org:10.18632/aging.101721

96 Hipkiss, A. R. On why decreasing protein synthesis can increase lifespan. *Mech Ageing Dev* **128**, 412-414 (2007). https://doi.org:10.1016/j.mad.2007.03.002

97 Bar, H., Strelkov, S. V., Sjoberg, G., Aebi, U. & Herrmann, H. The biology of desmin filaments: how do mutations affect their structure, assembly, and organisation? *J Struct Biol* **148**, 137-152 (2004). https://doi.org:10.1016/j.jsb.2004.04.003

98 Martinez-Laorden, E., Almela, P., Milanes, M. V. & Laorden, M. L. Expression of heat shock protein 27 and troponin T and troponin I after naloxone-precipitated morphine withdrawal. *Eur J Pharmacol* **766**, 142-150 (2015). https://doi.org:10.1016/j.ejphar.2015.10.006

99 Vander Heide, R. S. Increased expression of HSP27 protects canine myocytes from simulated ischemia-reperfusion injury. *Am J Physiol Heart Circ Physiol* **282**, H935-941 (2002). https://doi.org:10.1152/ajpheart.00660.2001

100 Chen, H. *et al.* Phosphorylated heat shock protein 27 is involved in enhanced heart tolerance to ischemia in short-term type 1 diabetic rats. *Acta Pharmacol Sin* **26**, 806-812 (2005). https://doi.org:10.1111/j.1745-7254.2005.00113.x

101 Weibel, E. R. *Stereological methods*. (Academic Press, 1979).

102 Palade, G. E. A study of fixation for electron microscopy. *J Exp Med* **95**, 285-298 (1952). https://doi.org:10.1084/jem.95.3.285

103 Goodman, C. A. & Hornberger, T. A. Measuring protein synthesis with SUnSET: a valid alternative to traditional techniques? *Exerc Sport Sci Rev* **41**, 107-115 (2013). https://doi.org:10.1097/JES.0b013e3182798a95

Total Word count without References ~12500

1142 104 Kayed, R. *et al.* Common structure of soluble amyloid oligomers implies common mechanism of
1143 pathogenesis. *Science* **300**, 486-489 (2003). https://doi.org:10.1126/science.1079469
1144 105 Wessel, D. & Flugge, U. I. A method for the quantitative recovery of protein in dilute solution in
1145 the presence of detergents and lipids. *Anal Biochem* **138**, 141-143 (1984).
1146 https://doi.org:10.1016/0003-2697(84)90782-6
1147 106 Ferreira, J. A. & Zwinderman, A. H. On the Benjamini-Hochberg method. *Ann Stat* **34**, 1827-1849
1148 (2006). https://doi.org:10.1214/009053606000000425

1149

1150

Total Word count without References ~12500

GRAPHICAL ABSTRACT

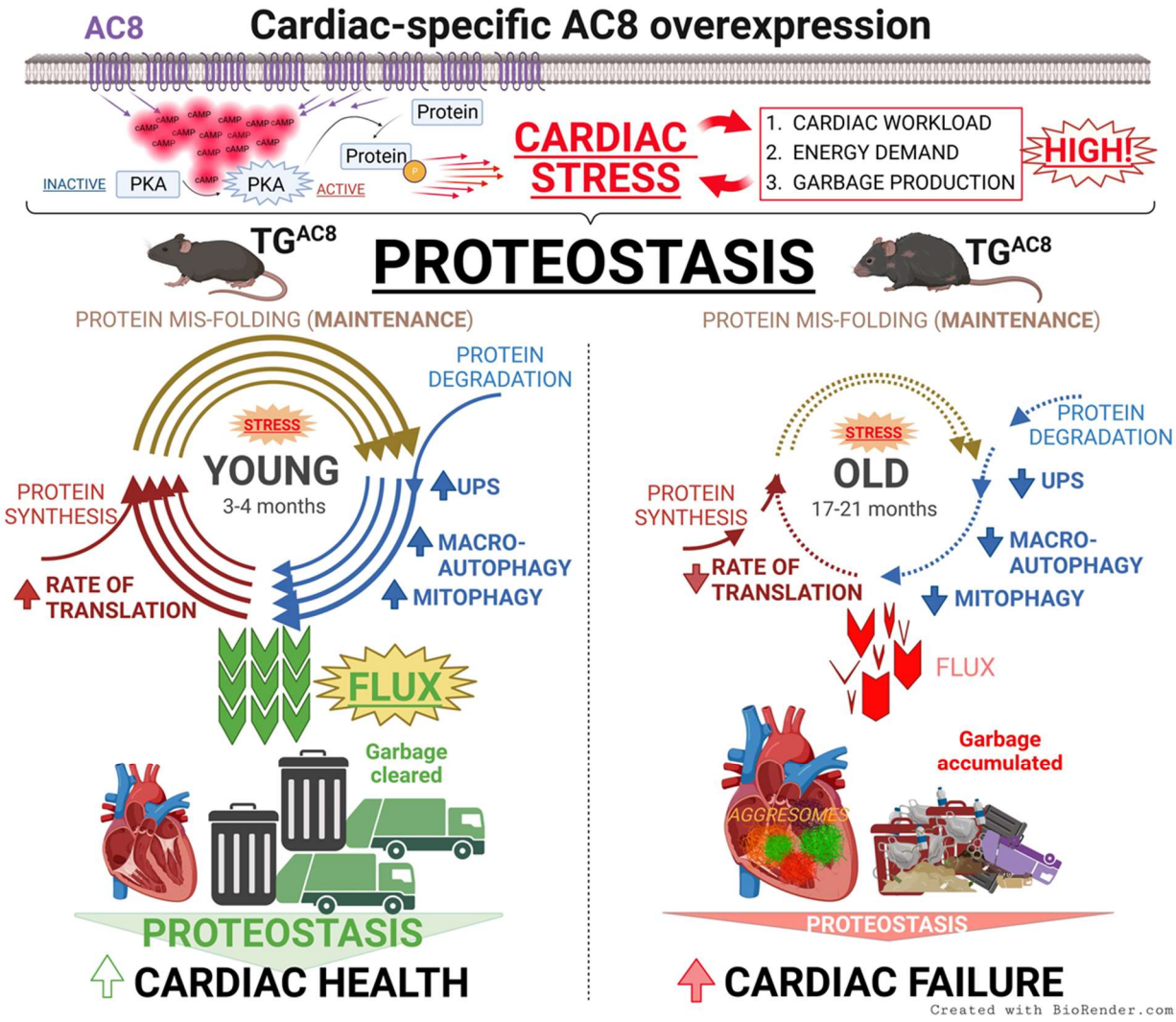

Total Word count without References ~12500

1153 **FIGURE 1**

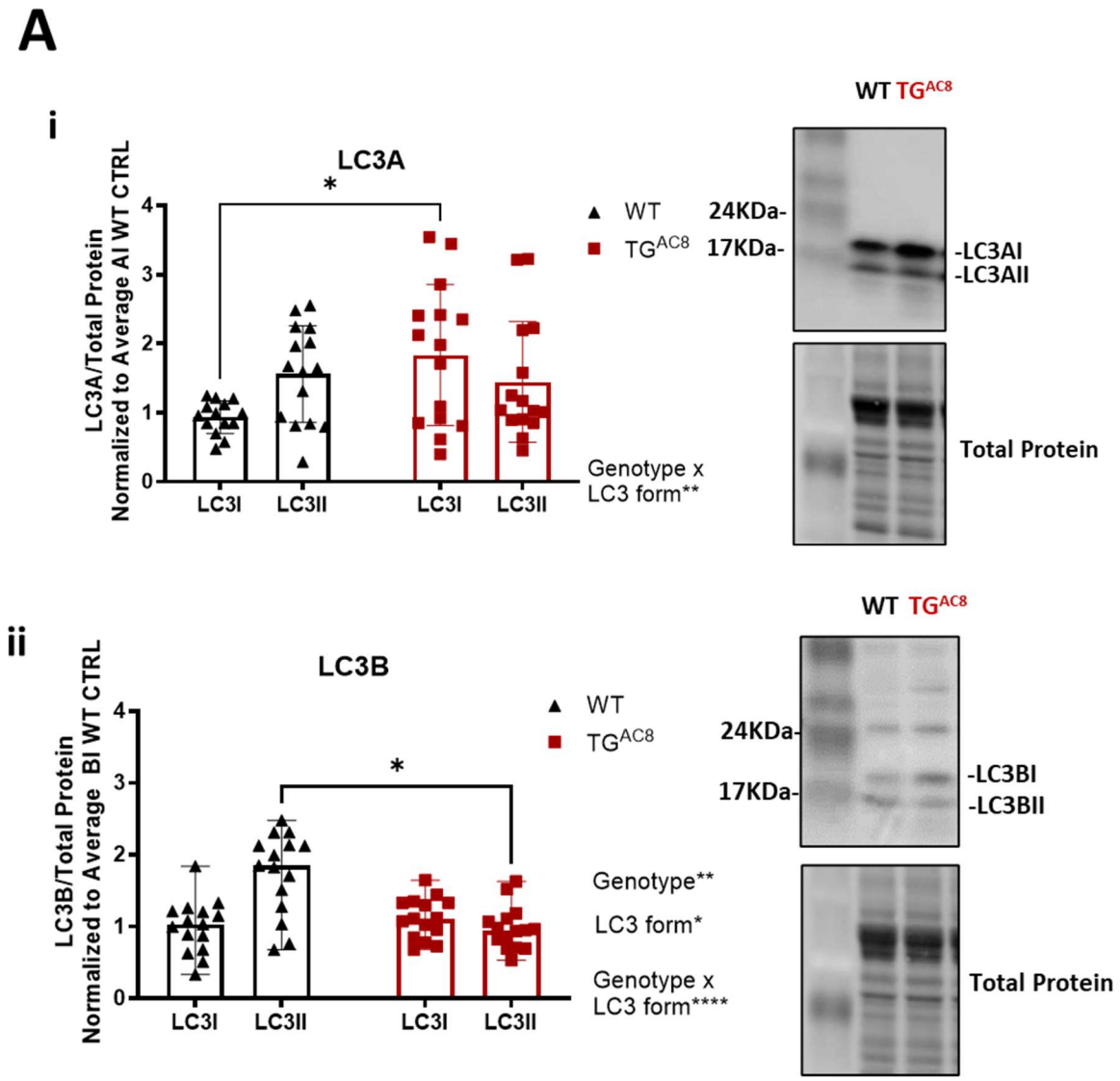

1154

1155

Total Word count without References ~12500

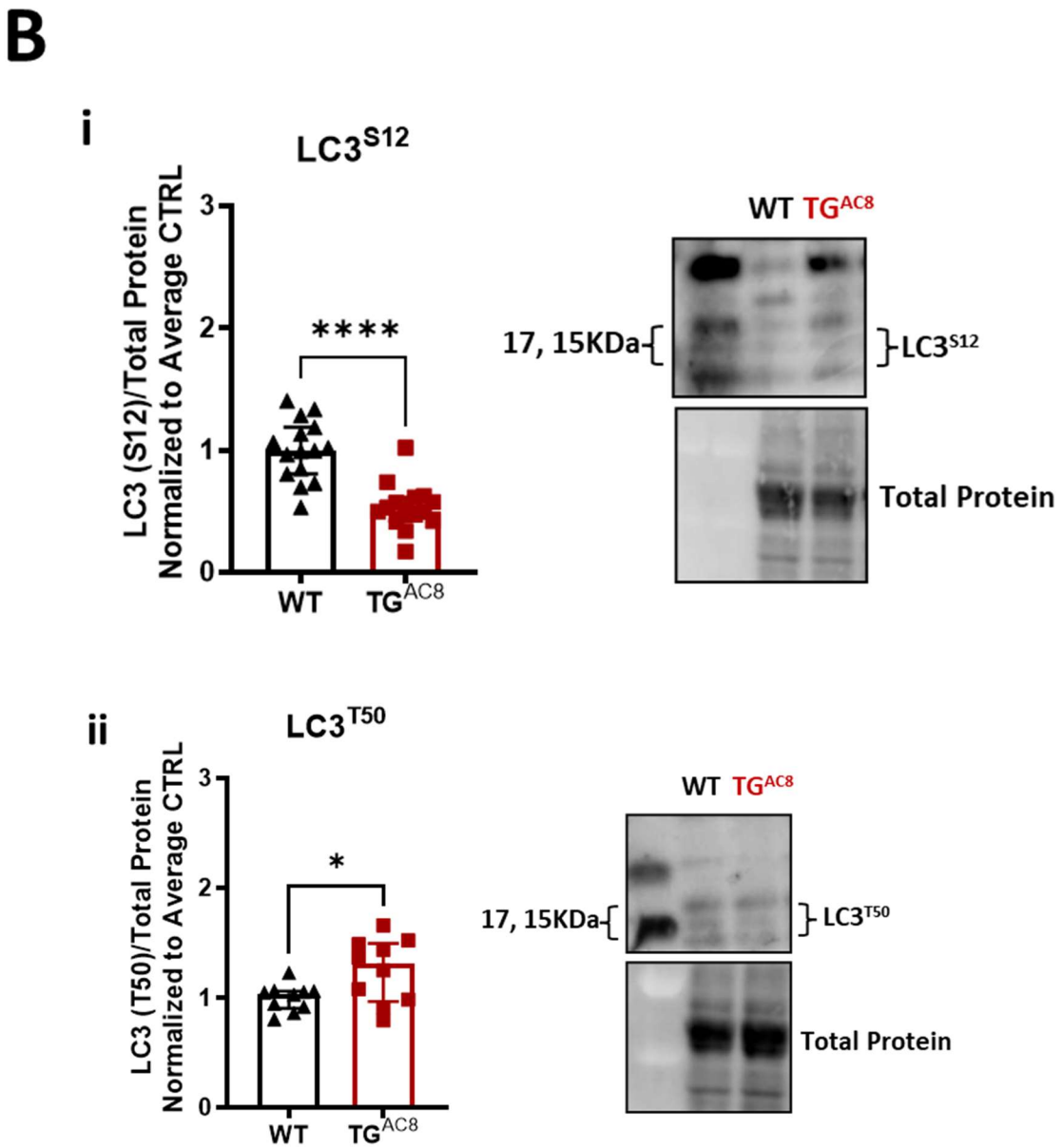

1156

1157

Total Word count without References ~12500

C

i

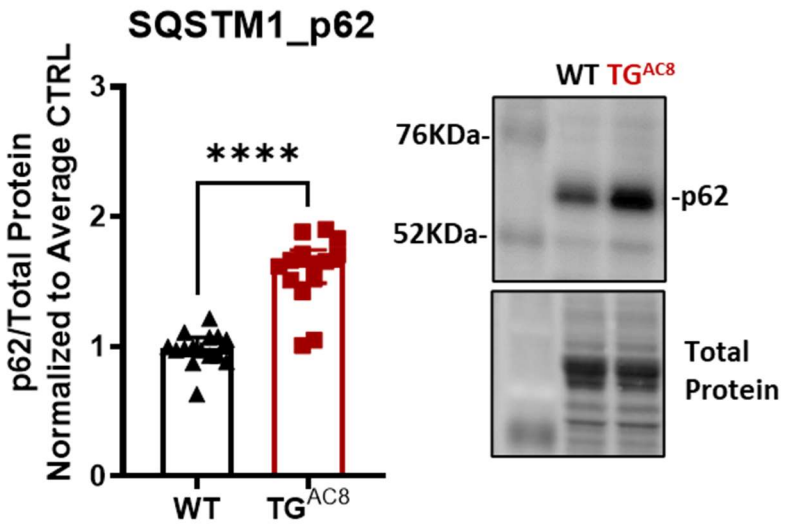

1158

ii

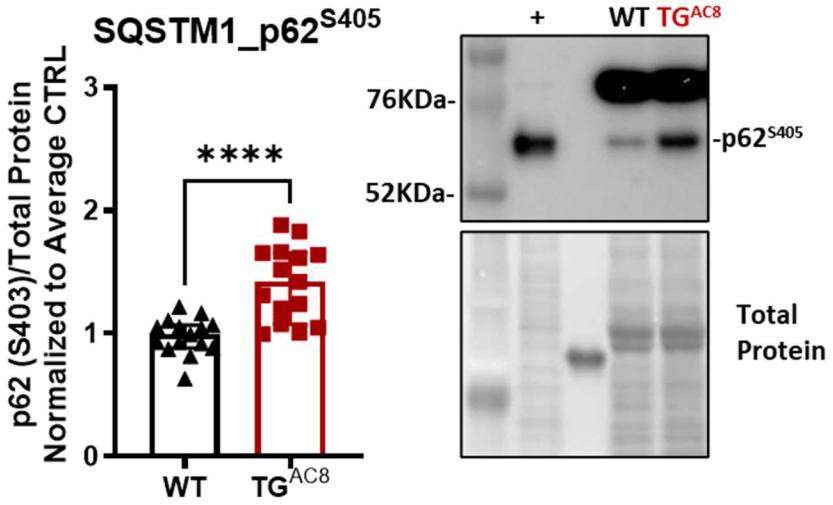

1159

Total Word count without References ~12500

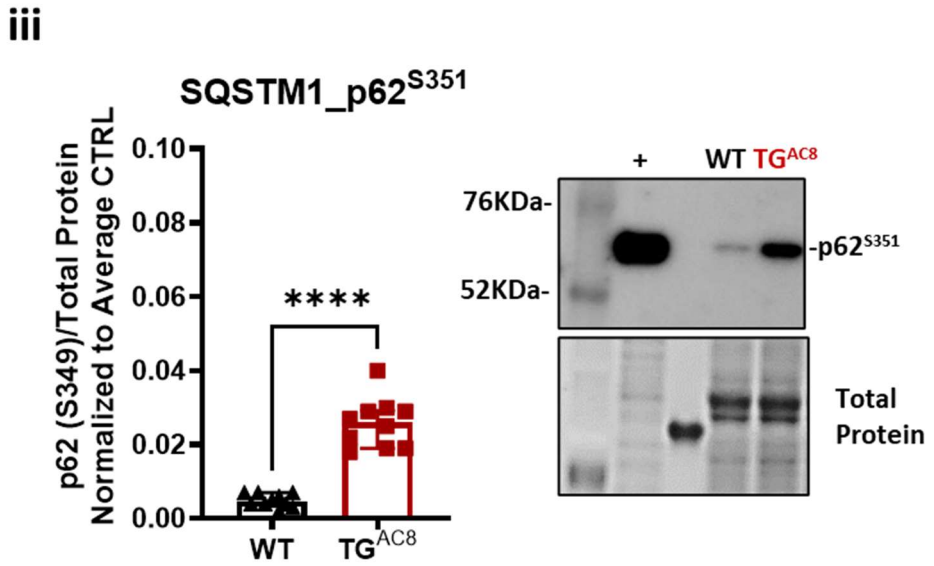

1160

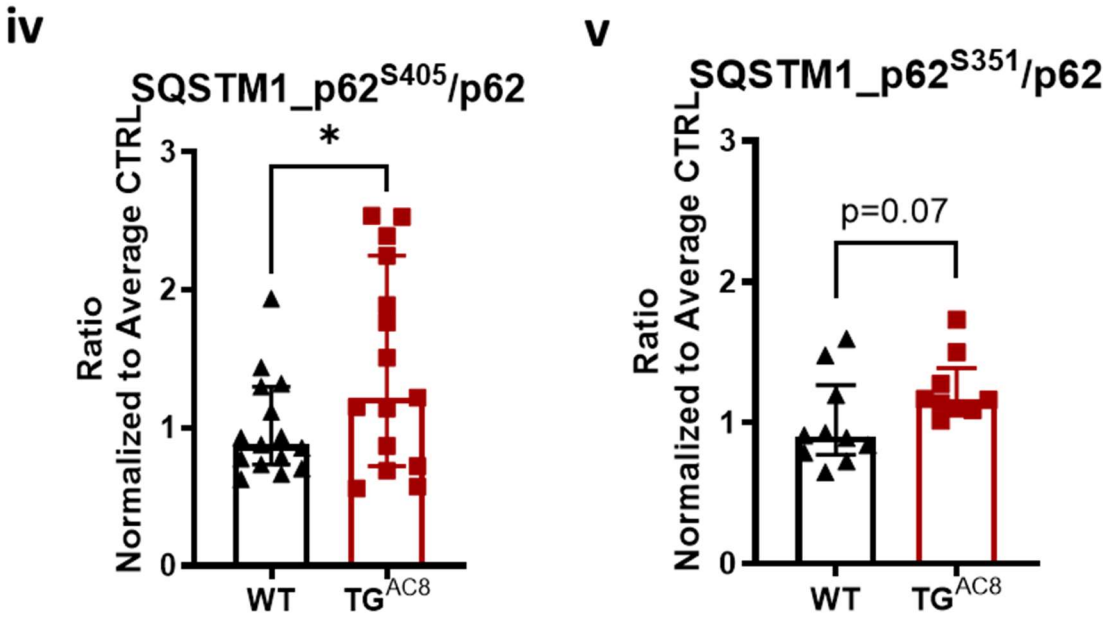

1161

1162 **FIGURE 2**

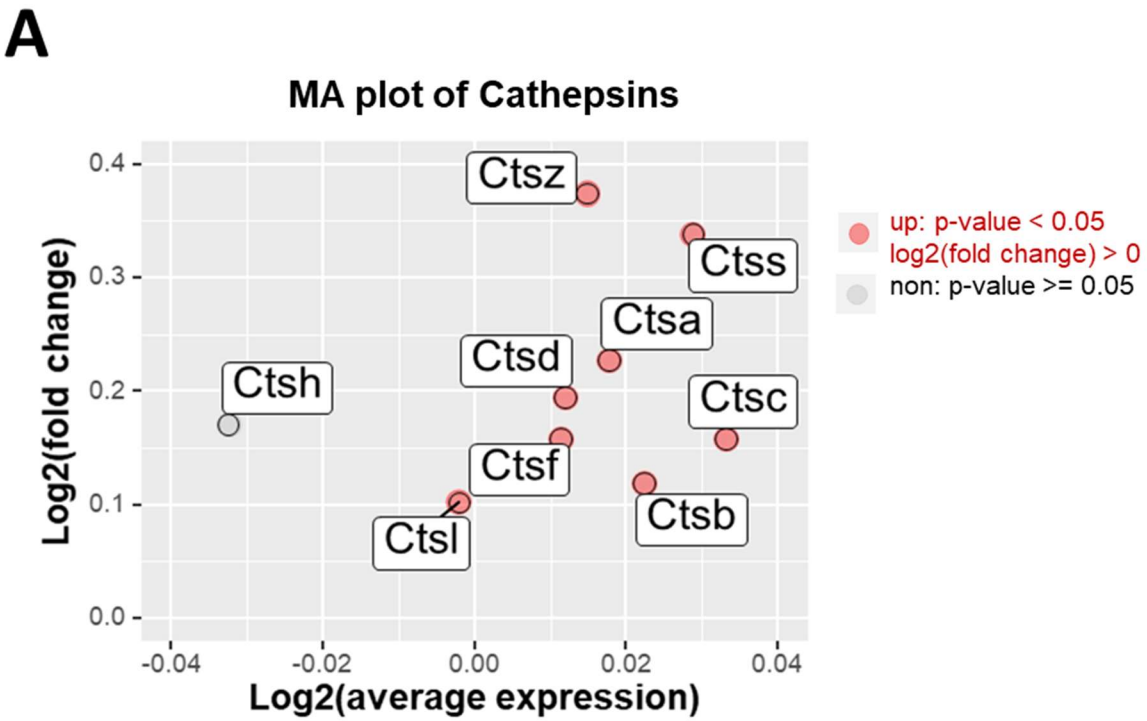

1163

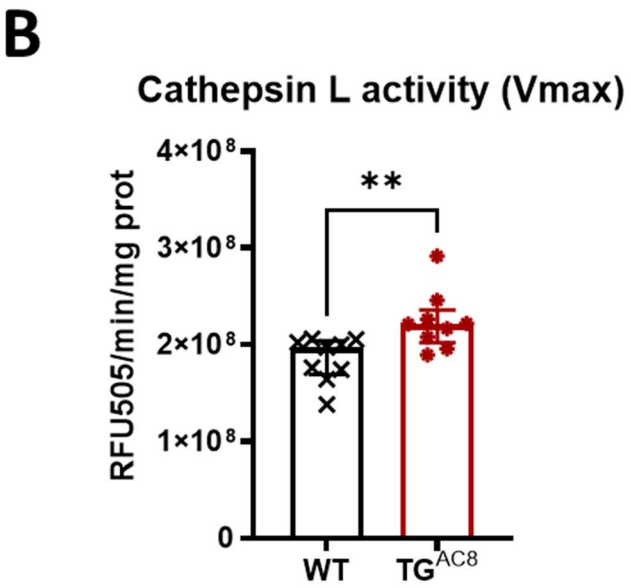

1164

Total Word count without References ~12500

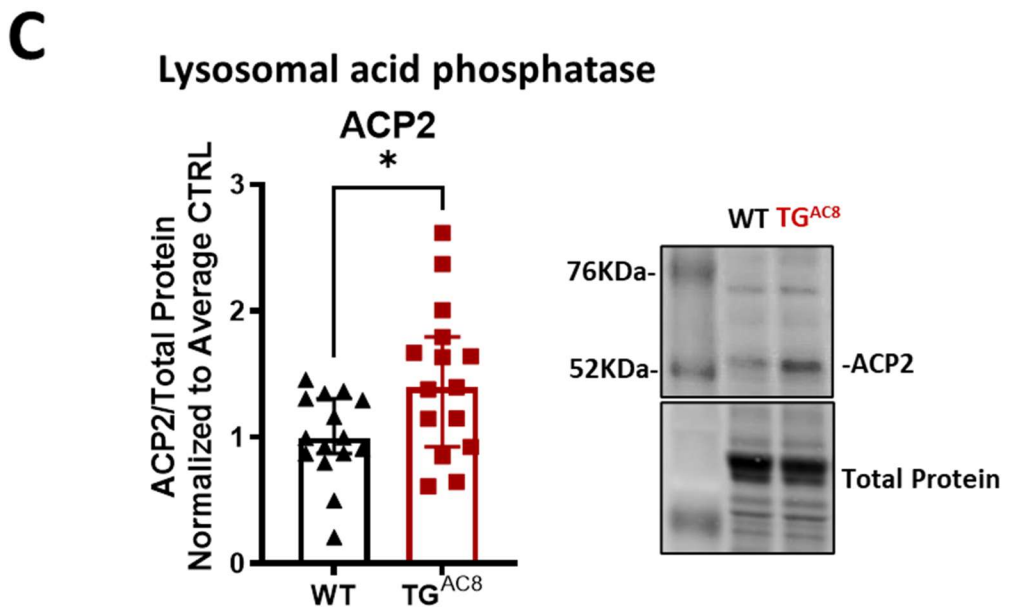

1165

1166 **FIGURE 3**

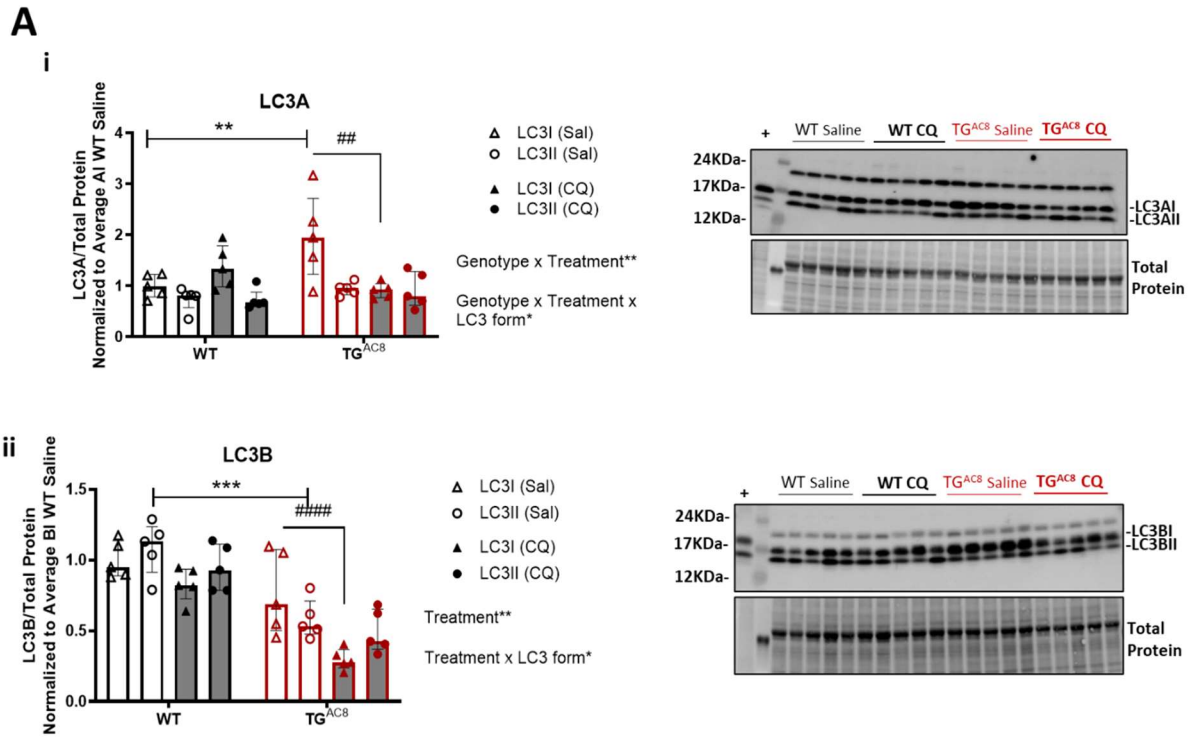

1167

1168

Total Word count without References ~12500

iii

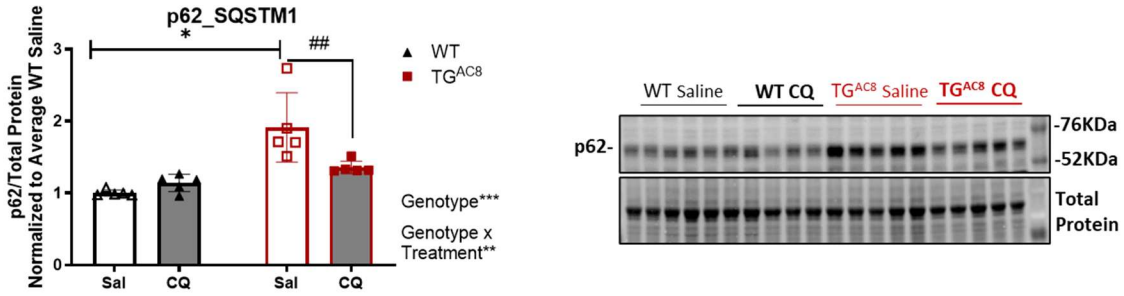

1169

B

i

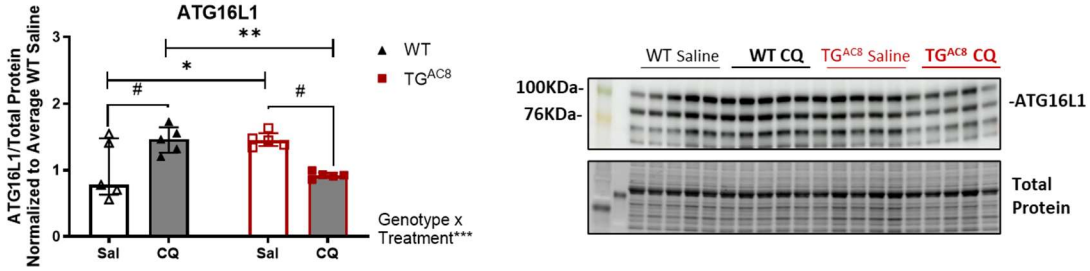

1170

ii

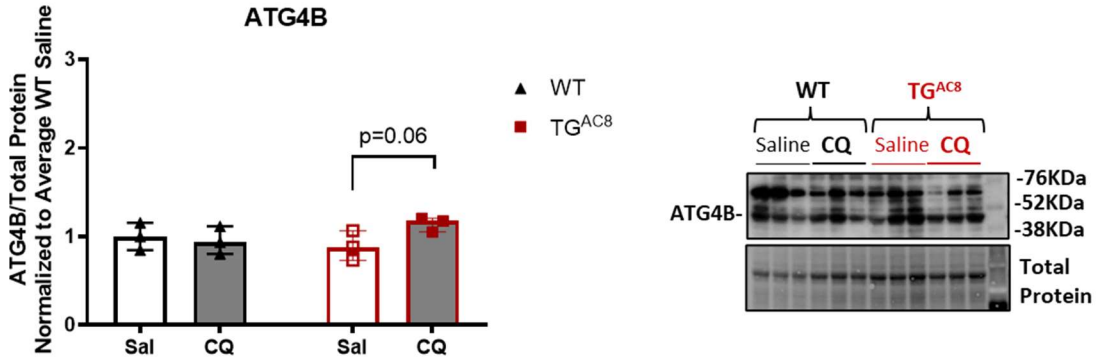

1171

iii

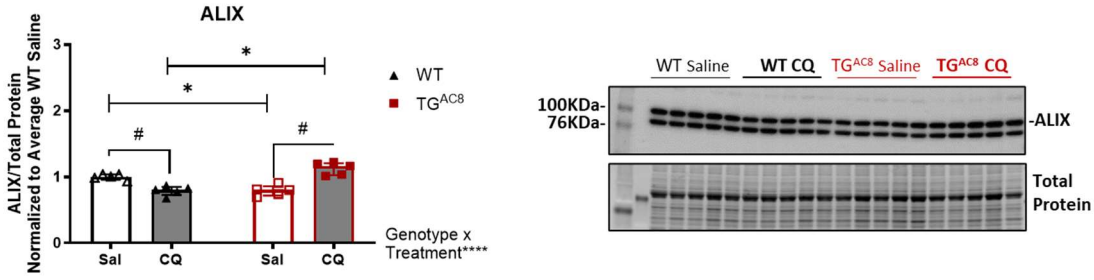

1172

Total Word count without References ~12500

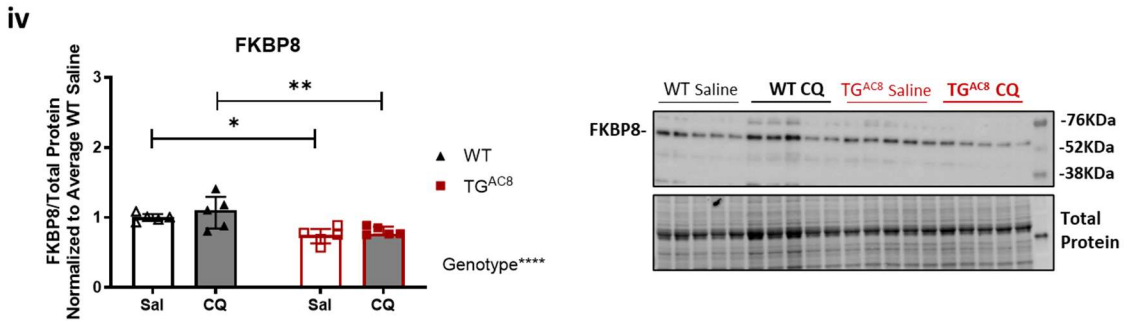

1173

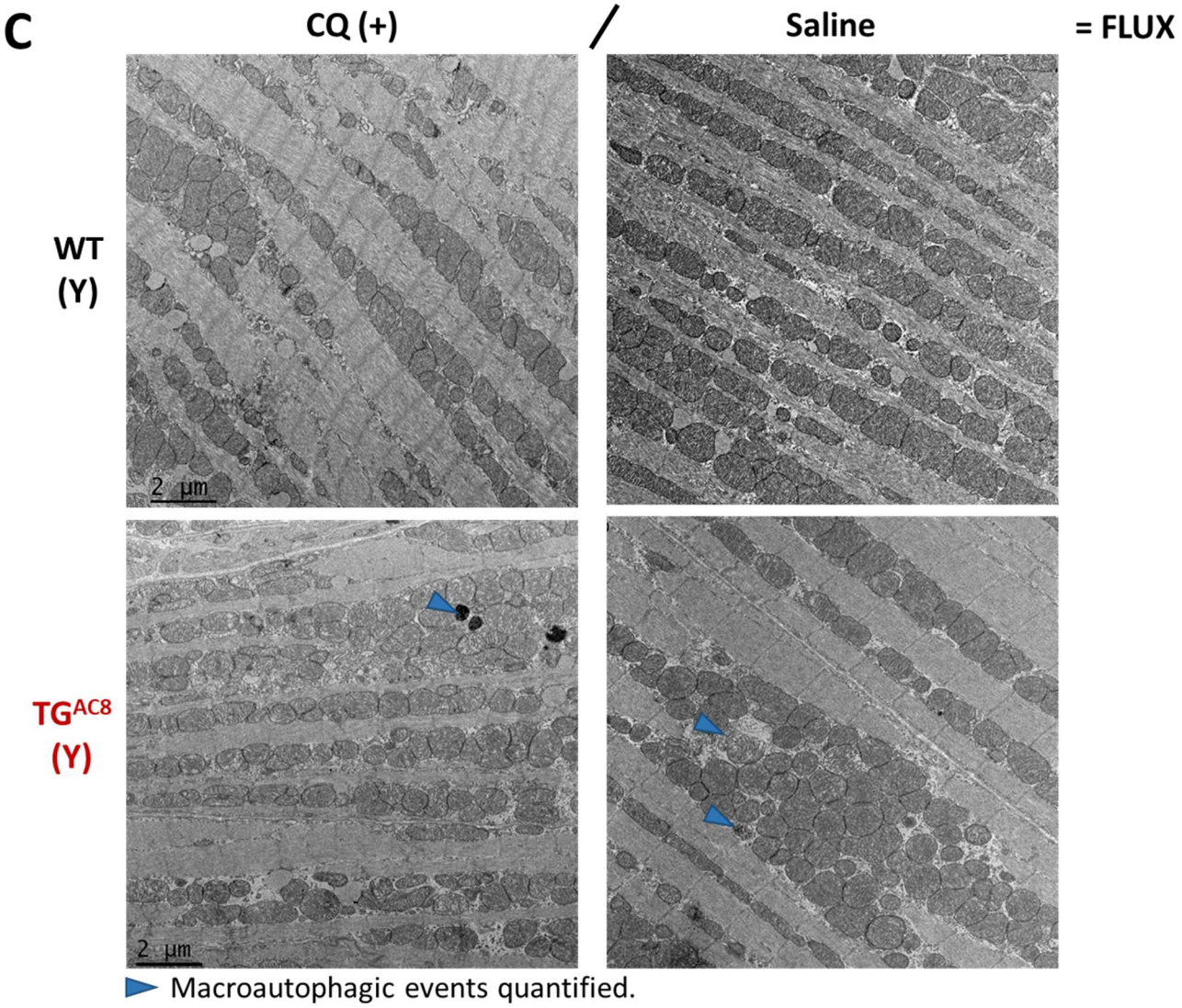

1174

Total Word count without References ~12500

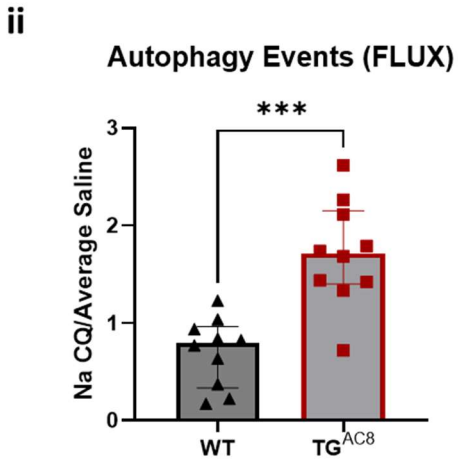

FIGURE 4

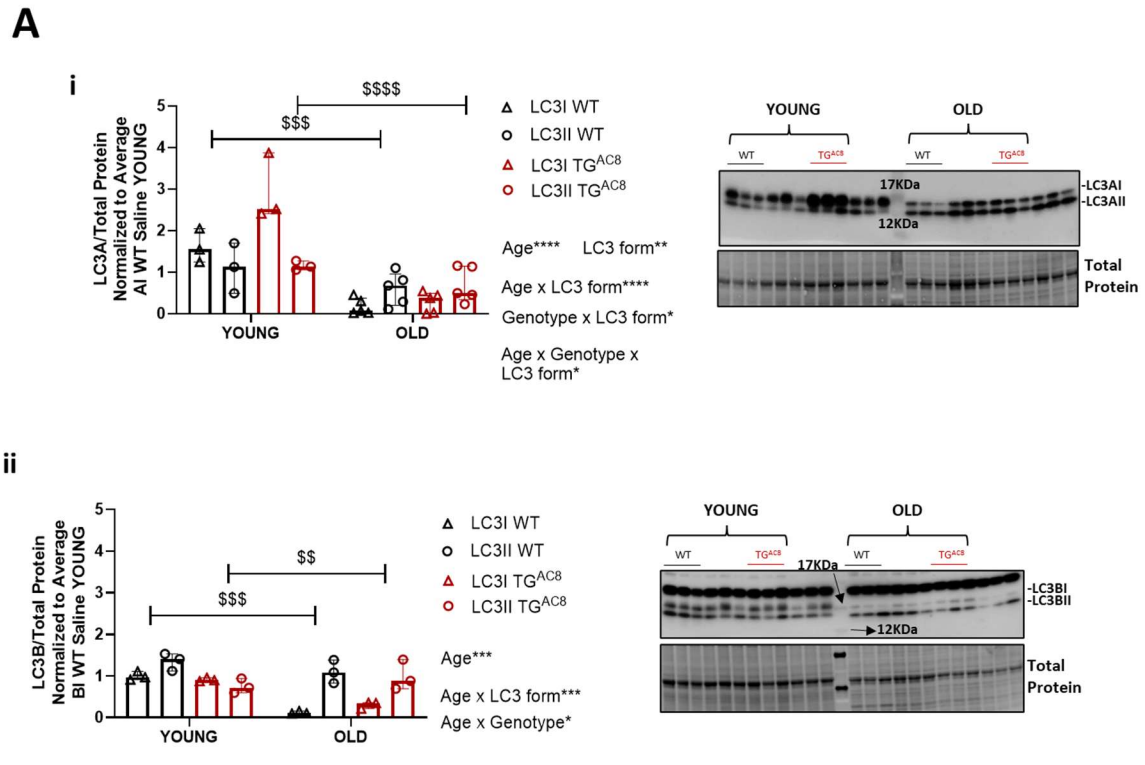

Total Word count without References ~12500

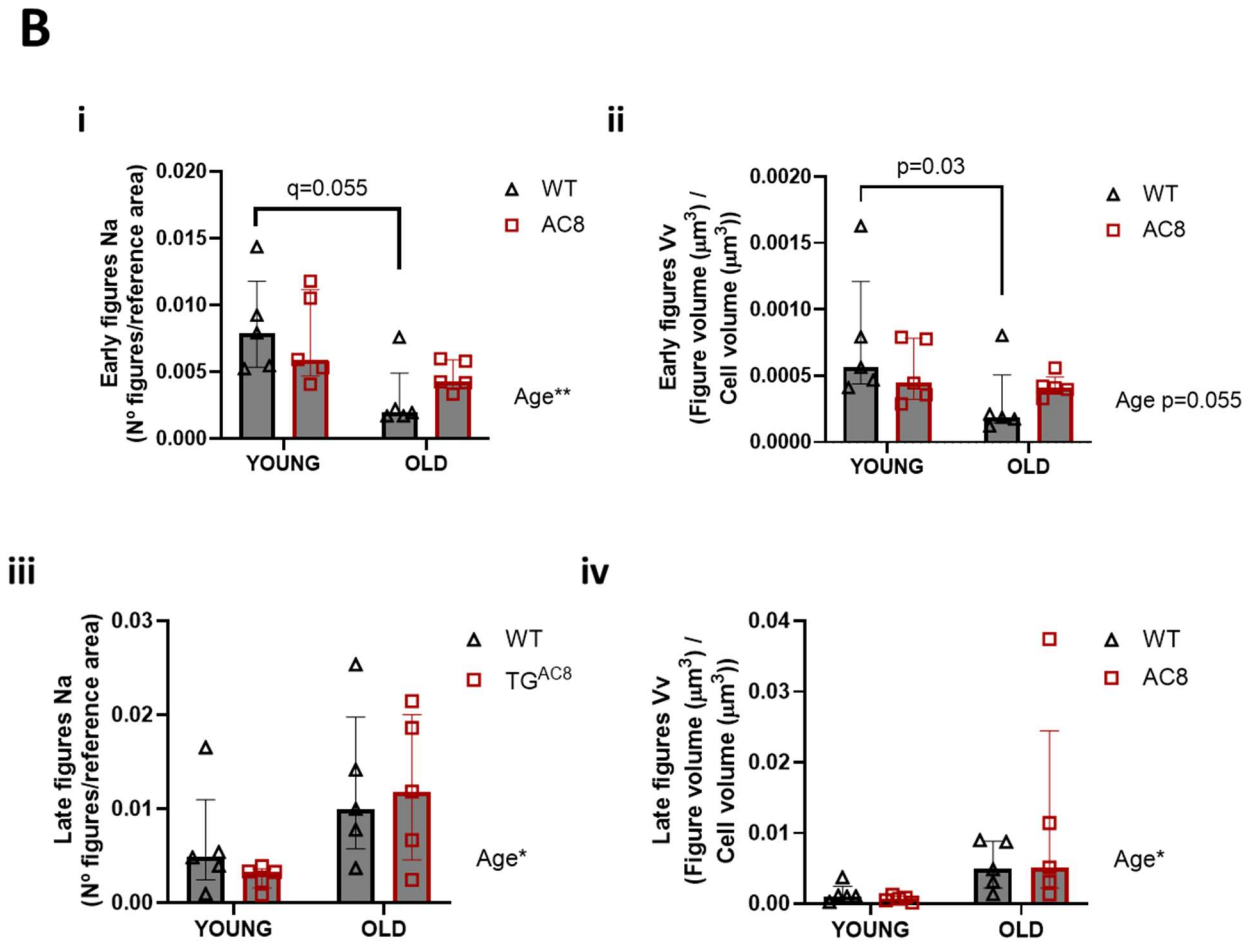

1179

1180

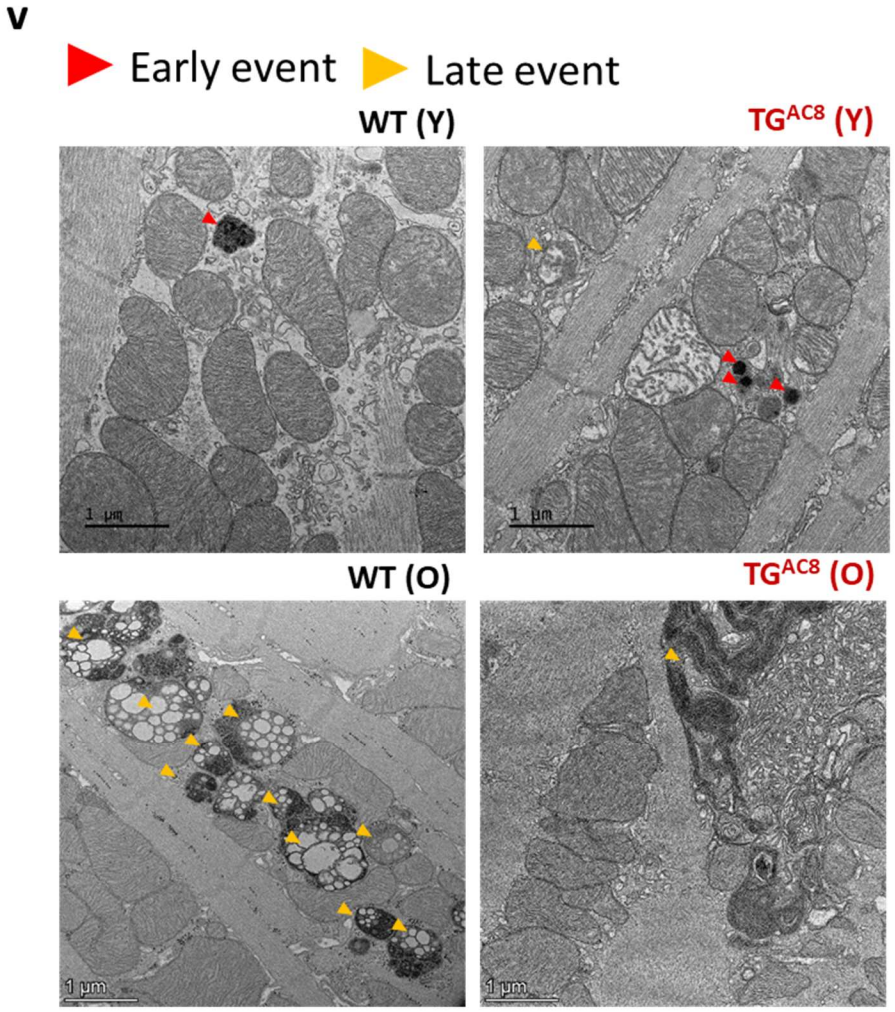

Early event (phagosomes, autophagosomes, lysosomes)

Late event (autophagolysosomes)

1181

Total Word count without References ~12500

C

i

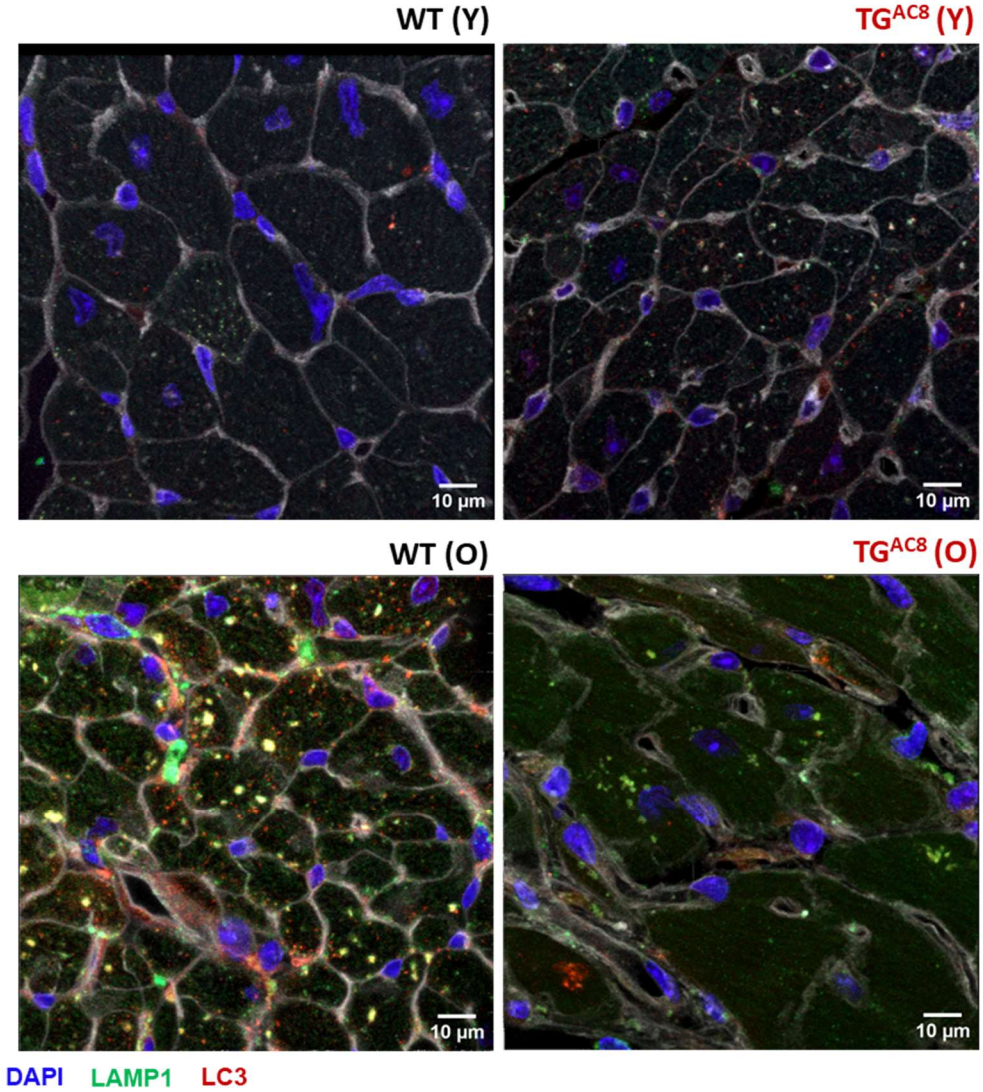

1182

ii

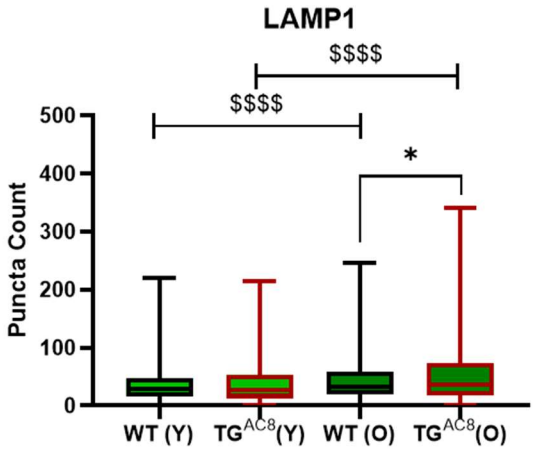

1183

iii

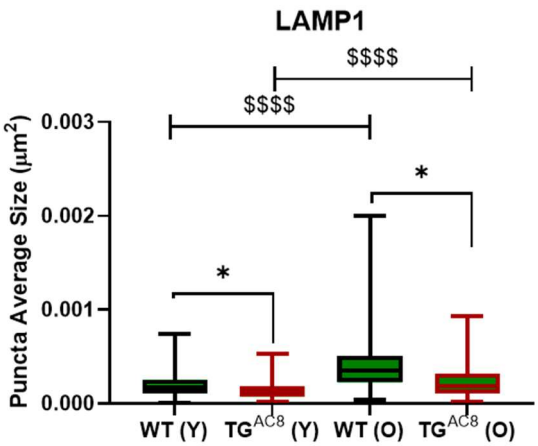

1184

iv

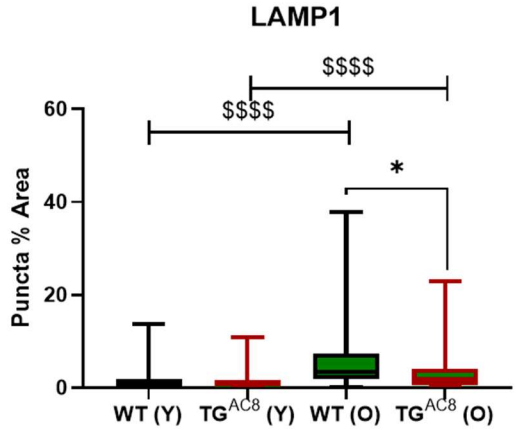

1185

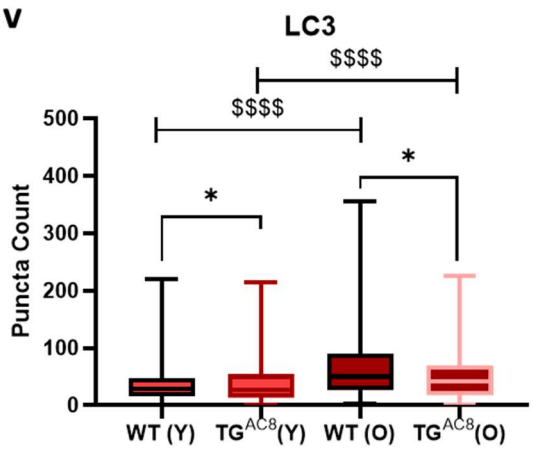
v
LC3
$$$$
$$$$
*
*
Puncta Count
500
400
300
200
100
0
WT (Y)
TG^AC8 (Y)
WT (O)
TG^AC8 (O)

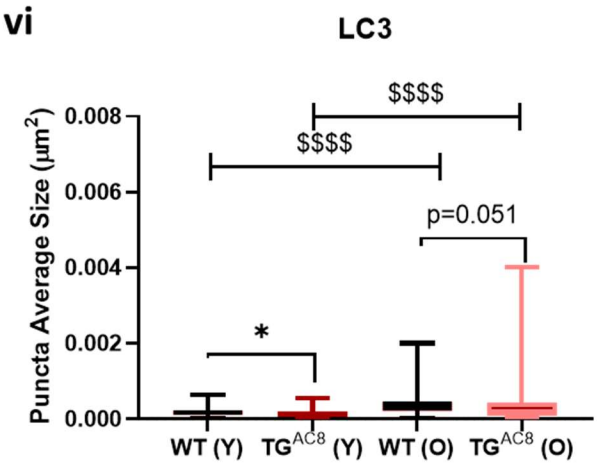
vi
LC3
$$$$
$$$$
p=0.051
*
Puncta Average Size (µm²)
0.008
0.006
0.004
0.002
0.000
WT (Y)
TG^AC8 (Y)
WT (O)
TG^AC8 (O)

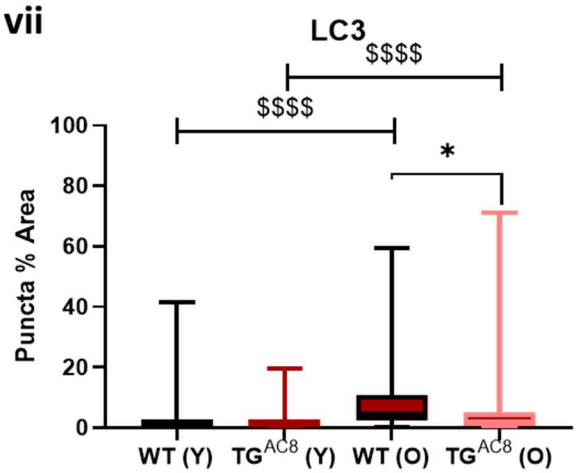
vii
LC3
$$$$
$$$$
*
Puncta % Area
100
80
60
40
20
0
WT (Y)
TG^AC8 (Y)
WT (O)
TG^AC8 (O)

D

i

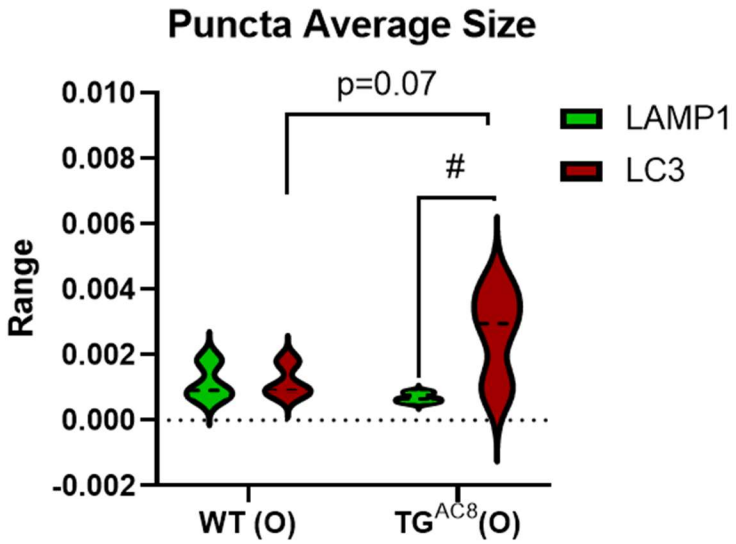

1191

ii

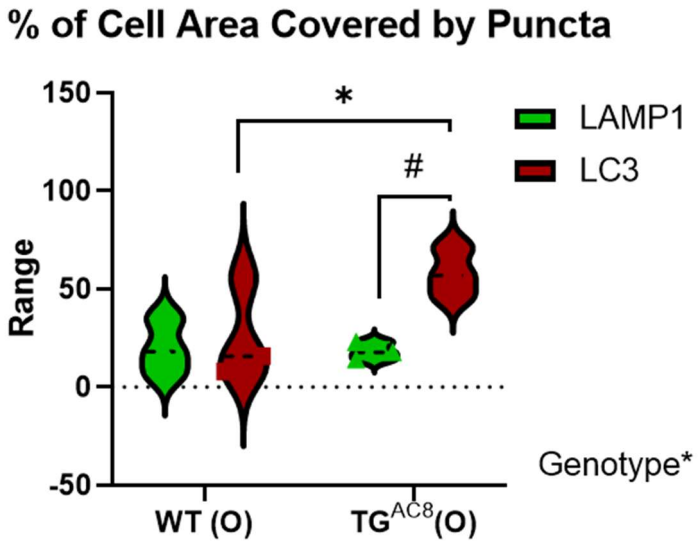

1192

Total Word count without References ~12500

E

i

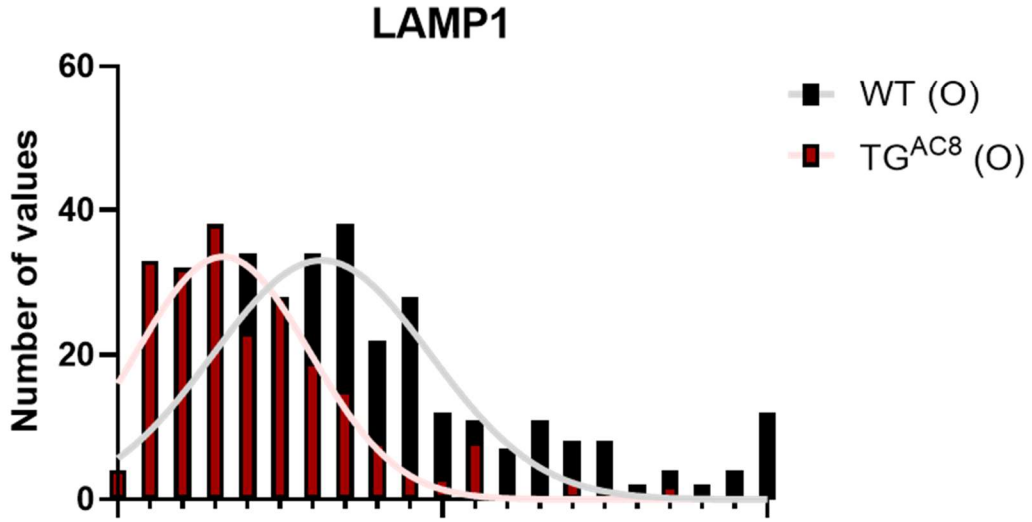

1193

ii

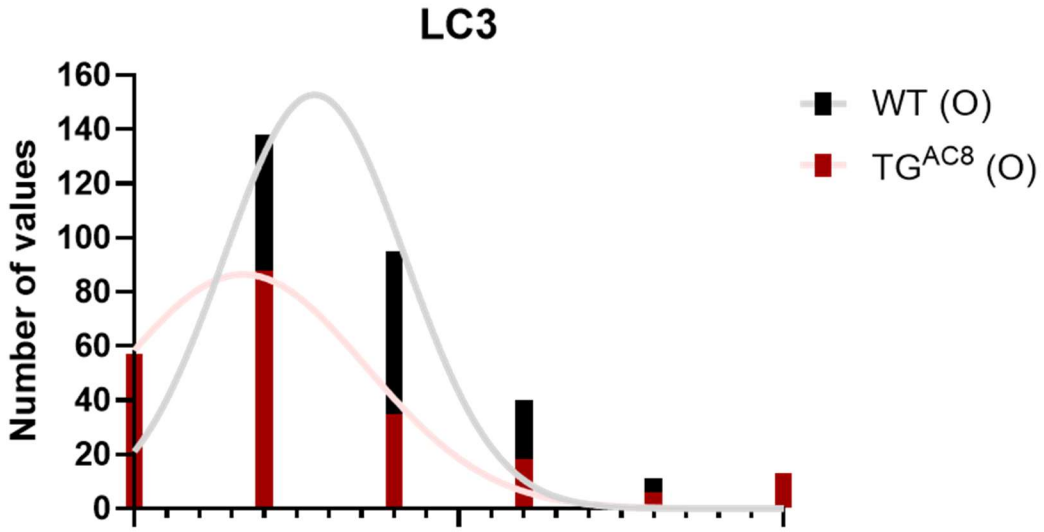

1194

Total Word count without References ~12500

FIGURE 5

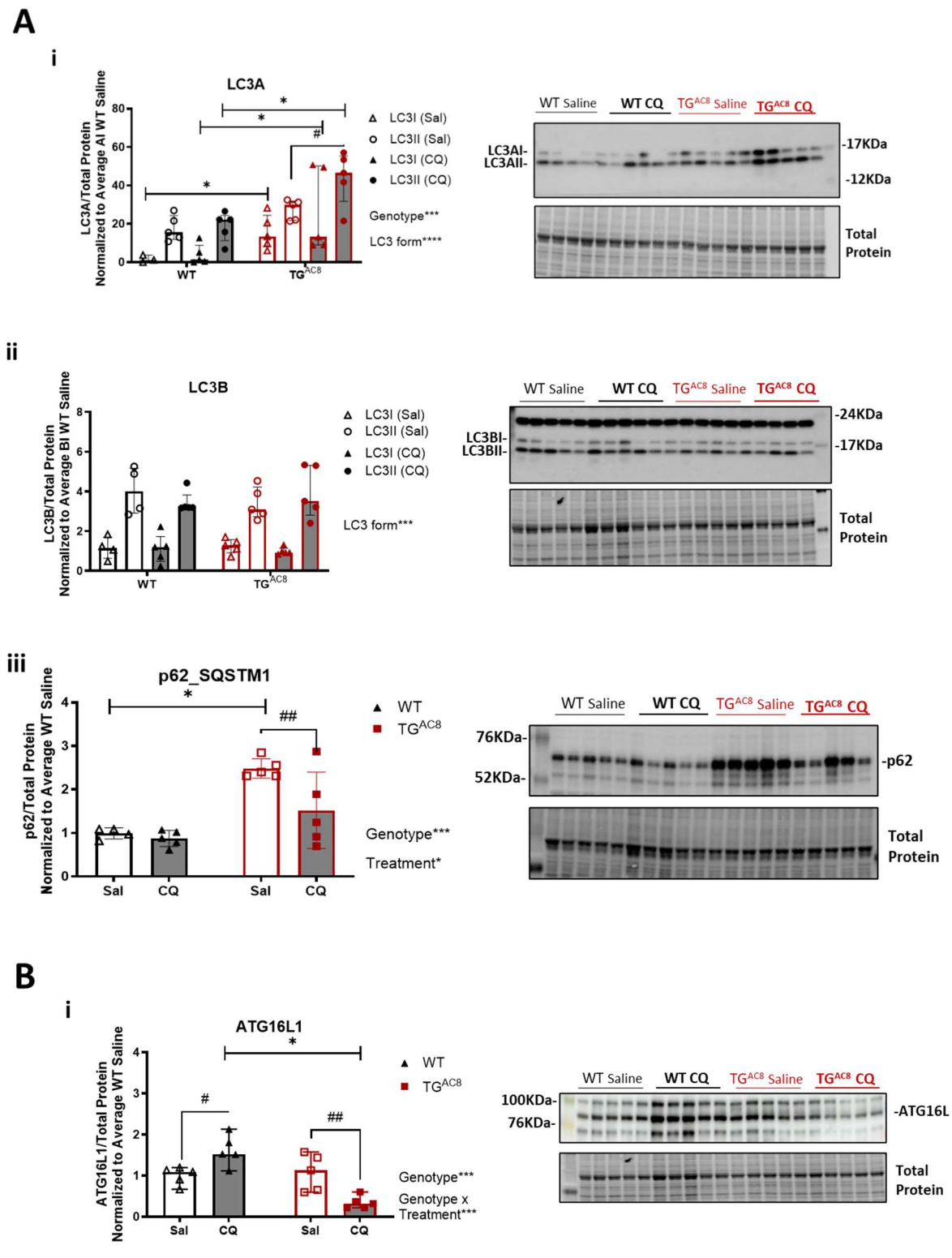

Total Word count without References ~12500

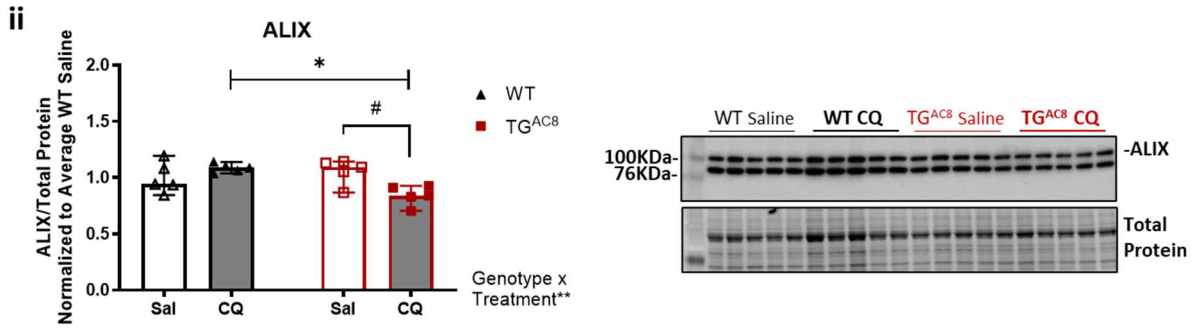

1200

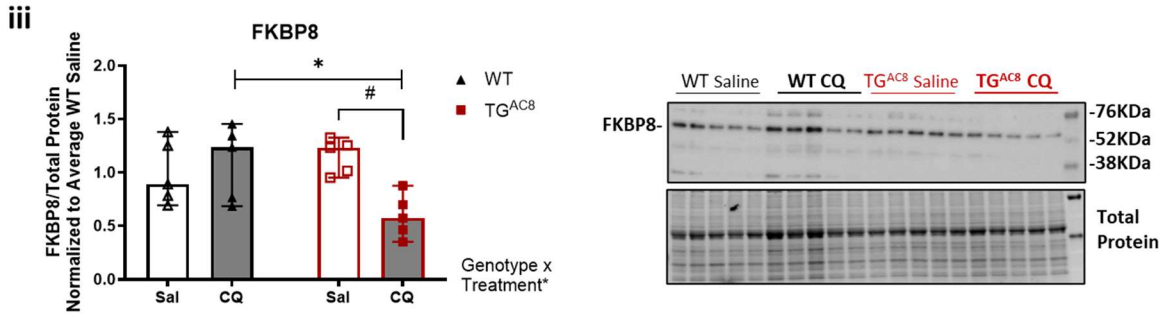

1201

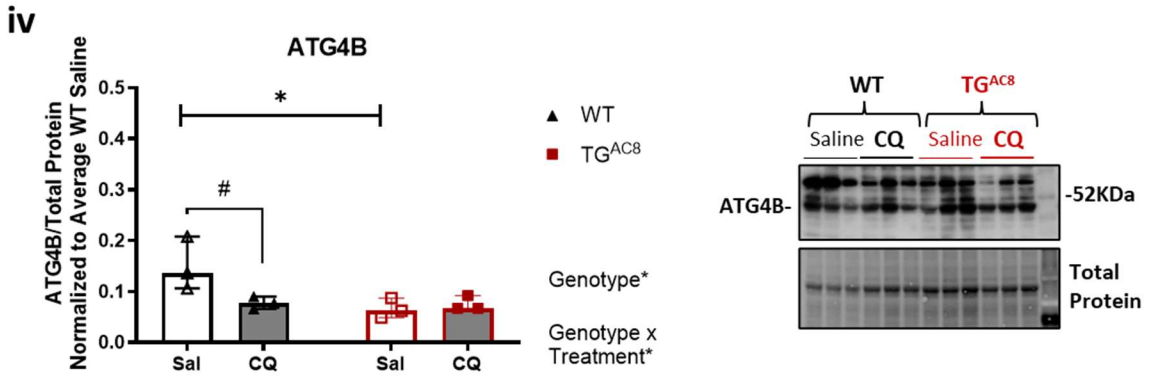

1202

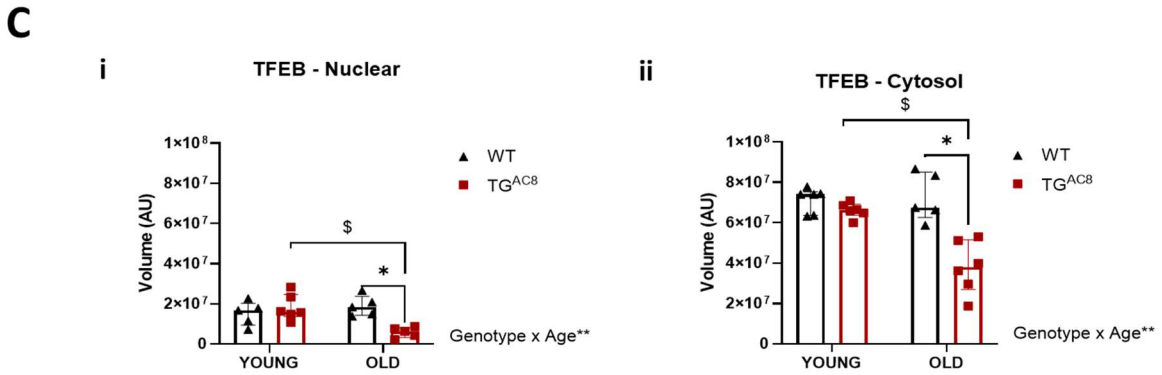

1203

Total Word count without References ~12500

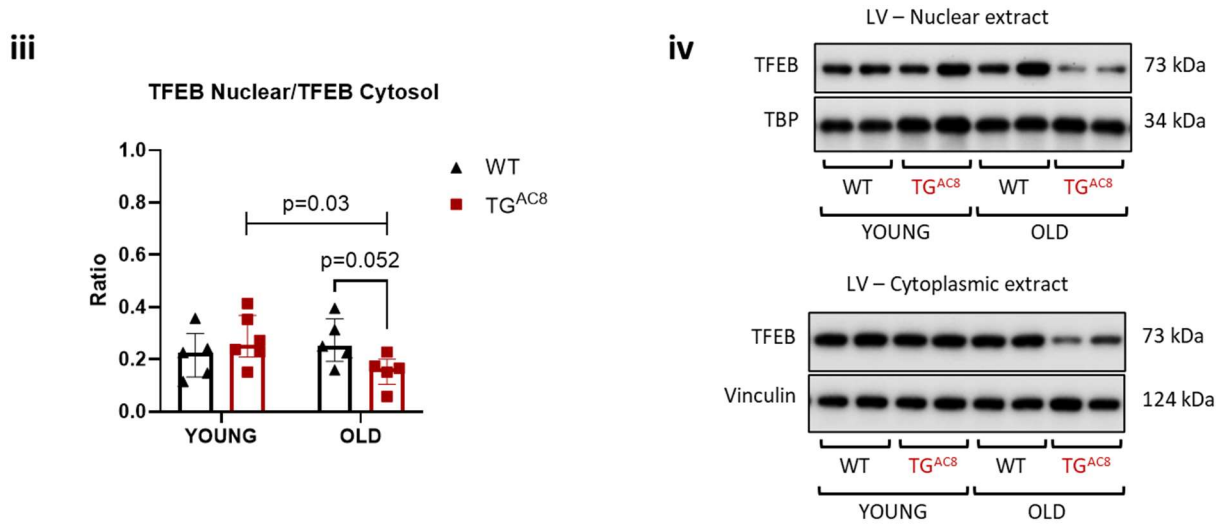

1204

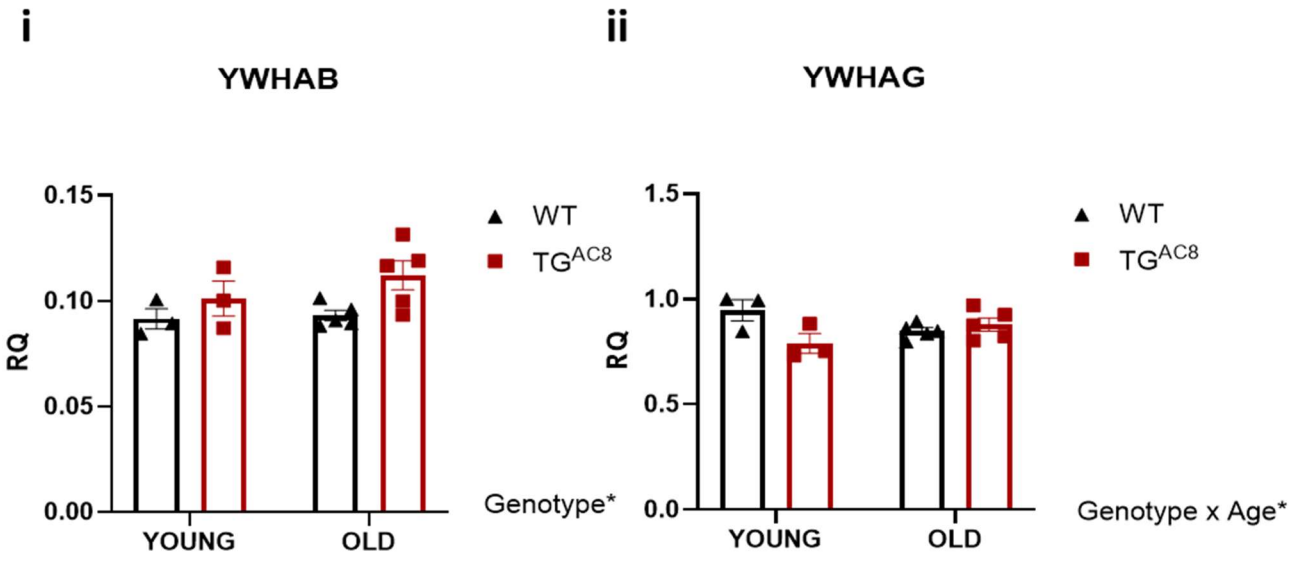

1205

Total Word count without References ~12500

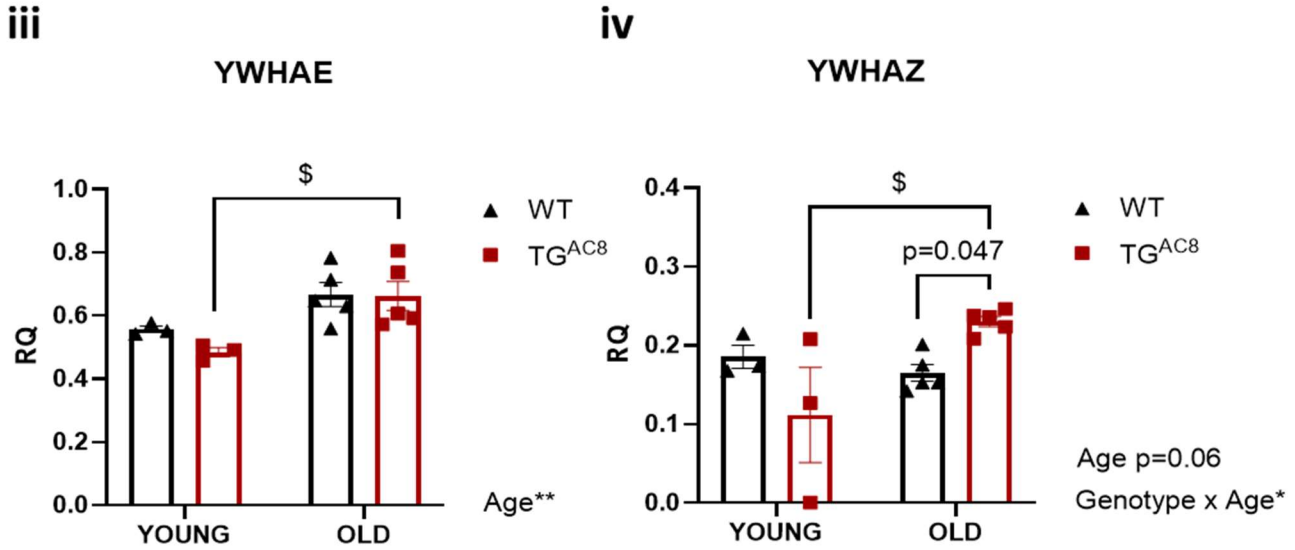

1206

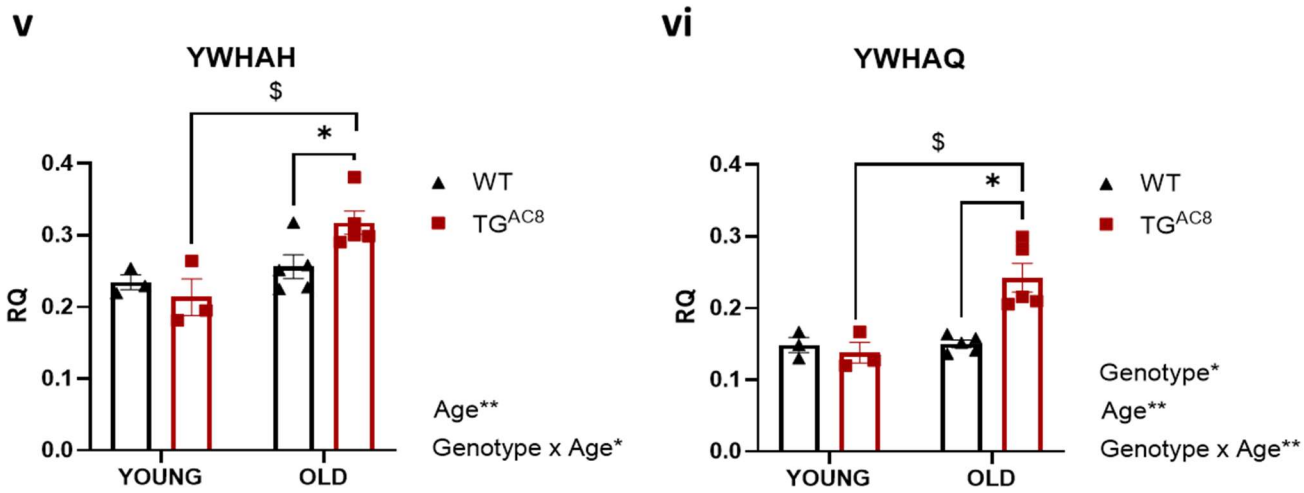

1207

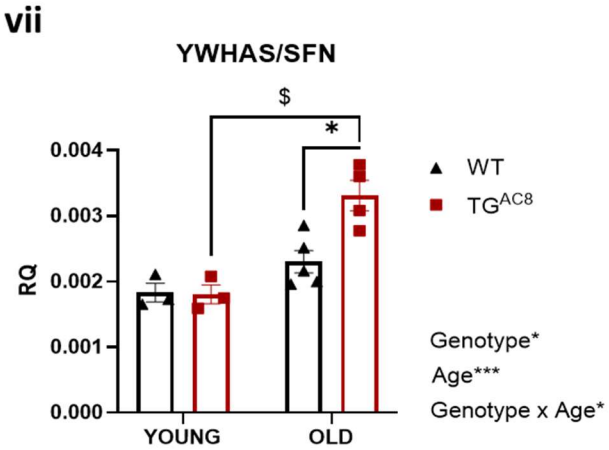

1208

Total Word count without References ~12500

FIGURE 6

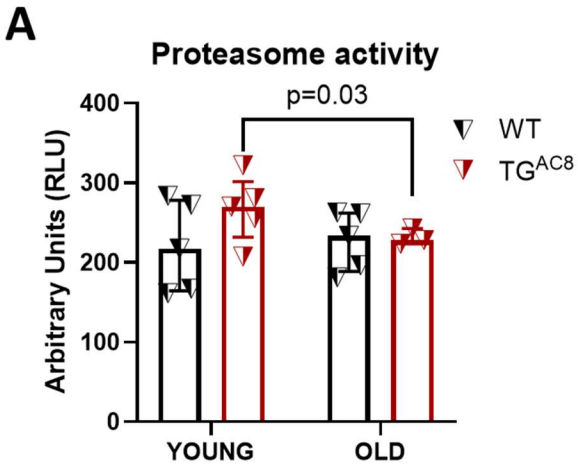

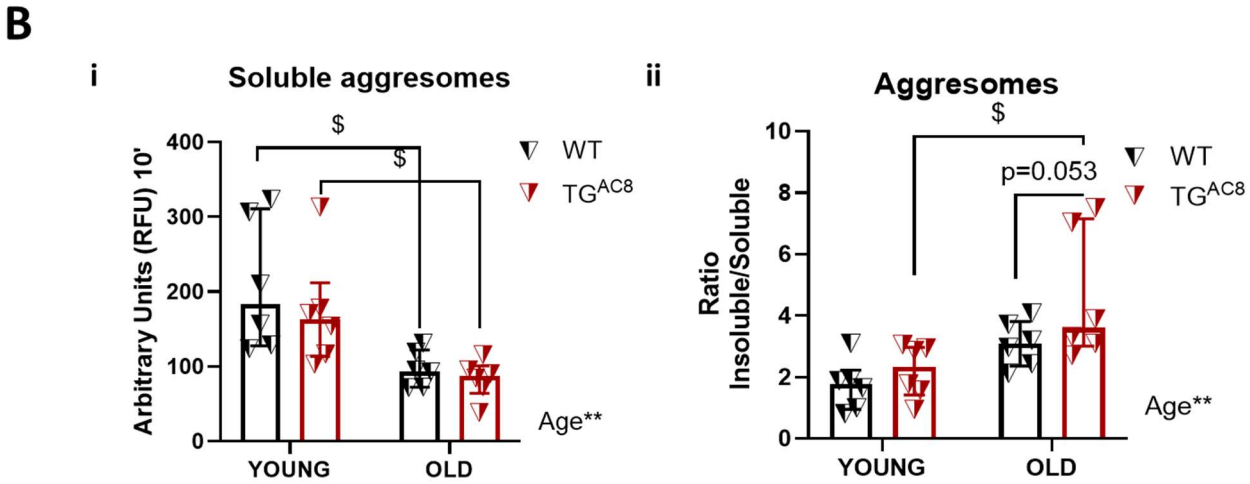

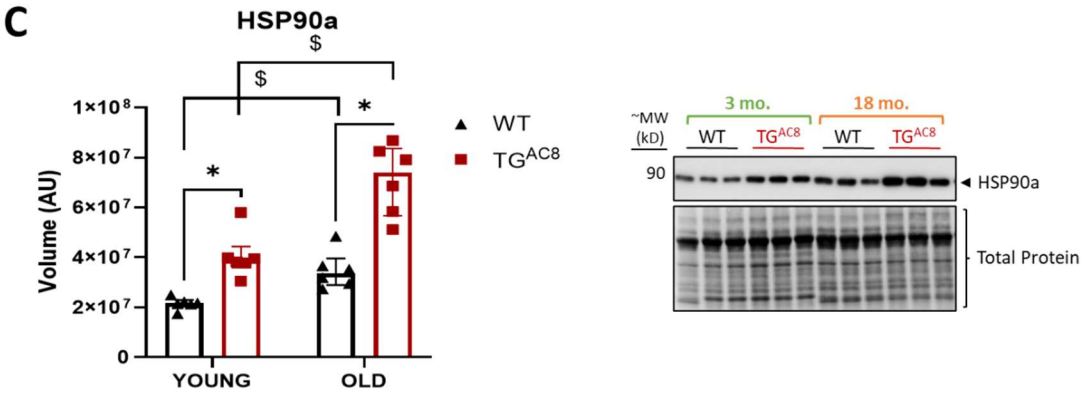

Total Word count without References ~12500

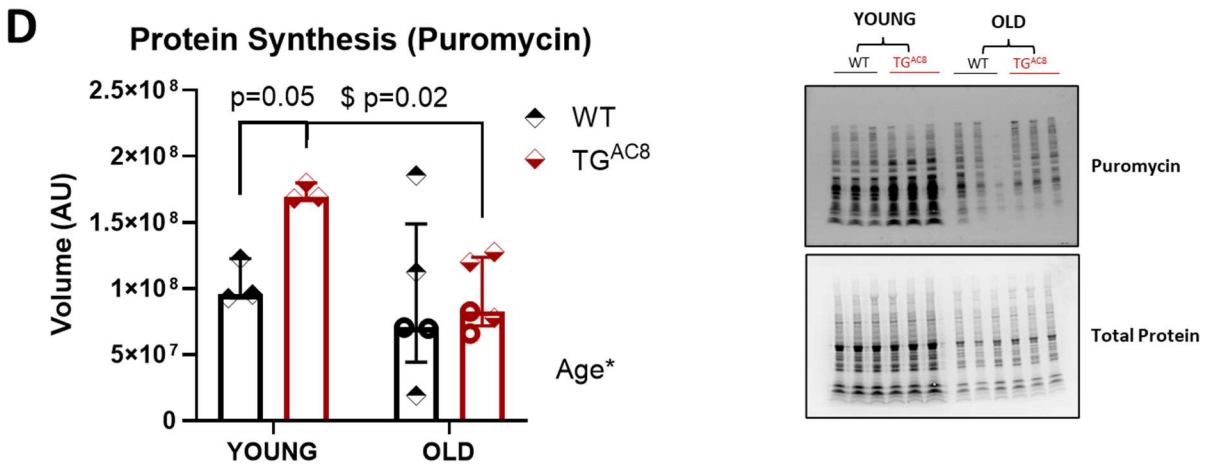

1213

1214 **FIGURE 7**

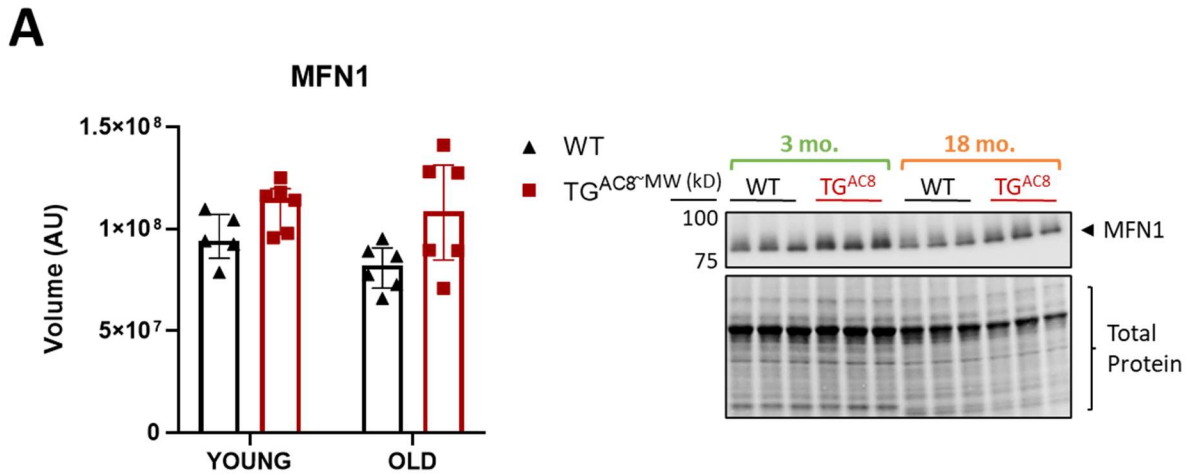

1215

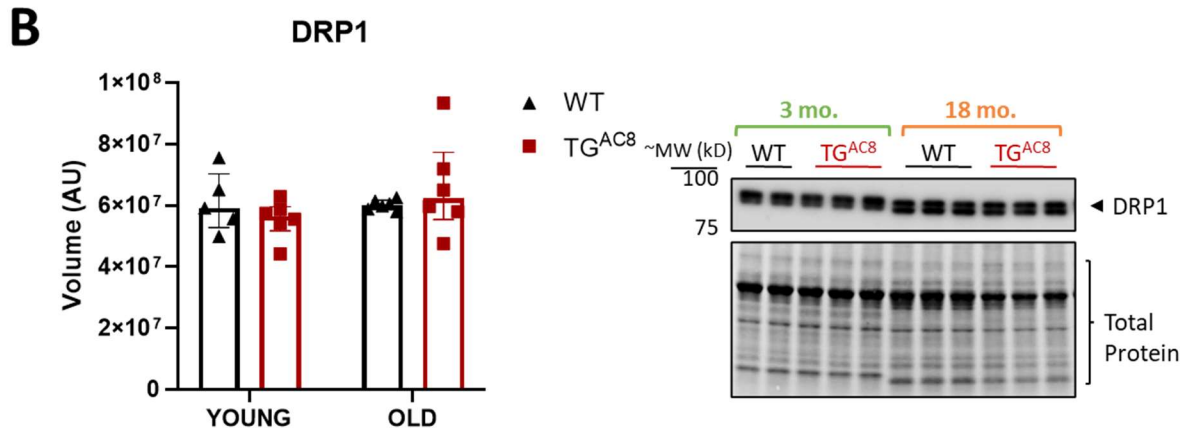

1216

Total Word count without References ~12500

C

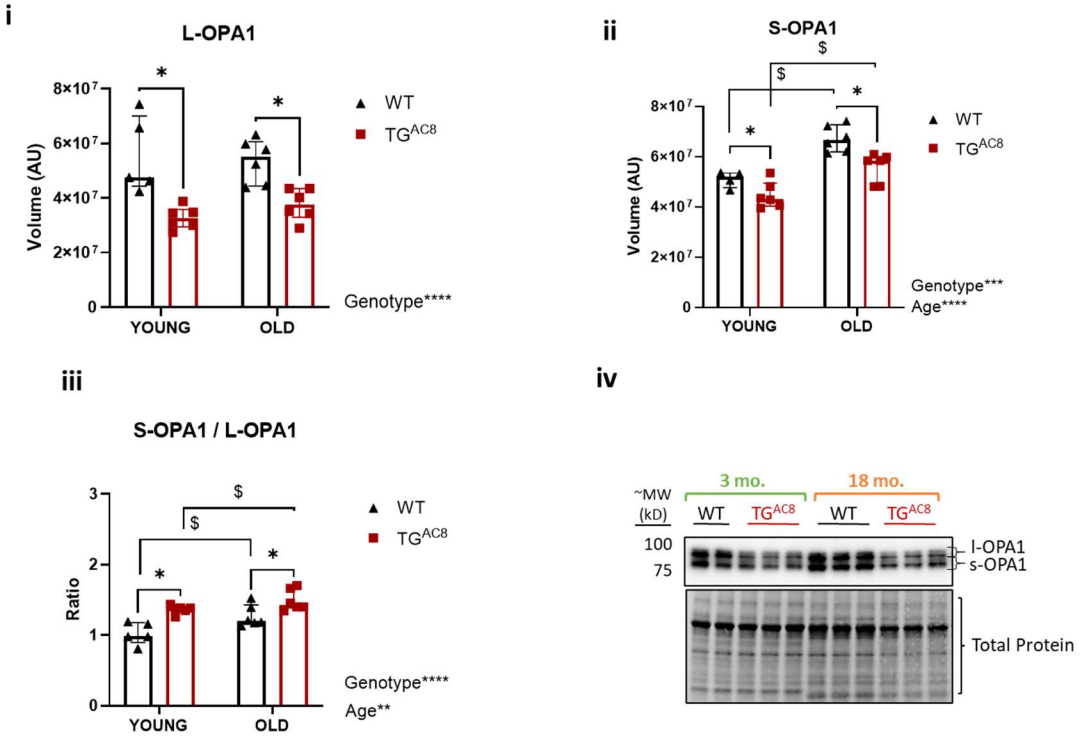

1217

D

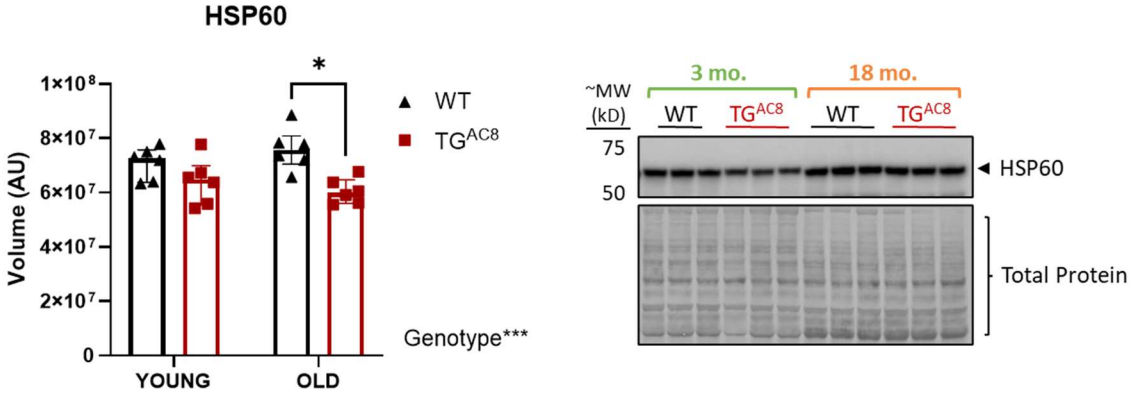

1218

Total Word count without References ~12500

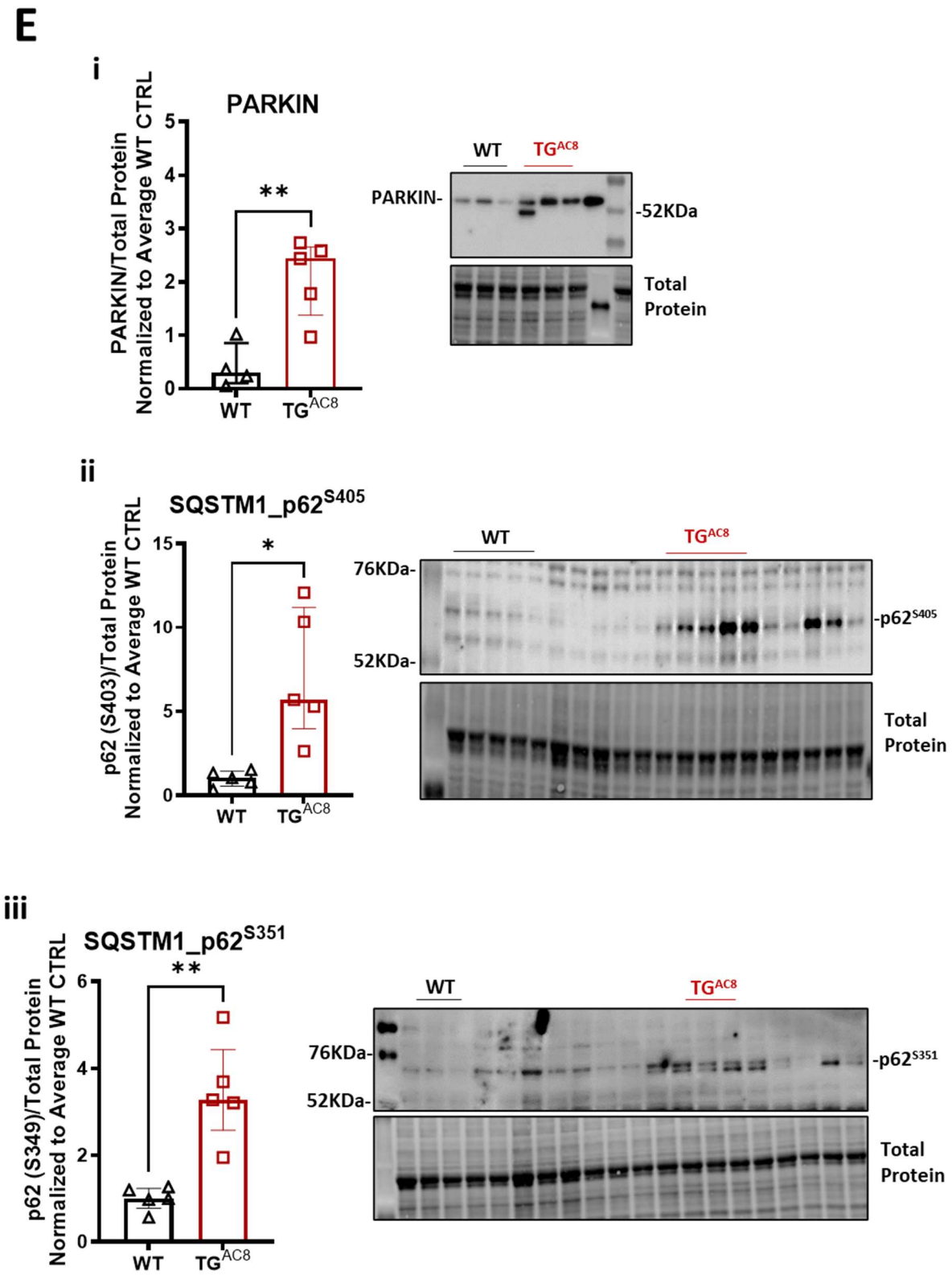

Total Word count without References ~12500

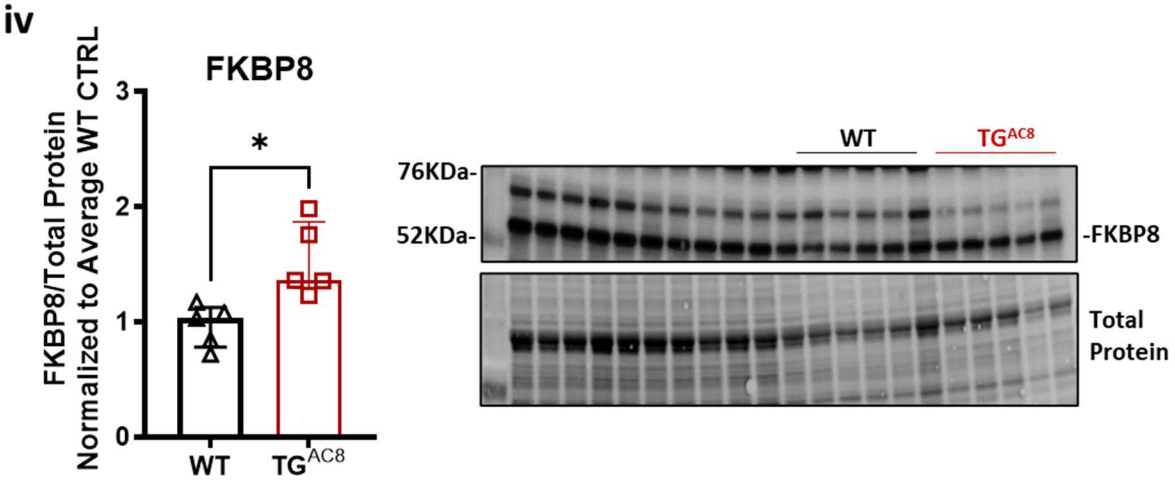

1221

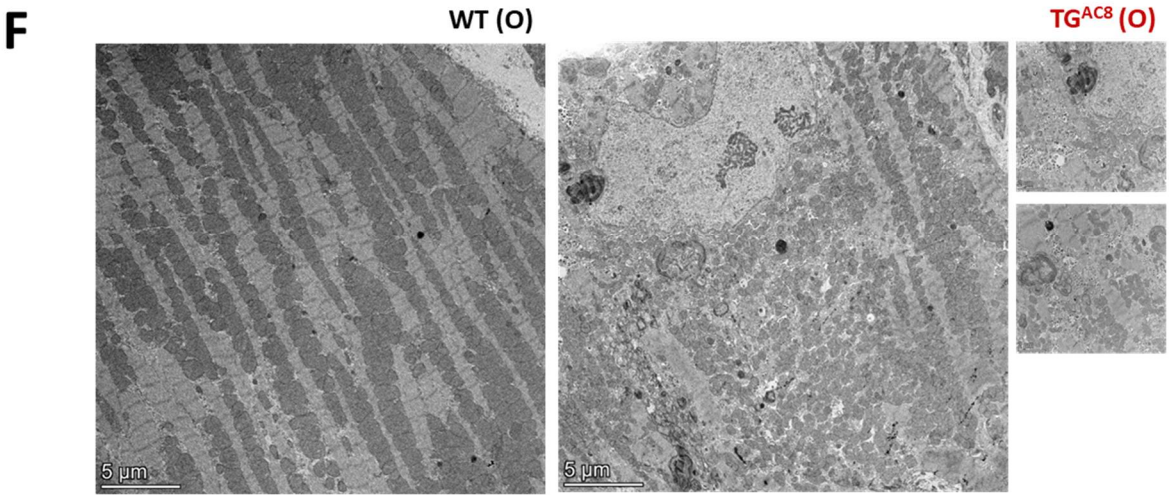

1222

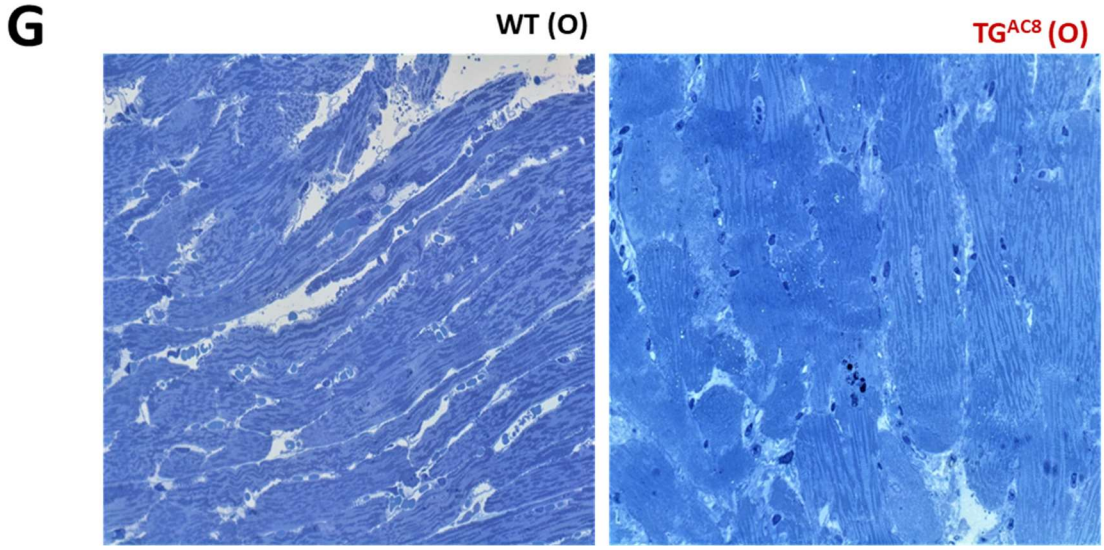

1223

Total Word count without References ~12500

1224 **FIGURE 8**

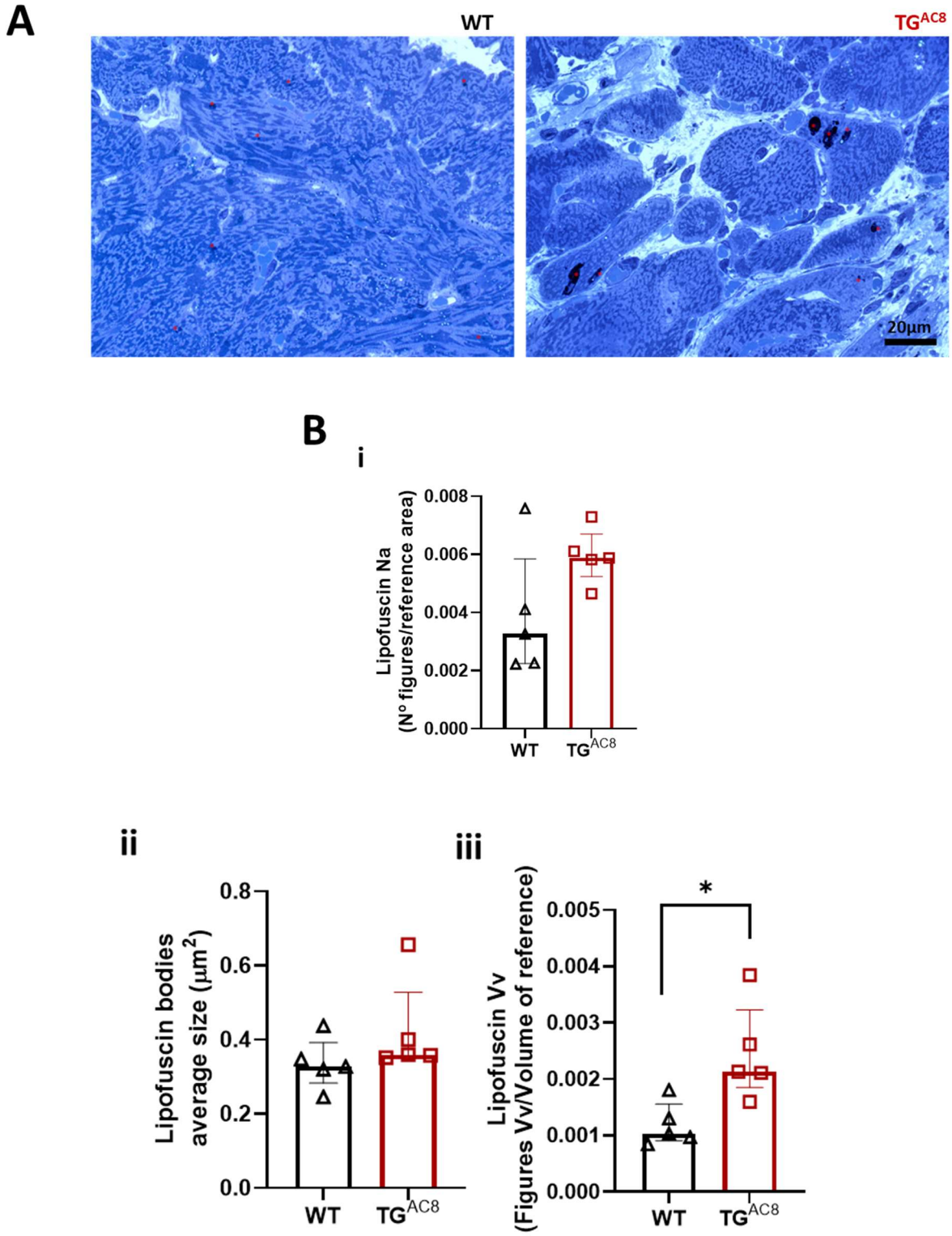

1225

1226

1227

Total Word count without References ~12500

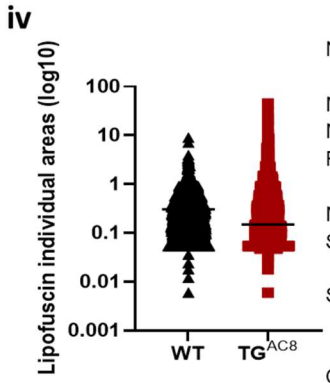

	WT	TG^{AC8}
Number of values	3188	4875
Minimum	0.006000	0.006000
Maximum	8.940	44.76
Range	8.934	44.75
Mean	0.3060	0.4133
Std. Deviation	0.4190	1.181
Std. Error of Mean	0.007422	0.01692
Coefficient of variation	137.0%	285.7%

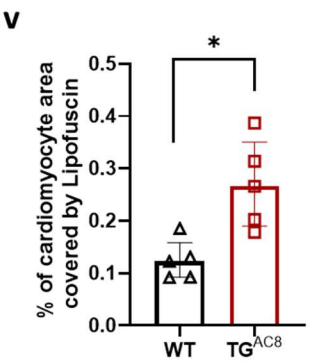

1228

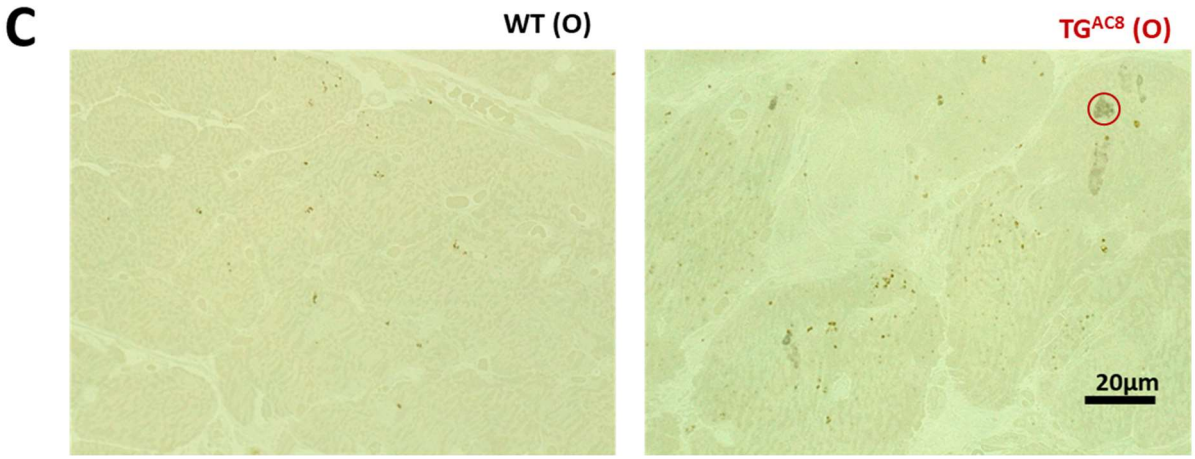

1229

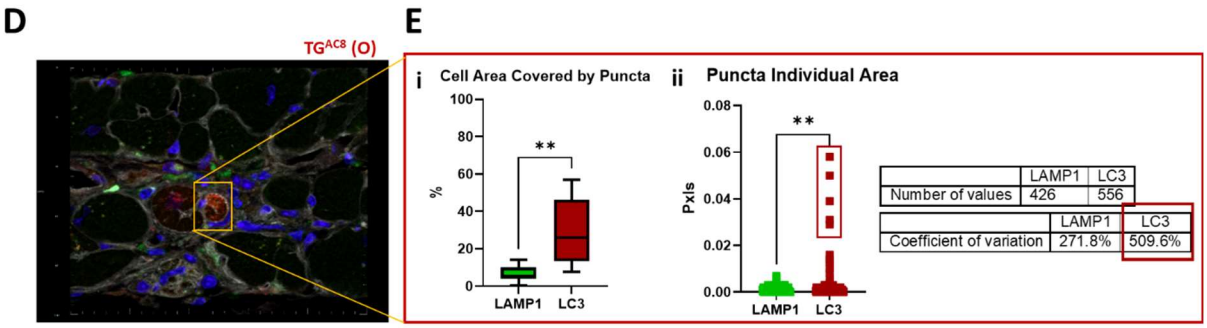

	LAMP1	LC3
Number of values	426	556

	LAMP1	LC3
Coefficient of variation	271.8%	509.6%

1230

Total Word count without References ~12500

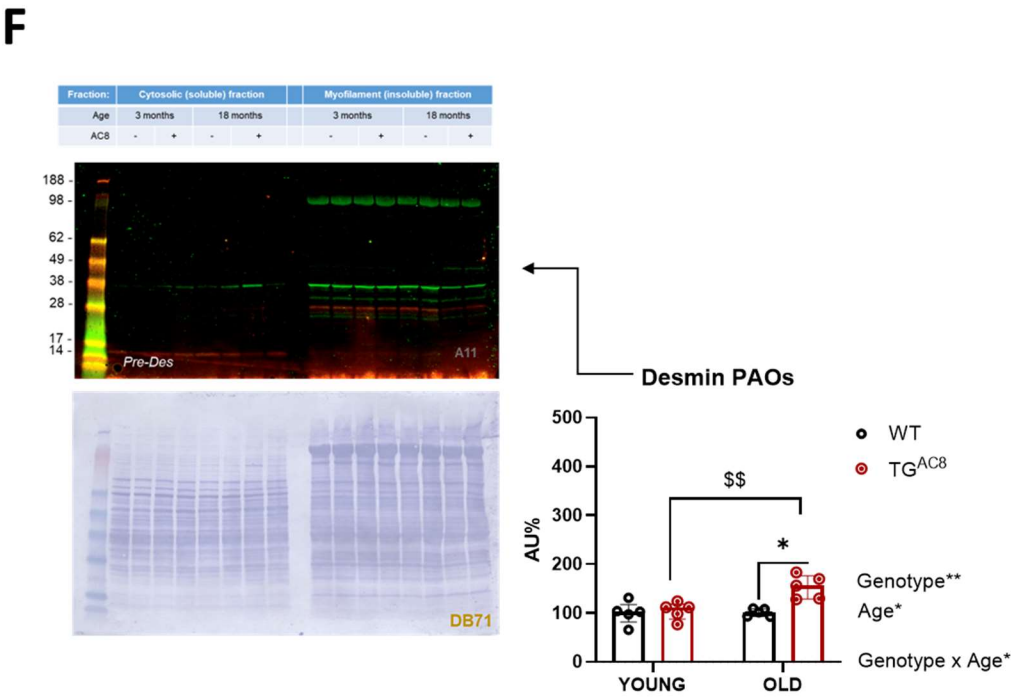

1231

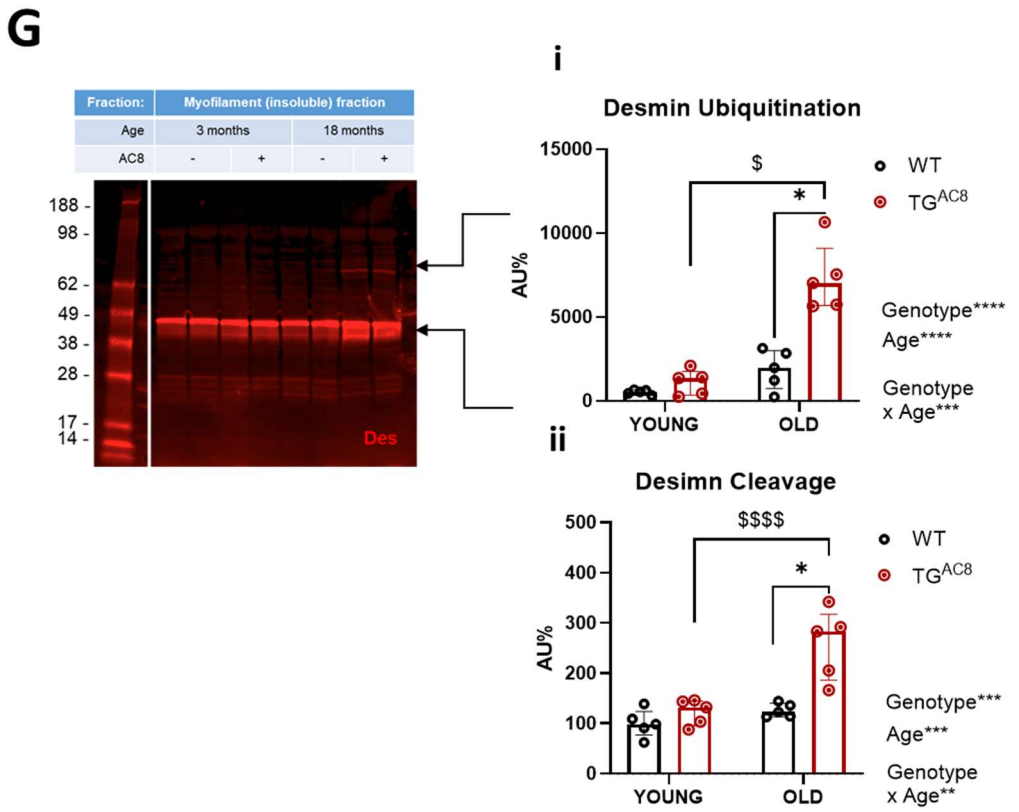

1232

Total Word count without References ~12500

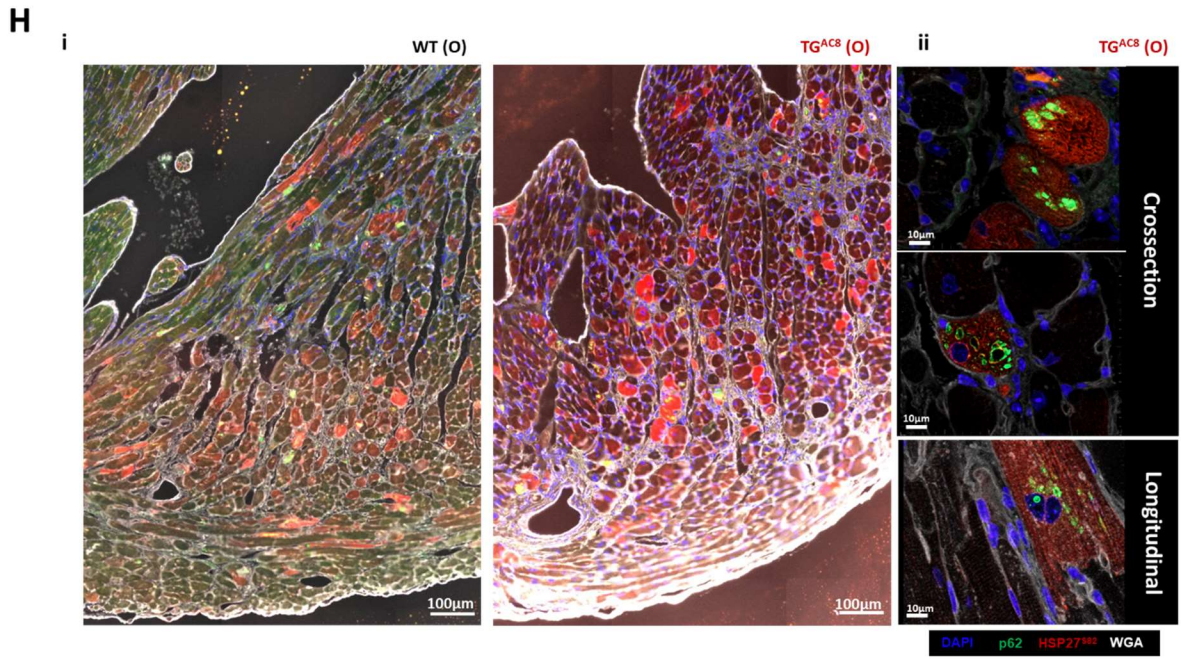

Figure 8

1233

1234 **FIGURE 9**

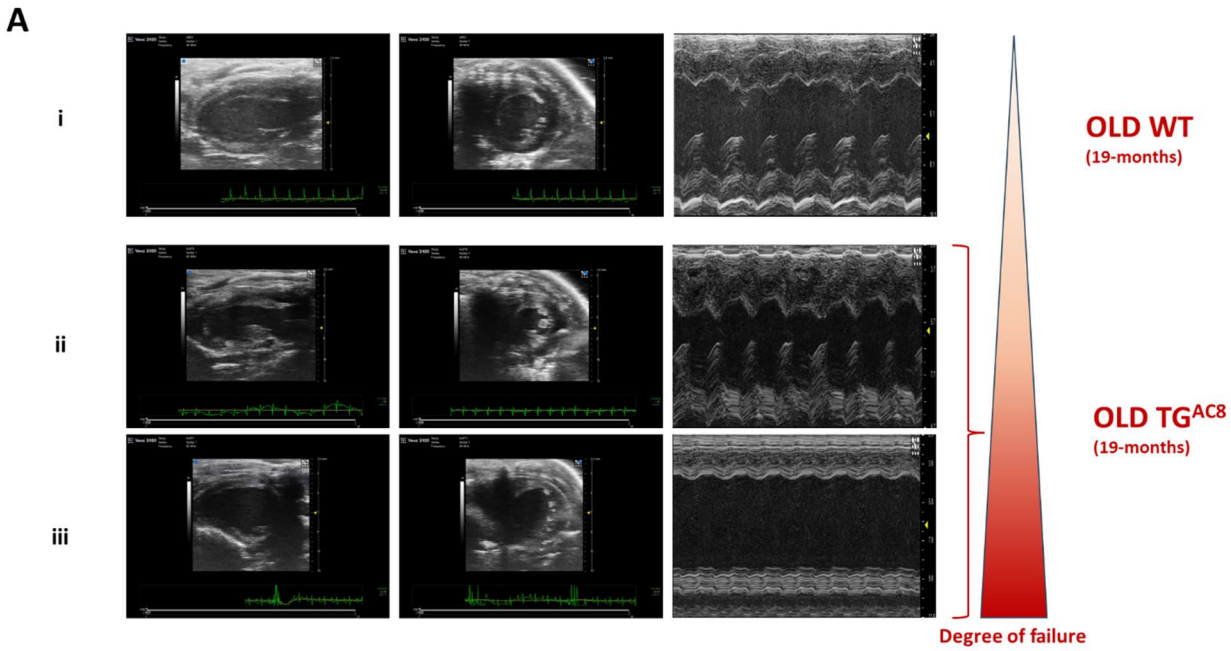

1235

Total Word count without References ~12500

B

i

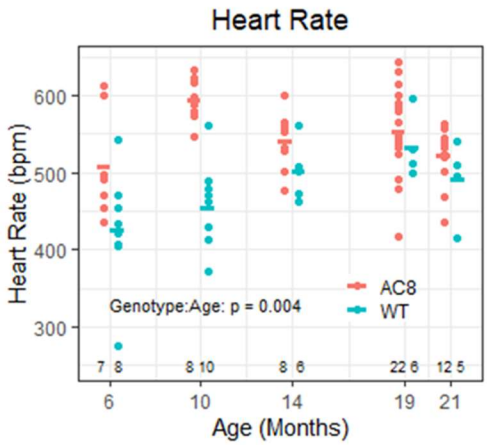

ii

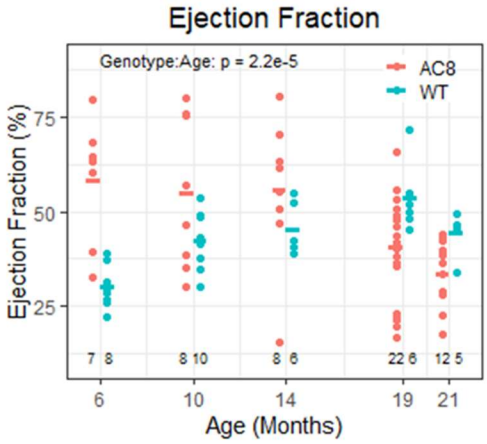

1236

C

i

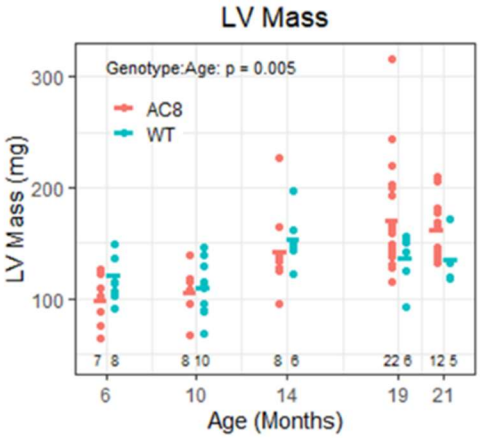

ii

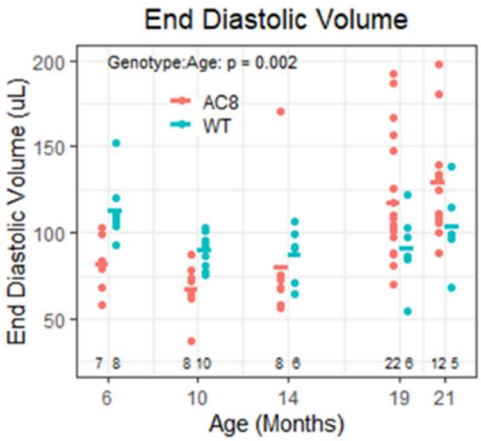

1237

iii

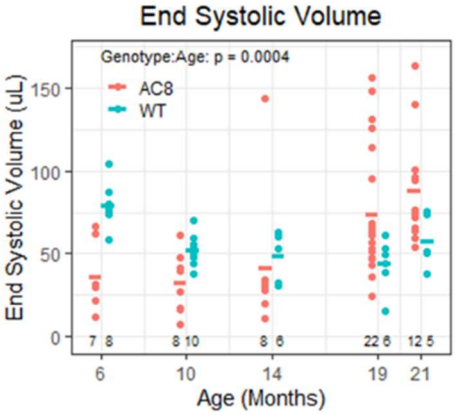

1238

1239 # FIGURE LEGENDS

1240 **Figure 1. Selective and non-selective autophagy are both upregulated in TG^{AC8} at**
1241 **3-4 months of age.**

1242 Bar graphs and Western blot analysis of autophagy markers LC3 and its phosphorylation
1243 in young TG^{AC8} and wild type littermates (WT) at 3-4 months of age (n=15 mice per
1244 group). Data are presented as the median ±interquartile range. **Ai**), LC3A; **Aii**), LC3B;
1245 **Bi**), LC3^{S12}; **Bii**), LC3^{T50}. **Ci**), p62; **Cii**), p62^{S405}; **C**), p62^{S351}; **D**), p62^{S405}/p62 ratio; **E**),
1246 p62^{S351}/p62 ratio. **Ai-ii**: A 3-way ANOVA with mixed-effect model for repeated
1247 measurements, followed by Original FDR method of Benjamini and Hochberg post-hoc
1248 multi-comparison test was used. **B and C**: Unpaired 2-tailed Student's tests with Welch's
1249 correction was used. Symbol * indicates significant ($p<0.05$) differences between
1250 genotypes (WT vs TG^{AC8}).

1251 **Figure 2. Lysosomal hydrolases are upregulated in TG^{AC8} at 3-4 months of age.**

1252 **A**), MA plot showing enrichment in the relative amount of lysosomal cathepsin obtained
1253 from OMICs data in TG^{AC8} at 3-4 months of age. **B**), Cathepsin L1 activity measured in
1254 TG^{AC8} and WT littermates at 3-4 months of age (n=6 mice per group). Activity was
1255 measured at V_{max}, and it is plotted as emitted fluorescence per mL, per mg of protein. **C**),
1256 Bar graphs and Western blot analysis of the lysosomal acid phosphatase, ACP2 (n=15
1257 mice per group). Unpaired 2-tailed Student t test was used in **B** and unpaired 2-tailed
1258 Student t test with Welch's correction was used in **C**. Data are presented as the median
1259 ±interquartile range. Symbol * indicates significant ($p<0.05$) differences between
1260 genotypes (WT vs TG^{AC8}).

1261 **Figure 3. Autophagic flux is enhanced in TG^{AC8} at 3-4 months of age.**

1262 TG^{AC8} and WT at 3-4 months of age were treated by intraperitoneal administration (IP) of
1263 chloroquine (CQ) (50 mg/kg) or saline, and LVs were collected 3 hours after drug
1264 administration and snap-frozen for analysis of autophagy markers LC3, p62, ATG16L1,
1265 ATG4B, ALIX and FKBP8 (n=5 mice per group). Bar graphs and Western blot analysis of
1266 **Ai**), LC3A; **Aii**), LC3B; **Aiii**), p62; **Bi**), ATG16L1; **Bii**), ATG4B; **Biii**), ALIX; **Biv**), FKBP8;
1267 **Ci**), TEM representative micrographs and **Cii**) Paired quantification of macroautophagic
1268 figures, normalized to average WT saline. **Ai-ii**: A three-way ANOVA with repeated
1269 measurements, followed by Original FDR method of Benjamini and Hochberg post-hoc
1270 multi-comparison test was used. **Aiii and B**: A two-way ANOVA, followed by Original FDR
1271 method of Benjamini and Hochberg post-hoc multi-comparison test was used. **C**:
1272 Unpaired 2-tailed Student t test with Welch's correction was used. Data are presented as
1273 the median ±interquartile range. Symbols * # indicate significant ($p<0.05$) differences:
1274 between genotypes* (WT vs TG^{AC8}), between treatments# (CQ vs saline).

1275 Ai), LC3A; Aii), LC3B; Aiii), p62; Bi), ATG16L1; Bii), ATG4B; Biii), ALIX; Biv), FKBP8; Ci),
1276 TEM representative micrographs and Cii) Paired quantification of macroautophagic
1277 figures, normalized to average WT saline. Ai-ii: A three-way ANOVA with repeated
1278 measurements, followed by Original FDR method of Benjamini and Hochberg post-hoc
1279 multi-comparison test was used. Aiii and B: A two-way ANOVA, followed by Original FDR
1280 method of Benjamini and Hochberg post-hoc multi-comparison test was used. C:
1281 Unpaired 2-tailed Student t test with Welch's correction was used. Data are presented as
1282 the median ±interquartile range. Symbols * # indicate significant ($p<0.05$) differences:
1283 between genotypes* (WT vs TGAC8), between treatments# (CQ vs saline).

1284 **Figure 4. Autophagy failure in aged TG^{AC8} increases inclusions' aggregation and**
1285 size heterogeneity.
1286 (**A**) Bar graphs and Western blot analysis of autophagy markers LC3, and (**B**) bar graphs
1287 showing event quantification of macroautophagic figures (TEM) and (**C**) of endogenous
1288 LC3^{+}- and LAMP1^{+}-puncta (IHC) in TG^{AC8} and WT at 3-4 months (n=3-5 mice per group)
1289 and 21 months of age (n=5 mice per group) LAMP1^{+}-puncta are in green, LC3^{+}-puncta
1290 are in red. **Ai**), LC3A; **Aii**), LC3B. Quantification of early events **Bi**), number of per
1291 reference area; **Bii**) volume per cell volume, and quantification of late events; **Biii**),
1292 number of per reference area; **Biv**) volumes per cell volume; **Bv**) TEM representative
1293 images. **Ci**), IHC representative images; **Cii**), quantification of LAMP1^{+}-puncta count;
1294 **Ciii**), quantification of LAMP1^{+}-puncta average size; **Civ**) quantification of the % of cell
1295 area covered by LAMP1^{+}-puncta; **Cv**), quantification of LC3^{+}-puncta count; **Cvi**),
1296 quantification of LC3^{+}-puncta average size; **Cvii**) quantification of the % of cell area
1297 covered by LC3^{+}-puncta; **Di**), Range of LAMP1^{+}- and LC3^{+}-puncta average size in TG^{AC8}
1298 and WT at 21 months of age; **Dii**), Range of the % of cell area covered by LAMP1^{+}- and
1299 LC3^{+}-puncta in TG^{AC8} and WT at 21 months of age; **Ei-ii**) LAMP1^{+}- and LC3^{+}-puncta size
1300 distribution in TG^{AC8} and WT at 21 months of age. **A**: A three-way ANOVA with repeated
1301 measurements, followed by Original FDR method of Benjamini and Hochberg post-hoc
1302 multi-comparison test was used. **B**, **C**, and **D**, A two-way ANOVA, followed by Original
1303 FDR method of Benjamini and Hochberg post-hoc multi-comparison test was used. Data
1304 are presented as the median ±range in **A**, and as median ±interquartile range in all others.
1305 Symbols * $ indicate significant ($p<0.05$) differences: between genotypes* (WT vs TG^{AC8}),
1306 between ages$^{\$}$ (young vs old) and between markers$^{\#}$ (LAMP1 vs LC3).

1307 **Figure 5. Accelerated autophagic flux in young TGAC8 heart becomes maladaptive**
1308 **and insufficient in old age, leading to more severe suppression of the autophagy**
1309 **program.**

1310 **A-B** TG^{AC8} and WT littermates at 21 months of age were treated by intraperitoneal
1311 administration (IP) with chloroquine (CQ) (50 mg/kg) or saline, and LVs (n=5 mice per
1312 group) were collected 3 hours after and snap-frozen for analysis of autophagy markers
1313 LC3, p62, ATG16L1, ALIX, FKBP8 and ATG4B. Bar graphs and Western blot analysis of
1314 **Ai**), LC3A; **Aii**), LC3B; **Aiii**), total p62; **Bi**), ATG16L1; **Bii**),.ALIX; **Biii**), FKBP8;
1315 **Biv**),.ATG4B; **C** Total TFEB protein levels in cytosolic and nuclear enriched fractions in
1316 young (3-4 months of age) and old (20 months of age) TG^{AC8} and WT littermates (n=5
1317 mice per group). **Ci**), Total TFEB in nuclear fraction; **Cii**), Total TFEB in cytosolic fraction;
1318 **Ciii**), TFEB Nuclear/TFEB Cytosol ratio; **Civ**), Representative WB images of nuclear and
1319 cytoplasmic extracts. **D** Quantification of 14-3-3s transcripts in young and old TG^{AC8} and
1320 WT littermates using the primers indicated in Supplemental Table 2 (n=3-5 mice per
1321 group). HPRT was used as housekeeping gene. **Di**), YWHAB transcript **Dii**), YWHAG
1322 transcript; **Diii**), YWHAE transcript; **Dii**), YWHAZ transcript; **Dv**), YWHAH transcript; **Dvi**),
1323 YWHAQ transcript and **Dvii**), SFN transcript. **Ai-ii**: A three-way ANOVA with repeated
1324 measurements, followed by Original FDR method of Benjamini and Hochberg post-hoc
1325 multi-comparison test was used. **Aiii, B, C and D**, A two-way ANOVA, followed by Original
1326 FDR method of Benjamini and Hochberg post-hoc multi-comparison test was used. Data
1327 are presented as the median ±interquartile range except for qPCR, which are presented
1328 as the mean ±SEM. Symbols * $ # indicate significant (<0.05) differences between:

1329 genotypes* (WT vs TG^{AC8}), between ages$ (young vs old), between treatments# (CQ vs
1330 saline).

1331 **Figure 6. Proteostasis dysregulation is more severe in old TGAC8 heart.**

1332 Bar graphs of **A**), Proteasome activity assessment and of **B**), Aggregates quantification
1333 in soluble fractions and the ratio of insoluble vs soluble protein aggregates in young (3-4
1334 months) and old (17-18 months) TG^{AC8} and age-matched WT (n=3-5 per group). **C**) Bar
1335 graphs and Western blot analysis of the stress marker HSP90. **D**) TG^{AC8} and WT at 19
1336 months of age (n=5 mice per group) were treated by intraperitoneal administration (IP)
1337 with puromycin (0.022g/g mouse) according to the SUnSET method, and LVs were
1338 collected 30 minutes after drug administration and snap-frozen for puromycin analysis.
1339 **A-D**, A two-way ANOVA, followed by Original FDR method of Benjamini and Hochberg
1340 post-hoc multi-comparison test was used. Data are presented as the median
1341 ±interquartile range. Symbols * $ # indicate significant (<0.05) differences between
1342 genotypes* (WT vs TG^{AC8}), between ages$ (young vs old).

1343 **Figure 7. PQC insufficiency leads to mitochondria dysfunction and disruption of**
1344 **the mitochondrial network in old TGAC8 heart.**

1345 Bar graphs and Western blot analysis of mitochondrial markers in young (3-4 months)
1346 and old (19 months) TG^{AC8} and WT littermates (n=5 mice per group). **A**), MFN1; **B**),
1347 DRP1; **Ci**) L-OPA1; **Cii**) S-OPA1; **Ciii**) S-OPA/L-OPA1 ratio; **Civ**) representative WB
1348 images; **D**) HSP60; **Ei**) PARKIN ; **Eii**) $p62^{S405}$; **Eiii**) $p62^{S351}$; **Eiv**) FKBP8; **F**) representative
1349 TEM and **G**) light microscopy images of semithin sections showing disrupted
1350 mitochondrial network. **A-D**: A two-way ANOVA, followed by Original FDR method of
1351 Benjamini and Hochberg post-hoc multi-comparison test was used. **E**: Unpaired 2-tailed

1352 Student t test with Welch's correction was used. Data are presented as the median
1353 ±interquartile range. Symbols * $ indicate significant (<0.05) differences between
1354 genotypes* (WT vs TG^{AC8}), between ages$ (young vs old).

1355 **Figure 8. Proteostasis dysregulation from PQC insufficiency leads to increased**
1356 **lipofuscin accumulation and deposition of desmin Pre-Amyloid Oligomers (PAOs)**
1357 **in aged TGAC8.**

1358 Bar graphs representing the quantification of undigested material (LF and desmin) in old
1359 TG^{AC8} and WT LVs (n=5 per group); **A**), representative semi-thin staining of lipofuscin
1360 bodies; **Bi**), number of lipofuscin figures per reference area; **Bii**), average size of
1361 lipofuscin bodies; **Biii**), volume of figures per volume of reference area; **Biv**), violin plot
1362 showing the more aberrant sizes of lipofuscin bodies; **Bv**), percentage of cardiomyocyte
1363 area covered by lipofuscin; **C**), representative image of Palade-staining of TEM semi-thin
1364 sections showing the presence of brown-to-blueish/black pigments in old TG^{AC8}; **D**),
1365 representative image of IHC sections showing cardiomyocytes covered with $LC3^{+}$-
1366 inclusions in old TG^{AC8}; **Ei**), quantification of cell area covered by $LAMP1^{+}$- and $LC3^{+}$-
1367 inclusions in old TG^{AC8}; **Eii**), quantification $LAMP1^{+}$- and $LC3^{+}$-puncta individual areas in
1368 old TG^{AC8}; **F**), soluble and insoluble (myofilament-enriched) fractions probed with the A11
1369 antibody for pre-amyloid oligomers (top), and total protein staining with Direct
1370 Blue71/DB71 (bottom), with relative densitometry analysis; **G**), insoluble (myofilament-
1371 enriched) fractions probed with the desmin antibody, and relative densitometry for **i**)
1372 ubiquitinated and **ii**) cleaved desmin proteoforms; **H**), representative IHC staining old
1373 TG^{AC8} and WT littermates with $HSP27^{S86}$ (red), p62 (green), and wheat germ agglutinin
1374 WGA (white) while nuclei are in blue (DAPI); **B-E**: Unpaired 2-tailed Student t test with

1375 Welch's correction was used. **F-G**: A two-way ANOVA, followed by Original FDR method
1376 of Benjamini and Hochberg post-hoc multi-comparison test was used. Data are presented
1377 as the median ±interquartile range. Symbols * $ indicate significant differences ($p<0.05$)
1378 between genotypes* (WT vs TG^{AC8}), between ages$ (young vs old).

1379 **Figure 9. Heart damage by PQC insufficiency and mitochondrial dysfunction leads**
1380 **to heart failure contributing to TGAC8 accelerated cardiac aging.**

1381 **A**), Representative images of echocardiograms in old TG^{AC8} and WT littermates (N=6-15
1382 mice per group). Echocardiographic parameters **Bi**), heart rate (HR); **Bii**), ejection fraction
1383 (EF); **Ci**), left ventricular mass (LVM); **Cii**), end diastolic volume (EDV); **Ciii**), end systolic
1384 volume (ESV). Data are presented as mean along with all the data points. 2-way mixed
1385 ANOVAs was employed for the analyses. Statistical significance was assumed at $p<0.05$.

1386 # EXTENDED DATA FIGURE 2

Relative Cathepsin Expression in YOUNG WT/TG^{AC8}

Protein Name	Symbol	log2(average expression)	log2(fold change)	p-value
Lysosomal protective protein	Ctsa	0.017702383	0.216799716	0.004513026
Cathepsin B	Ctsb	0.022381593	0.120723106	0.0254094
Dipeptidyl peptidase 1	Ctsc	0.033052876	0.167723218	0.028205766
Cathepsin D	Ctsd	0.011868307	0.164671994	0.033523037
Cathepsin F	Ctsf	0.011385877	0.134158334	0.03797905
Pro-cathepsin H	Ctsh	-0.032543079	0.171483139	0.115212134
Cathepsin L1	Ctsl	-0.002089995	0.082015669	0.037159714
Cathepsin S	Ctss	0.028762851	0.317183952	0.007053072
Cathepsin Z	Ctsz	0.014751699	0.403327276	0.008561447

1387

Total Word count without References ~12500

EXTENDED DATA FIGURE 3

S1

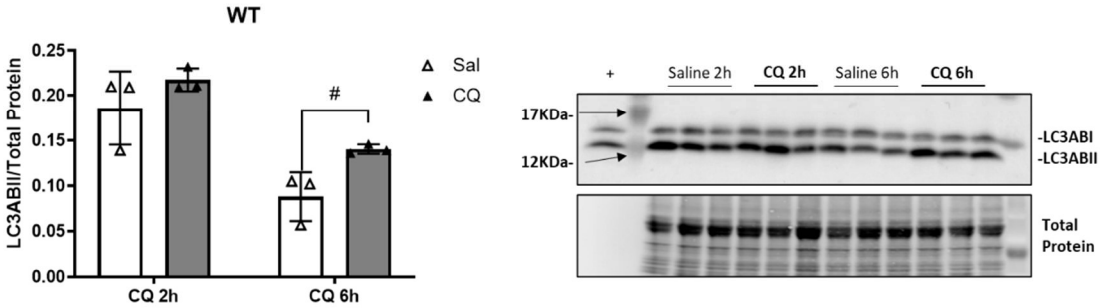

EXTENDED DATA FIGURE 4

S2

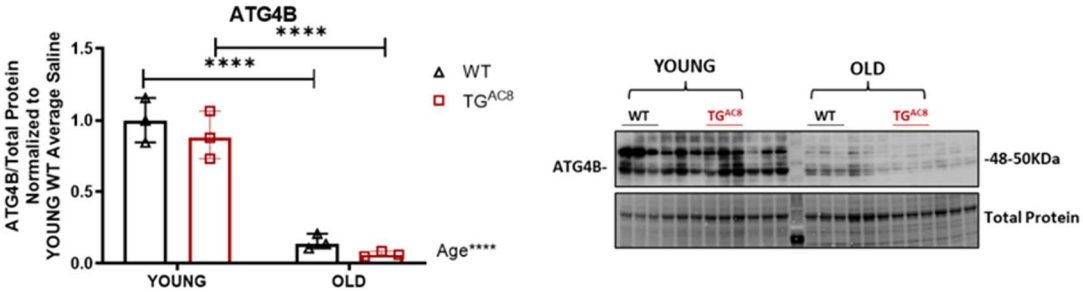

Total Word count without References ~12500

EXTENDED DATA FIGURE 5

S3

i

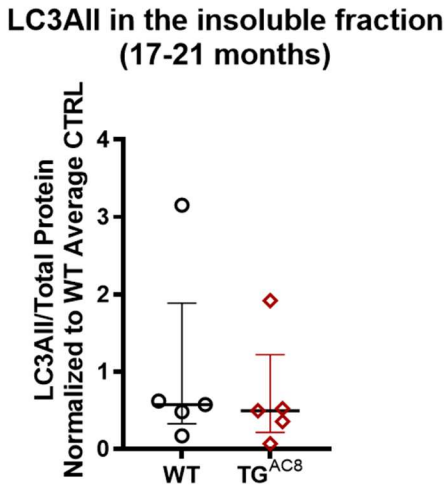

ii

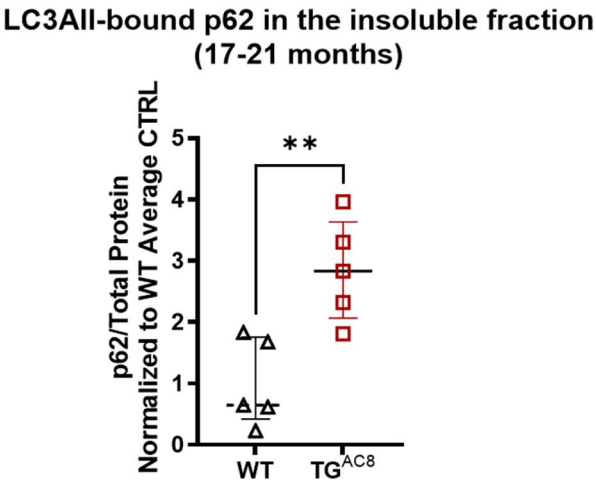

iii

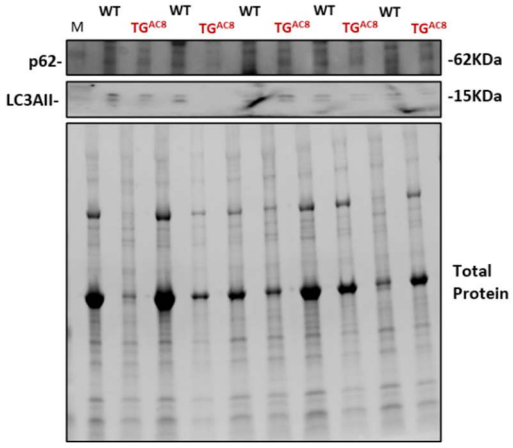

Total Word count without References ~12500

S4

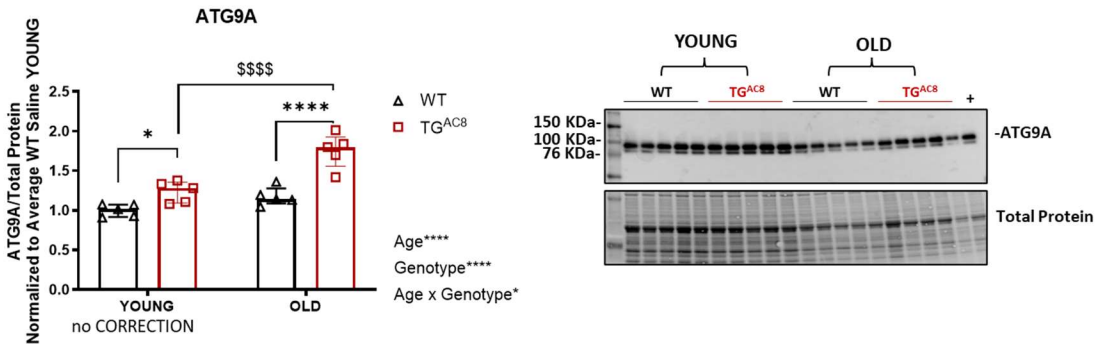

1395

S5

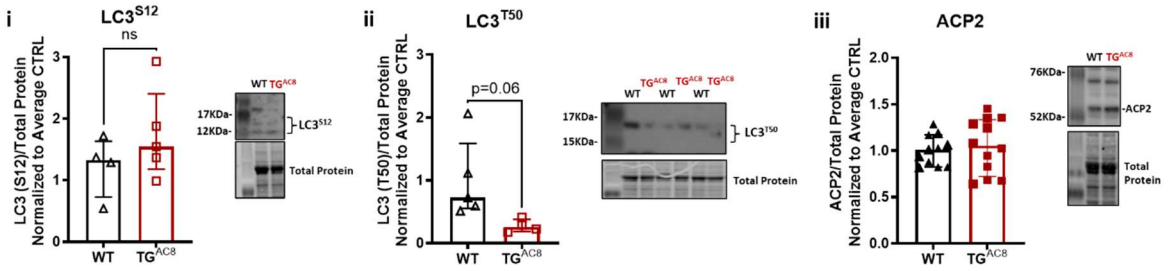

1396

S6

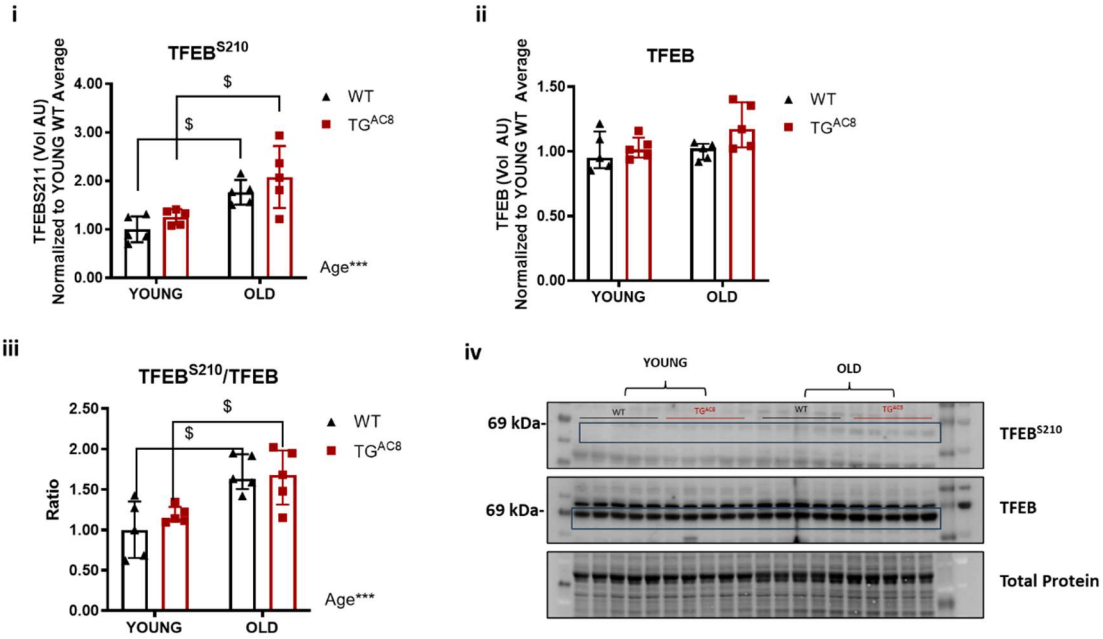

1397

1398 # EXTENDED DATA FIGURE LEGENDS

1399 **Extended Data Figure 2 -Table. Relative Cathepsin Expression in TG^{AC8} and WT**
1400 **littermates at 3-4 months of age.**

1401 MA plot of relative cathepsin expression (proteOMICs) in TG^{AC8} LVs at 3-4 months of age.

1402 **Extended Data Figure 3 - Figure S1. Chloroquine (CQ) time-course in WT at 3-4**
1403 **months of age.**

1404 Bar graphs and Western blot analysis of LC3II in WT (3-4 months of age) treated by
1405 intraperitoneal administration (IP) of chloroquine (CQ) (50 mg/kg) or saline. LVs were
1406 collected 2 hours and 6 hours after drug administration and snap-frozen (n=3 mice per
1407 group). A two-way ANOVA, followed by Original FDR method of Benjamini and Hochberg
1408 post-hoc multi-comparison test was used. Data are presented as the median
1409 ±interquartile range. # indicates significant ($p<0.05$) differences between treatments (CQ
1410 vs saline).

1411 **Extended Data Figure 4 - Figure S2. ATG4B is reduced with age in TG^{AC8} and WT**
1412 **littermates.**

1413 Bar graphs and Western blot analysis of ATG4B in TG^{AC8} and WT at 3-4 months (n=3-5
1414 mice per group) and 21 months of age (n=5 mice per group). A two-way ANOVA, followed
1415 by Original FDR method of Benjamini and Hochberg post-hoc multi-comparison test was
1416 used. Data are presented as the median ±range. Symbols * indicate significant ($p<0.05$)
1417 differences between ages (young vs old).

1418 **Extended Data Figure 5 - Figure S3. Assessment of LC3AII and *LC3AII-bound* p62**
1419 **in insoluble fractions (pellets) in aged TG^{AC8} and WT littermates (17-21 months of**
1420 **age)**

1421 Pellets from total protein lysates (RIPA) were lysed with WB loading buffer and protein
1422 resolved with SDS-PAGE. Proteins were then transferred onto PVDF and probed with
1423 LC3A and p62 antibodies, as indicated in the WB methods section. N=5 mice per group,
1424 TG^{AC8} and WT littermates (21 months of age). Unpaired 2-tailed Student t test with
1425 Welch's correction was used. Data are presented as the median ±interquartile range.
1426 Symbols * indicate significant ($p<0.05$) differences between genotypes (WT vs TG^{AC8}). **i**),
1427 LC3AII; **ii**), LC3AII-bound p62; **iii**), Paired WB blot image.

1428 **Extended Data Figure 5 - Figure S4. ATG9A is increased in old TG^{AC8} heart.**

1429 Bar graphs and Western blot analysis of ATG9A in TG^{AC8} and WT at 3-4 months and 21
1430 months of age (n=5 mice per group). A two-way ANOVA, followed by Original FDR
1431 method of Benjamini and Hochberg post-hoc multi-comparison test was used. Data are
1432 presented as the median ±interquartile range. Symbols * $^{\$}$ indicate significant ($p<0.05$)
1433 differences between genotypes* (WT vs TG^{AC8}), between ages$^{\$}$ (young vs old).

1434 **Extended Data Figure 5 - Figure S5. $LC3^{S12}$, $LC3^{T50}$ and ACP2 assessment.**

1435 Bar graphs and Western blot analysis of autophagy markers in old (19 months) TG^{AC8}
1436 and WT littermates (n=5-15 mice per group) **i**), $LC3^{S12}$; **ii**), $LC3^{T50}$; **iii**) ACP2. Unpaired 2-
1437 tailed Student t test with Welch's correction was used. Data are presented as the median
1438 ±interquartile range.

1439 **Extended Data Figure 5 - Figure S6. TFEB^{S210} and its ratio to total TFEB increase**
1440 **with aging both in TG^{AC8} and age-matched WT littermates.**

1441 Bar graphs and Western blot analysis of TFEB and its phosphoform TFEB^{S210} in TG^{AC8}
1442 and WT at 3-4 months and 21 months of age (n=5 mice per group). **i**), TFEB^{S210}; **ii**), total
1443 TFEB; **iii**), TFEB^{S210}/TFEB ratio; **iv**), WB representative image. A two-way ANOVA,
1444 followed by Original FDR method of Benjamini and Hochberg post-hoc multi-comparison
1445 test was used. Data are presented as the median ±interquartile range. Symbols $^{\$}$ indicate
1446 significant ($p<0.05$) differences between ages (young vs old).

1447 # SUPPLEMENT DATA – TABLE 1

Primary Antibodies used in WB analyses

Target Protein	Company	Cat. No.	Dilution
ACP2	Proteintech	15236-1-AP	1:1000
ALIX/PDCD6IP	Proteintech	12422-1-AP	1:1000
ATG16L1	Abcam	ab187671	1:1000
ATG4B	Abcam	ab199537	1:1000
ATG9A	Abcam	ab108338	1:1000
DRP1	Cell Signaling Technology	8570	1:1000
FKBP8	ThermoFisher Scientific	PA5-96573	1:500
HSP60	Abcam	ab190828	1:1000
HSP90a	ThermoFisher Scientific	PA3-013	1:1000
LC3A	Abcam	ab52628	1:1000
LC3B	Novus Biologicals	NB100-2220	1:1000
LC3AB	Cell Signaling Technology	4108	1:1000
$LC3^{S12}$	Bio Vision	6951	1:1000
$LC3^{T50}$	Abcam	ab204297	1:1000
MFN1	Abcam	ab221661	1:1000
OPA1	ThermoFisher Scientific	MA5-16149	1:1000
p62/sequestosome 1	Abcam	ab56416	1:1000
$p62^{S349}$	Cell Signaling Technology	16177	1:1000
$p62^{S403}$	Cell Signaling Technology	39786	1:1000
PARKIN	ThermoFisher Scientific	39-0900	1:1000
Puromycin	Sigma	MABE343	1:25000
TBP	Cell Signaling Technology	8515	1:1000
TFEB	ThermoFisher Scientific	PA5-96632	1:1000
$TFEB^{S211}$	Cell Signaling Technology	37681	1:5000
Vinculin	Cell Signaling Technology	13901	1:10000

1448

Total Word count without References ~12500

1449 # SUPPLEMENT DATA – TABLE 2

Primers for qPCR		
Target Gene	**Sequence**	**Amplicon Size**
HPRT. F	CTTCCTCCTCAGACCGCTTTT	97bp
HPRT. R	CATAACCTGGTTCATCATCGCTAA	
YWHAB. F	GCGCTGAATTTCTCAGTCTTTTACT	96bp
YWHAB. R	CTCAGCAATCGCCTCATCAA	
YWHAE. F	TGAGGCGCCGCCATT	78bp
YWHAE. R	ACGGATGGAAGCGGATAGC	
YWHAH. F	ATCTGTATTGGCAGCACAGCTATT	77bp
YWHAH. R	GCCCATGAAGGTTTATCTGAAACT	
YWHAG. F	GCCAAGACCGCCTTCGA	83bp
YWHAG. R	TGCATGATCAGAGTGGAGTCCTT	
YWHAQ. F	GGCGATGATCGAAAACAAACA	80bp
YWHAQ. R	TGCATCTCCTTCTTGCTTATATCAA	
YWHAZ. F	AAGGCCTGGAGCACTTGTGA	84bp
YWHAZ. R	CAAGAGTGTGCACGCAGACA	
Sfn. F	CCGCAGAACCCAGCGTTA	65bp
Sfn. R	GACTGCGAGGATGGACAGACA	

1450

1451 # SUPPLEMENT DATA – TABLE 3

Autophagy Pathway (ProteOMICs) in YOUNG TG^{AC8} vs WT

Symbol	Entrez Gene Name	Entrez G	Expr Ot	Expr p-value
ATG3	autophagy related 3	Atg3	11.349	0.0153
ATG9A	autophagy related 9A	Atg9a	30.993	0.016
ATG13	autophagy related 13	Atg13	21.004	0.0255
BECN1	beclin 1	Becn1	14.637	0.000037
CTSA	cathepsin A	Ctsa	16.215	0.00451
CTSB	cathepsin B	Ctsb	8.728	0.0254
CTSC	cathepsin C	Ctsc	12.328	0.0282
CTSD	cathepsin D	Ctsd	12.091	0.0335
CTSF	cathepsin F	Ctsf	9.745	0.038
CTSS	cathepsin S	Ctss	24.59	0.00705
CTSV	cathepsin V	Ctsl	5.85	0.0372
CTSZ	cathepsin Z	Ctsz	32.255	0.00856
LAMP1	lysosomal associated membrane protein 1	Lamp1	9.427	0.0149
LAMP2	lysosomal associated membrane protein 2	Lamp2	17.389	0.00142
MAP1LC3A	microtubule associated protein 1 light chain 3 alpha	Map1lc3a	-45.27	0.0423
PIK3C3	phosphatidylinositol 3-kinase catalytic subunit type 3	Pik3c3	16.209	0.00709
PIK3R4	phosphoinositide-3-kinase regulatory subunit 4	Pik3r4	12.184	0.00452
RB1CC1	RB1 inducible coiled-coil 1	Rb1cc1	8.639	0.047
SQSTM1	sequestosome 1	Sqstm1	22.553	0.00374
STX17	syntaxin 17	Stx17	21.775	0.0379
ULK1	unc-51 like autophagy activating kinase 1	Ulk1	14.444	0.04

1452

1453 # SUPPLEMENT DATA – TABLE 4

Phagosome Formation Pathway (ProteOMICs) in YOUNG WT/TG^{AC8}

Symbol	Entrez Gene Name	Entrez Ge	Expr Ot	Expr p-v
FCER1G	Fc epsilon receptor Ig	Fcer1g	48.805	0.00259
FN1	fibronectin 1	Fn1	19.588	0.00179
FNBP1	formin binding protein 1	Fnbp1	13.954	0.000824
ITGA2	integrin subunit alpha 2	Itga2	33.08	0.0254
ITGA5	integrin subunit alpha 5	Itga5	15.639	0.0272
ITGB2	integrin subunit beta 2	Itgb2	26.988	0.00412
MBL2	mannose binding lectin 2	Mbl2	21.695	0.0033
MRC1	mannose receptor C-type 1	Mrc1	26.984	0.0147
MRC2	mannose receptor C type 2	Mrc2	14.806	0.0297
PDIA3	protein disulfide isomerase family A member 3	Pdia3	13.635	0.00757
PIK3C3	phosphatidylinositol 3-kinase catalytic subunit type 3	Pik3c3	16.209	0.00709
PIK3CB	phosphatidylinositol-4,5-bisphosphate 3-kinase catalytic subunit bet	Pik3cb	13.834	0.0183
PIK3R1	phosphoinositide-3-kinase regulatory subunit 1	Pik3r1	8.8	0.0168
PIK3R4	phosphoinositide-3-kinase regulatory subunit 4	Pik3r4	12.184	0.00452
PLCG2	phospholipase C gamma 2	Plcg2	14.581	0.00011
PRKCI	protein kinase C iota	Prkci	23.901	0.0307
RAC2	Rac family small GTPase 2	Rac2	34.574	0.0489
RHOB	ras homolog family member B	Rhob	9.77	0.0167
RHOG	ras homolog family member G	Rhog	14.423	0.0036
RHOT1	ras homolog family member T1	Rhot1	8.752	0.0124
RHOT2	ras homolog family member T2	Rhot2	5.576	0.018
SYK	spleen associated tyrosine kinase	Syk	16.644	0.0139
VTN	vitronectin	Vtn	33.51	0.00764

1454

Total Word count without References ~12500

1455 # SUPPLEMENT DATA – TABLE 5

Phagosome Maturation Pathway (ProteOMICs) in YOUNG WT/TG^{AC8}

Symbol	Entrez Gene Name	Entrez Gene/	Expr Ot	Expr p-va
ATP6V0A1	ATPase H+ transporting V0 subunit a1	Atp6v0a1	11.991	0.0486
ATP6V0D1	ATPase H+ transporting V0 subunit d1	Atp6v0d1	16.118	0.00755
ATP6V1A	ATPase H+ transporting V1 subunit A	Atp6v1a	10.447	0.0188
ATP6V1B2	ATPase H+ transporting V1 subunit B2	Atp6v1b2	7.786	0.00817
ATP6V1F	ATPase H+ transporting V1 subunit F	Atp6v1f	8.739	0.047
ATP6V1H	ATPase H+ transporting V1 subunit H	Atp6v1h	12.95	0.00459
B2M	beta-2-microglobulin	B2m	16.883	0.0403
CANX	calnexin	Canx	10.298	0.00522
CTSA	cathepsin A	Ctsa	16.215	0.00451
CTSB	cathepsin B	Ctsb	8.728	0.0254
CTSC	cathepsin C	Ctsc	12.328	0.0282
CTSD	cathepsin D	Ctsd	12.091	0.0335
CTSF	cathepsin F	Ctsf	9.745	0.038
CTSS	cathepsin S	Ctss	24.59	0.00705
CTSV		Ctsl	5.85	0.0372
CTSZ	cathepsin Z	Ctsz	32.255	0.00856
DCTN4	dynactin subunit 4	Dctn4	9.453	0.00641
DYNC1LI2	dynein cytoplasmic 1 light intermediate chain 2	Dync1li2	10.201	0.0127
GPAA1	glycosylphosphatidylinositol anchor attachment 1	Gpaa1	14.343	0.00188
HLA-A	major histocompatibility complex, class I, A	H2-D1	8.857	0.039
LAMP1	lysosomal associated membrane protein 1	Lamp1	9.427	0.0149
LAMP2	lysosomal associated membrane protein 2	Lamp2	17.389	0.00142
NAPA	NSF attachment protein alpha	Napa	8.606	0.00126
NAPG	NSF attachment protein gamma	Napg	7.666	0.0255
NCF1	neutrophil cytosolic factor 1	Ncf1	55.062	0.0231
NSF	N-ethylmaleimide sensitive factor, vesicle fusing ATPase	Nsf	5.425	0.0259
PIK3C3	phosphatidylinositol 3-kinase catalytic subunit type 3	Pik3c3	16.209	0.00709
PRDX1		Prdx1	16.381	9.22E-07
PRDX2	peroxiredoxin 2	Prdx2	6.909	0.00636
PRDX5	peroxiredoxin 5	Prdx5	-3.968	0.0034
RAB5B	RAB5B, member RAS oncogene family	Rab5b	5.72	0.0287
STX16	syntaxin 16	Stx16	9.904	0.0404
TSG101	tumor susceptibility 101	Tsg101	6.717	0.00715
TUBA8	tubulin alpha 8	Tuba8	5.722	0.0253
TUBB	tubulin beta class I	Tubb5	14.606	0.014
TUBB4B	tubulin beta 4B class IVb	Tubb4b	9.131	0.00805
TUBB6	tubulin beta 6 class V	Tubb6	21.975	0.00626
VPS37A	VPS37A subunit of ESCRT-I	Vps37a	6.268	0.0305

1456

Total Word count without References ~12500

SUPPLEMENT DATA – PATHWAY FOR TABLE 3

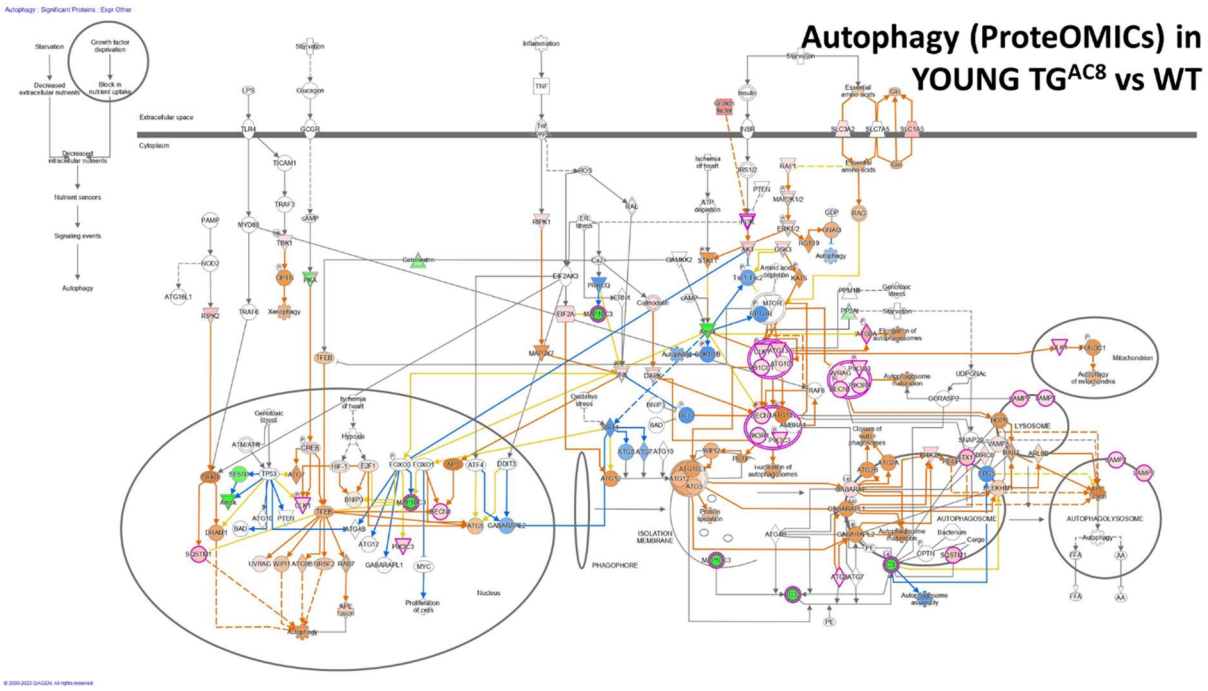

Total Word count without References ~12500

SUPPLEMENT DATA – PATHWAY FOR TABLE 4

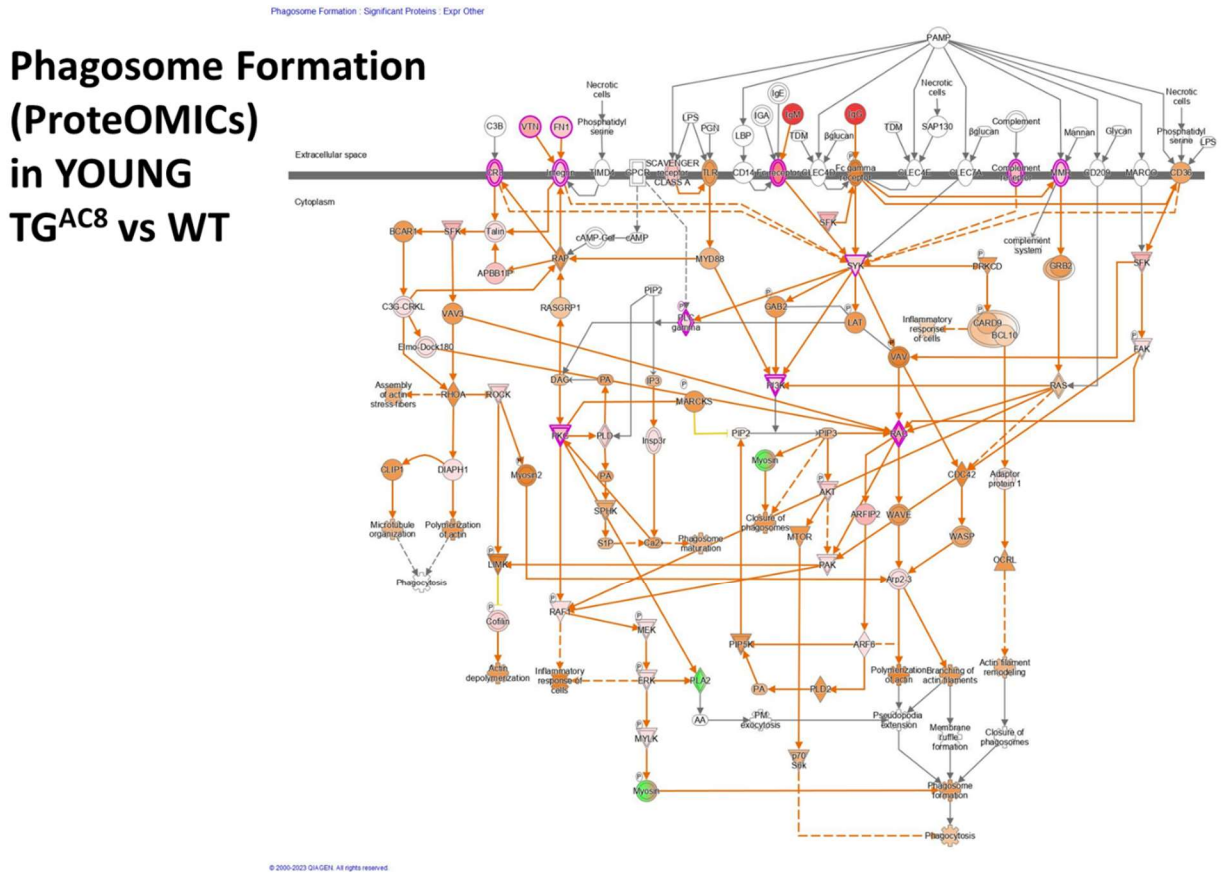

Total Word count without References ~12500

SUPPLEMENT DATA – PATHWAY FOR TABLE 5

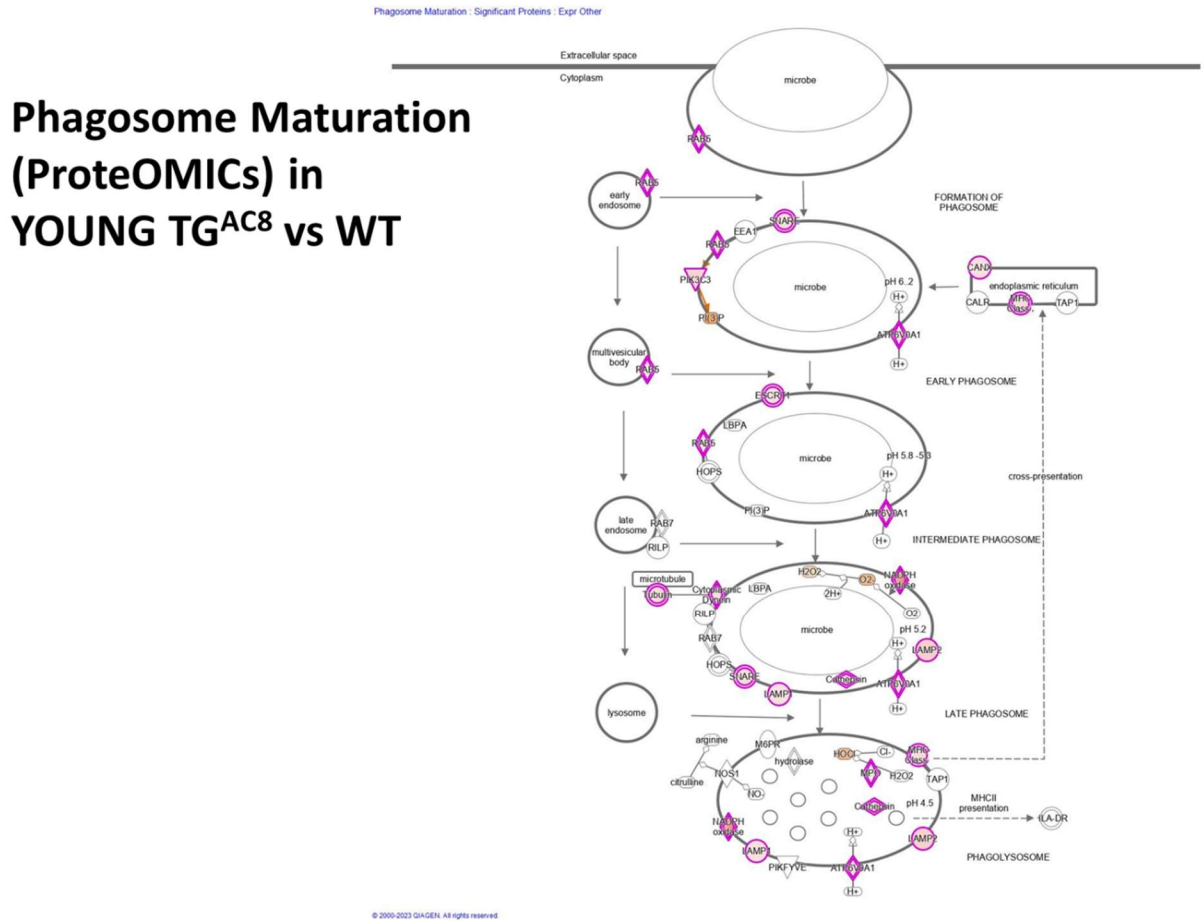

1463 # SUPPLEMENTAL DATA FIGURE LEGENDS

1464 **Table 1. Primary antibodies used in WB.**

1465 **Table 2. List of primers used in qPCR.**

1466 **Table 3. List of players (proteOMICs) in the Autophagy Pathway in TG^{AC8} and WT**

1467 **littermates at 3-4 months of age.**

1468 **Table 4. List of players (proteOMICs) in the Phagosome Formation Pathway in**

1469 **TG^{AC8} and WT littermates at 3-4 months of age.**

1470 **Table 5. List of players (proteOMICs) in the Phagosome Maturation Pathway in**

1471 **TG^{AC8} and WT littermates at 3-4 months of age.**

1472 **Pathway 3 for Table 3. Autophagy Pathway (proteOMICs) in TG^{AC8} and WT**

1473 **littermates at 3-4 months of age.**

1474 **Pathway 4 for Table 4. Phagosome Formation Pathway (proteOMICs) in TG^{AC8} and**

1475 **WT littermates at 3-4 months of age.**

1476 **Pathway 5 for Table 5. Phagosome Maturation Pathway (proteOMICs) in TG^{AC8} and**

1477 **WT littermates at 3-4 months of age.**